

Design principles for low-dimensional supramolecular systems at metal surfaces

THÈSE No 2849 (2003)

présentée à la Faculté Science de Base

Institut de Physique des Nanostructures

Section de Physique

ÉCOLE POLYTECHNIQUE FÉDÉRALE DE LAUSANNE

*pour l'obtention du grade de Docteur ès sciences
par*

ALEXANDRE DMITRIEV

*physicien diplômé de l'Université Fédérale de Rostov, Russie
et de nationalité russe*

acceptée sur proposition du jury:

Prof. K. Kern, directeur de thèse

Prof. K. Wandelt, rapporteur

Prof. E. Meyer, rapporteur

Prof. H. Brune, rapporteur

Lausanne, EPFL

2003

Résumé

Les principes pour obtenir par assemblage modulaire des architectures supramoléculaires fonctionelles de basse dimensionalité sont étudiés et appliqués à pour la fabrication de divers nanosystèmes sur des surfaces. Deux voies principales sont explorées pour l'auto-organisation supramoléculaire sur des surfaces: l'utilisation des liaisons hydrogène et la coordination métallo-organique. L'avancée principale a été réalisée dans la deuxième voie. Pour celle-ci on présentera une nouvelle approche qui a pour but de fabriquer des structures supramoléculaires de basse dimension. L'application des principes de la chimie en solution et ceux de la chimie de coordination de l'état solide sur des surfaces est montrée comme étant une manière productive pour l'élaboration des architectures métallo-organiques fonctionnalisées, dont la morphologie et les propriétés, bien qu'ayant des analogies directes dans la chimie supramoléculaire de coordination conventionnelle, sont largement affectées par la symétrie et la nature du substrat. En fait, une classe totalement nouvelle d'architectures supramoléculaires est présentée et explorée.

Les systèmes supramoléculaires sont préparés *in situ* par croissance épitaxiale en jet moléculaire organique (OMBE) (pour les espèces organiques) et par évaporation thermique par bombardement électronique (pour les dépôts d'adatoms métalliques). Les structures ainsi formées sont ensuite caractérisées *in situ* par microscopie à effet tunnel (STM). Toutes les études ont été effectuées sur une surface de Cu(100) atomiquement propre.

Pour élucider les principes de l'assemblage modulaire des structures supramoléculaires fonctionelles de basse dimensionalité de simples acides carboxyliques polytopiques sont utilisés car ils sont bien appropriés pour former à la fois pour des architectures par liaison hydrogène et basées sur des liaisons métallo-organiques.

L'influence des liaisons hydrogènes sur l'auto-organisation est illustrée par l'adsorption et l'organisation supramoléculaire de l'acide trimésique (TMA) - 1,3,5-tricarboxylique acide benzoïque $C_6H_3(COOH)_3$ et de l'acide trimellitique (TMLA) - 1,2,4-tricarboxylique acide benzoïque $C_6H_3(COOH)_3$ - sur une surface de Cu(100).

La structure des arrangements supramoléculaires a été caractérisée dans l'espace réel avec une résolution sub-moléculaire. A basse température (200 K) des réseaux bidimensionnels de molécules de TMA se développent par formation de liaisons hydrogènes entre les espèces adsorbées à plat sur la surface, de manière semblable à l'organisation de ces molécules sous forme cristalline. A température ambiante des arrangements plus denses se forment, qui sont associés à une géométrie des molécules debout sur la surface grâce à la formation de carboxylate. Les molécules de TMLA prochirales ne montrent pas d'organisation particulière sur un substrat à basse température, par contre, sur un substrat à température élevée les molécules de TMLA sont partiellement déprotonées et adsorbées à plat, et forment de larges domaines homochiraux.

L'utilisation de liaisons de coordination métal-organique pour obtenir une architecture supramoléculaire en surface est explicitée et étudiée à partir de molécules de TMA et de TMLA pour les ligands organiques (L) et d'atomes de Cu et de Fe pour les centres de coordination (M). L'observation en temps réel et à l'échelle nanométrique de la formation des complexes de coordination de TMA interagissant avec les atomes de cuivre a été effectuée. Les molécules de TMA agissant comme des rotors moléculaires fonctionnent comme un piège dynamique pour les atomes métalliques de surface. La caractérisation dynamique, en temps réel, de la formation des arrangements unidentates $\text{Cu}(\text{TMA})_4$ a été réalisée. Les processus élémentaires des réactions de formation et de dissociation, de rotation et de diffusion des différentes espèces sont suivis à l'échelle de la molécule. De plus les énergies correspondantes ont été évaluées en mesurant les taux de réaction.

Dans les étapes suivantes la synthèse des systèmes métallo-organiques multicomposants et complexes a été explorée. Premièrement, la génération de chiralité dans des complexes de coordination unidimensionnels composés de TMA et de Fe a été caractérisée, démontrant qu'un complexe planaire de type ML_4 peut être chiral à deux dimensions quand des ligands symétriques bidentate sont liés à l'atome métallique (qui représente le centre stéréogénique) dans un mode organisée unidentate. En développant cette idée, la fabrication contrôlée de réseaux de coordination chiraux nanoporeux est présentée grâce à l'assemblage hiérarchique de TMA et des atomes de Fe sur la surface.

Deuxièmement, la fabrication de systèmes monocouches hybrides composés de molécules de TMLA et d'atomes de Fe et contenant des centres magnétiques rationnellement placés, est réalisée. Les structures synthétisées démontrent la possibilité d'établir sur des surfaces des architectures métallo-organiques fonctionnelles qui comportent différents centres magnétiques positionnés avec grande précision.

Finallement, les réseaux métallo-organiques possédant des morphologies variables sont construits avec des molécules de TMLA et des centres de Fe. Ce dernier exemple démontre la polyvalence extrême de la coordination métal-organique en surface et donne la perspective d'explorer de nombreuses fonctionnalités à partir de systèmes supramoléculaires assemblées avec cette approche.

Abstract

The design principles for the fabrication of low-dimensional supramolecular architectures by the modular assembly of functional components are investigated and applied for the construction of diverse surface-supported nanosystems. Two main routes are explored, relying on hydrogen-bonding and metal-ligand interactions. The major emphasis is put on the latter approach, where a novel concept to design low-dimensional metal-organic structures is introduced. The translation of the principles of solution and solid state coordination chemistry to surface systems is demonstrated to be a versatile way to obtain metal-organic architectures, whose topologies and functional properties, although having direct analogies with conventional bulk supramolecular coordination compounds, are to a large extent templated and controlled by the symmetry and the chemical nature of the substrate. In fact, an entirely new class of surface supramolecular architectures is introduced and explored.

The fabricated supramolecular systems are prepared *in situ* by organic molecular beam epitaxy (OMBE) (concerning the organic species) and electron-beam heating evaporation (with respect to metal adatoms deposition). The formed structures are characterized at the nanoscale by *in situ* scanning tunneling microscopy (STM). All experiments are conducted on atomically clean Cu(100) surface.

To elucidate the design principles of low-dimensional supramolecular self-assembly, simple polytopic carboxylic acid linkers were employed, which are appropriate both for H-bonded or metal-carboxylate based architectures.

Hydrogen-bond driven surface self-assembly is exemplified with the adsorption and supramolecular ordering of trimesic acid (TMA) - 1,3,5-benzenetricarboxylic acid $C_6H_3(COOH)_3$ and trimellitic acid (TMLA) - 1,2,4-benzenetricarboxylic acid $C_6H_3(COOH)_3$. The real-space structures of distinct self-assembled supramolecular aggregates at the molecular scale were elucidated. At low temperatures (200 K) two-dimensional networks evolve with TMA, reflecting extensive hydrogen bond formation of a flat-lying species, similar to supramolecular ordering in the bulk TMA crystal structure. At room temperature more densely packed stripe arrangements

form, which are associated with a bonding transition leading to an upright geometry due to carboxylate formation. Prochiral TMLA molecules do not show particular ordering at the cold substrate, however, when partially deprotonated and flat-adsorbed upon thermal annealing, they are engaged in chiral recognition to form homochiral extended domains.

The paradigm for supramolecular design at surfaces exploiting coordination bonding is formulated and studied by employing the molecules TMA and TMLA as organic ligands (L) and Cu or Fe atoms as transition metal coordination centers (M). Single-molecule real-time monitoring of the formation and decay of coordination compounds from TMA interacting with Cu adatoms was achieved at room temperature. The TMA molecules acting as molecular rotors are found to operate as a dynamical trap for the metal atoms. Real-time measurements reveal the dynamics of the resulting unidentate $\text{Cu}(\text{TMA})_4$ cloverleaf arrangement. Single events of association and dissociation reactions involving rotation and diffusion in individual reactant and product species are followed one molecule at a time. From measured reaction rates the corresponding energetics were quantified.

In subsequent steps the genuine synthesis of intricate multicomponent metal-organic systems was explored.

Firstly, chirality generation in one-dimensional coordination complexes of TMA and Fe was characterized, evidencing that a square-planar ML_4 complex can be chiral in two dimensions when symmetric bidentate ligands are employed which link to the metal atom (representing the stereogenic center) in an organized unidentate fashion. Developing this idea, the rational design of nanoporous two-dimensional chiral coordination networks via hierarchical assembly of TMA and Fe atoms at surfaces is presented.

Secondly, the fabrication of a hybrid monolayer system of TMLA molecules and Fe atoms, containing rationally positioned magnetic centers has been achieved. The synthesized structure demonstrates the possibility of building functional surface-supported metal-organic architectures, comprising individual magnetic centers, positioned with extreme accuracy.

Finally, nanoporous metal-organic coordination networks with tunable topologies are constructed out of TMLA molecules and Fe. This last example underlines the extreme versatility provided by the metal-organic coordination at surfaces and the prospects to explore diverse functionalities of supramolecular systems, assembled with this approach.

Abbreviations and Common Symbols

AFM	Atomic Force Microscopy
CMOS	Complementary Metal-Oxide Semiconductor
DFT	Density Functional Theory
HOMO	Highest Occupied Molecular Orbital
L	Ligand
(L)DOS	(Local) Density Of States
LEED	Low-Energy Electron Diffraction
LUMO	Lowest Unoccupied Molecular Orbital
M	Metal
ML	Monolayer
MOCN	Metal-Organic Coordination Network
MOSFET	Metal-Oxide Semiconductor Field Effect Transistor
NEXAFS	Near-Edge X-rays Absorption Fine Structure
OMBE	Organic Molecular Beam Epitaxy
STIS	Scanning Tunneling Inelastic Spectroscopy
STM	Scanning Tunneling Microscopy
TMA	1,3,5-Benzenetricarboxylic acid, trimesic acid
TMLA	1,2,4-Benzenetricarboxylic acid, trimellitic acid
TPA	1,4-Benzenedicarboxylic acid, terephthalic acid
UHV	Ultra-High Vacuum
XPS	X-ray Photoelectron Spectroscopy

a_0	surface lattice constant
D_0	pre-exponential factor for tracer diffusion
E	energy with respect to the Fermi energy
E_b	binding energy of adsorbates
E_F	Fermi energy
E_m	energy barrier for surface migration
$f(E, T)$	Fermi-Dirac distribution
fcc	face cubic centered
hcp	hexagonal close-packed
I	tunneling current
i	tunneling current per energy unit
m_e	free electron mass, $m_e = 9.11 \cdot 10^{-31}$ kg
s	tip-sample distance
T	temperature
V	electric potential of sample with respect to tip
W	work function
δ	delta function
θ	surface coverage
\hbar	Planck constant, $\hbar = \frac{h}{2\pi} = 1.05 \cdot 10^{-34}$ Js
ν_0	attempt frequency
ν_s	hopping rate
π	pi, $\pi = 3.14$
ρ	electronic density of states
2D	Two-Dimensional
3D	Three-Dimensional

Contents

Résumé	iii
Abstract	vii
Abbreviations and Common Symbols	ix
Contents	xi
1 Introduction	1
2 Experimental	15
2.1 Experimental Methods	15
2.2 Experimental Set-up	20
2.3 Sample Preparation	24
3 Bonding and Ordering of Mellitic Acids on Cu(100)	27
3.1 Trimesic Acid	29
3.2 Trimellitic Acid	37
4 Assembly of Coordination Systems at Surfaces	43
4.1 Coordination Reactions Followed in Real-Time	45
4.2 Direct Insight Into Mononuclear Chiral Compounds	53
4.3 Hierarchical Self-Assembly	58
4.4 Print Boards of Magnetic Centers	65
4.5 Metal-Organic Coordination Networks	70
5 Outlook	77

Bibliography	80
Acknowledgements	97
Curriculum vitae	99
Publications	101

Chapter 1

Introduction: The Keys to the World of Nano and Supramolecular Self-Assembly

The beginning of 21st century is marked in material science by establishing it among both the highly promising and highly hyped areas of knowledge: the reason are the four letters - 'nano' - which are promised to revolutionize the world as we know it.

It seems that about the only thing that nanotechnology won't deliver is the eradication of taxes. [1]

Traditionally chemistry is manipulating matter on the nanometer scale by covalent synthesis of molecular species from smaller constituents. On the other hand life science at the nanoscale is known in biology since decades: just as now it is time to *rendre hommage* to Watson and Crick, who initiated molecular structural biology 50 years ago by determining the DNA double-helix structure - one of the primal naturally occurring nanoscopic functional entities [2]. Nature provides the principles of nanotechnological approaches, which are intrinsic for all living matter and which are fundamental for the origin and functioning of life. Exploring them in connection with material science, however, was seeking for long a major motivation from the side of physics.

Paradoxically, the minds have not turned to so called 'bio-nanotechnology' (which is related to biological or biomedical systems) before semiconductor physics started

to rule the ideas and provided prospects how to adopt the richness of naturally occurring nano-systems for our computational needs. In his famous visionary talk "There's Plenty of Room at the Bottom" Richard Feynman outlined how to merge chemistry, biology and physics to produce materials, whose functional units would be of a nanoscopic dimensions and whose capability in information storage would be comparable with the molecular structures known in biology [3].

The avalanche development of complementary metal-oxide semiconductor (CMOS)-based integrated circuit technology started in 1947 with the invention of the first transistor by John Bardeen and Walter Brattain at Bell Labs, followed by the development of the first integrated circuit in 1958 by Jack Kilby, rapidly went on in the 60-70s with the patenting of the first metal-oxide semiconductor field-effect transistor (MOSFET) and is continuing to the present days with the development of increasingly refined (photo)lithographic methods. It successfully fueled the microelectronics and computation advances over the past four decades. And since miniaturization rules the world of microelectronics with its "Moore's law", introduced in 1965 by Intel co-founder Gordon Moore (a chemist!) and stating that the feature sizes of microelectronic devices shrink by half and the number of components on a chip quadruple every three years [4] - electronics at the atomic level will be the ultimate limit if this exponential route is to continue. Here comes 'nano'! However, bright prospects are shadowed by the Mother Nature - rather than reaching the atomic scale in the device size, fundamental physical limits will be imposed on the size of the narrowest feature of silicon devices - the gate oxide - as soon as it reaches a thickness of four layers [5,6]. Moreover, the problem of fabrication of integrated circuits with feature sizes less than 5 nm is currently an unresolved issue.

Primarily motivated by the development of microelectronics, nanotechnology soon appeared to bring dazzling perspectives to the overwhelming range of applicable knowledge, establishing itself as an intrinsically multidisciplinary science. Selected examples include the impact of nanoscale approach on science of catalysis [7], molecular machinery development [8,9], DNA-based biotechnology [10,11] or postgenomic research [12]. Moreover, nanotechnology seems to bridge the gap between top-down miniaturization, exemplified by photolithography, e-beam lithography or

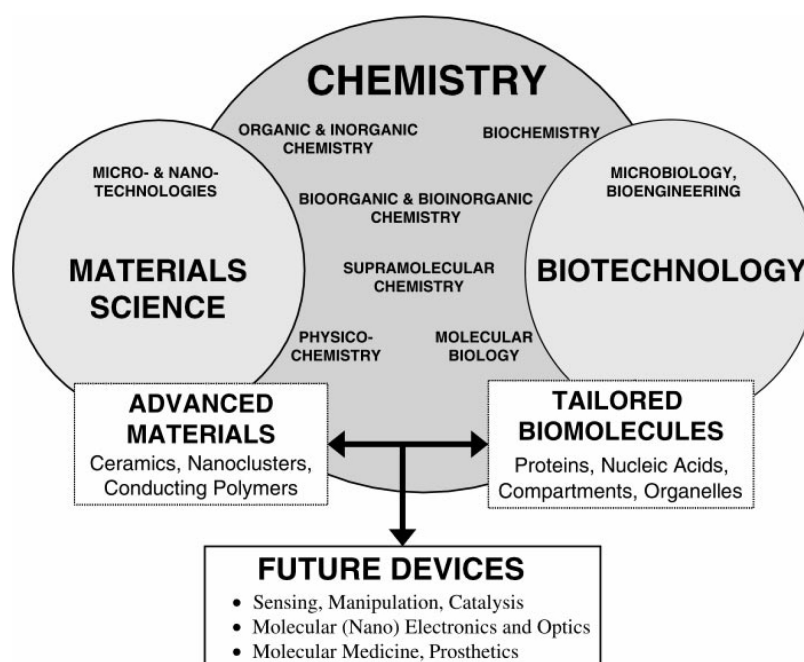


Figure 1.1: When Material Science, Chemistry and Biotechnology come together, the results of such a fusion promise to be bright. As for material science is concerned, "with the little help from" two other disciplines it can now manipulate the world of Nano. Major breakthroughs are still to come! (scheme is taken from [13]).

microcontact printing, and bottom-up strategies, explored by organic synthesis and supramolecular self-assembly. The area where biomolecular components, such as proteins and nucleic acids, meet nanoparticles comprised of metal and semiconductor material promises great future developments on the cross-road between chemistry, biotechnology and material science (Fig. 1.1, adopted from [13]). And it is indeed two-way traffic: when nanoscience brings to biotechnology its advances, such as quantum dots, to revolutionize *in vivo* imaging of the cell processes, biotechnologically selected peptides provide prospects for synthesis of durable magnetic architectures for high-density recording media [14].

Among endless number of faces for nanoscience, molecular scale electronics [15–17] - exploration of alternative paradigms aimed to avoid the dead-end of silicon technology miniaturization route - is of fundamental interest for microelectronics-related material science. Launched as a discipline by Aviram and Ratner in 1974 with their preparation and characterization of donor-acceptor species, conceived as donor-insulator-acceptor molecular diodes (rectifiers) [18], which are still ac-

tively discussed [19], molecular electronics developed promising routes for the replacement of CMOS-based devices by their molecular analogues. An entire collection of electronic components, needed for integrated circuitry, namely molecular diodes/rectifiers/transistors, molecular wires, molecular memory units and molecular switches or logic gates, was proposed and tested for the last decade of active research in the field [20–28]. Nevertheless it is still far away from any practical applications in information technologies. In particular, the fundamental principles of how individual molecular units should be positioned at specific sites where they operate are under current active discussion: whereas manual manipulation appears to be economically not viable, molecular self-assembly concepts are envisioned to play a major role here.

Molecular self-assembly relies on interactions between complex molecules containing specific functional groups. Both the local arrangement of these chemical groups and the physical properties (mechanical, optical etc.) resulting from organization at a larger scale provide the performance and functions needed in biological systems and materials. Self-assembly is abundant in nature, where the process is used to create complex functional biological structures with precision. Biological self-assembled structures are built up by a modular approach from simple, ordinary subunits, thus minimizing the amount of information required for a specific ensemble. The molecular level design of new materials by self-assembly [29–32] advanced extensively in the past decade under the banner of the multidisciplinary fields of crystal engineering [33, 34] and supramolecular chemistry [35–38]. If molecules are built by connecting atoms with covalent bonds, supermolecules are assembled on the next level of complexity by binding molecules with directional intermolecular interactions, non-covalent in their nature. Group properties of molecules are often different from those of individual ones - this trend potentially leads to unusual effects and exciting discoveries [39]. Supramolecular chemistry supplies molecular nanoscience with a wide range of tools for deliberate construction of non-covalently bonded self-assembled molecular architectures, whose complexity and functionality is tackling those common in biology: Natural supermolecules are abundant in biological systems, where their proper functioning is of crucial importance for life (see [40] and references therein).

We live, I regret to say, in an age of surfaces. Oscar Wilde

As a primal motivation of employing low-dimensional supramolecular self-assembly for nanoscience applications stems from the demands in shifting conventional CMOS-based technology towards molecular electronics, two-dimensionally confined media - surfaces - appear to be a natural environment to explore the potential of supramolecular chemistry with reduced dimensionality. Indeed, whereas non-covalently bonded supramolecular architectures are the classical subject of interest in solution and solid state chemistry [41, 42], surface-confined molecular nanostructures and single molecules have been extensively studied for last decade in particular due to ground breaking progress in surface-characterization techniques, especially in scanning local probes (see [43–45] and references therein). Feynman was motivating physical science to make electron microscopy two orders of magnitude more performant to get real-space insight at the atomic scale. In two dimensions it became a reality in the 80ies with the invention of scanning tunnelling microscopy [46]. The entire term nanoscience (and nanotechnology) have been strongly influenced by the introduction of STM and AFM, which provide unprecedented capabilities to image and manipulate matter at the atomic scale.

Recent studies evidence the value of this technique for the elucidation of fundamental phenomena in surface chemistry in exquisite detail: topology of supramolecular assemblies and molecular conformations [47–53], chiral specificity [54–57], pathways of chemical reactions [58–63], catalytic functionality [64].

Major types of non-covalent interactions, employed in supramolecular design, are: - electrostatic (which can vary from unselective ion pairing of singly charged species to highly selective interaction between two ions with another complementary intermolecular interaction); - ionic interaction (as employed in growth of ionic crystals or inter-protein interactions); - hydrophobic (with quite small energies stabilizing long-range two-dimensional structures in the absence of other interactions); - host-guest interactions (responsible for filling internal molecular cavities, functionalized with donor sites, by ionic species); - hydrogen bonding and metal-ligand coordination. We will put an emphasis on the latter two, since both are key interactions in living

biological matter and represent the pillars of supramolecular chemistry [36, 65, 66].

Hydrogen bonding is of pivotal importance in biological systems and in organic host-guest molecular complexes: structural aspects of DNA and DNA binding agents, protein conformations and folding, receptor functions are the examples where the natural chemistry of hydrogen bonding is extensively involved [67, 68]. Of all directional intermolecular interactions, hydrogen bonding is the most important one. Three dimensional structures may readily be fast and specifically assembled by hydrogen bonding, incorporating a large degree of flexibility due to weak intermolecular forces holding the molecules. As the interaction is weaker than covalent bonding and in the range of thermal energies at ambient conditions, it may be reversed - an intrinsic error correction mechanism is characteristic for hydrogen-bonded assemblies, which leads ultimately to the most thermodynamically favorable structures. An important feature of hydrogen bonding is cooperativity - being individually weak, together they become stronger, which enables noncovalent synthesis, based on the reversible formation of multiple hydrogen bonds to be accomplished. Hydrogen bonding is responsible for the determination of molecular conformation, molecular aggregation and functionality of a vast number of supramolecular systems [69–72].

At solid substrates, particularly on single crystal metal surfaces, hydrogen bonding was successfully explored for advanced supramolecular engineering, where its directionality facilitates fabrication of highly organized assemblies [52, 73–78]. Due to the great flexibility of this weak interaction, employing hydrogen bonding for the fabrication of surface-supported supramolecular architectures allows deliberate design of complex topologies with possible control over the final structures and functionalities [47].

The first part of the present thesis is concerned with surface-confined supramolecular engineering through hydrogen bonding (Chapter 3.1). As an exemplary model system for investigation, representative polytopic organic linkers - molecules of the mellitic acids series, namely 1,3,5-benzenetricarboxylic acid (trimesic acid, TMA) and 1,2,4-benzenetricarboxylic acid (trimellitic acid, TMLA), adsorbed on Cu(100) surface, are chosen (see Fig. 1.2 for the molecular structure of both species). The low-temperature ordering of these molecular species is governed by the directionality

of hydrogen bonding, arising upon lateral functional groups' coupling or the formation of classic supramolecular synthon - the carboxylic acid dimer [79].

For TMA it is important, that molecules adsorb in a flat-lying configuration at low-temperature. The supramolecular self-assembly in this case is affected by the potential corrugation of the surface, resulting in hydrogen bonding characterized by slightly altered distances compared to the solution or solid state chemistry cases for the same species. By contrast, a similar effect of the substrate potential prevents TMLA species to order into extended hydrogen-bonded structures due to the TMLA molecular geometry with reduced symmetry.

Furthermore the effect of carboxylic group deprotonation on the resulting supramolecular assemblies is discussed in detail.

Room temperature experiments suggest that for TMLA all carboxylic groups are intact and deprotonation does not occur even upon annealing up to 450 K. Only at monolayer coverage (or upon deposition at the substrate hold at 400 K) one carboxylic group of TMLA is deprotonated, which leads effectively to a nearly flat-lying adsorption geometry. This opens the possibility for the molecules to form extended chiral structures: being prochiral in 3D, TMLA upon 2D confinement is a chiral species and thus chiral recognition may occur.

Analogously, upon the loss of carboxylic acid hydrogens, the arrangement of TMA molecules undergoes a transition to new phases. This time carboxylates of up-right standing species bind to the substrate atoms, and the whole supramolecular architecture is weakly stabilized by lateral hydrogen bonding of still non-deprotonated carboxylic groups. However, despite the covalent character of the carboxylate bonding to the substrate atoms, this configuration does not show a long term stability. The presence of mobile copper adatoms on the Cu surface at room temperature favors the deprotonation of the remaining carboxylic groups, enforcing hydrogen-bonded assemblies to lose their integrity and eventually disappear. In fact, the low stability of TMA hydrogen-bonded structures at room (and elevated) temperatures and the ease for this molecule of deprotonation process, driven by the catalytic activity of the substrate, which creates reactive to metal ions carboxylate entities, opens up an alternative linkage to the H-bond in building supramolecular architectures - metal-ligand

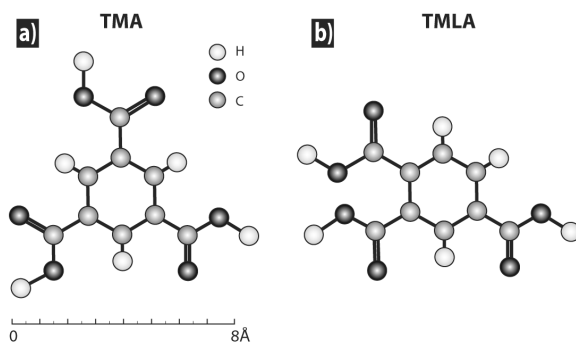


Figure 1.2: Molecular structure of (a) trimesic acid, (b) trimellitic acid

interactions.

Metal-ligand interactions are exploited to link organic species to transition metal centers. They are characterized by intermediate strength relative to weak interactions (as hydrogen bonding, discussed above) and strong covalent (e.g. carbon-carbon) bonds of most organic compounds [80]. Coordination chemistry is a key for understanding the mechanisms by which transition metal ions are taken up into living cells and handled inside for the purpose of storage or incorporation into essential enzymes - metal sites of bioinorganic systems provide the heart of enzymatic catalysis and play a fundamental role in the structure and function of proteins and nucleic acids (in their structural stabilization and catalytic functions) [81–84]. By straightforward analogy with biological systems, in synthetic supramolecular coordination chemistry there are distinct geometries of the coordinating ligands, which fit to the size, spin state and electron density of the various metal ions, and which orientate and adjust the metal ion for its proper function [85,86]. Since the introduction of the coordination concept by Alfred Werner [87], the use of transition metal centers and coordination chemistry for directing the formation of complex structures has evolved into one of the most widely used strategies for organizing molecular building blocks into supramolecular arrays [36, 88]. The predictable and directional bonding of organic ligands allows for the engineering of supramolecular coordination complexes with extraordinary structures and properties: rotaxanes and catenanes [89, 90], synthetic receptors - molecular cages [91–93], multicomponent assemblies such as chains, grids or helices [94–96] are already classical examples of coordination-driven self-assembly (two- and three-dimensional porous grid-like architectures are discussed in

detail later in the Section 4.5 of the Chapter 4).

Solid state chemistry takes advantage of the coordination bonding approach, since rational crystal engineering of solid materials is crucially dependent on predictability and rigidity - e.g. provided by organometallic compounds, where C-moieties of organic molecules couple to a metal [39,97]. Transition metal complexes play a tremendous role in catalysis. The mimics of enzymatic specificity in chemical asymmetric synthesis is tentatively approached by use of transition-metal-based catalysts [98], whereas supported metal-organic catalytic materials are expected to bridge the gap between homogeneous and heterogeneous catalysis, bringing the concepts and tools of chemistry to surface science [99–102]. Molecular magnetism constitutes another promising facet of modern coordination chemistry and the field has produced in recent years magnificent solid-state structures with intriguing magnetic properties [103,104]. Cooperative magnetic behavior can be found in zero- [105–107], one- [108–110], two- [111–113] or three-dimensional [114] metal-organic architectures. Moreover, spin cross-over phenomena are observed for this type of compounds [115–118].

The link of supramolecular coordination chemistry to molecular electronics becomes evident in this case: surface-supported molecular magnetic architectures [119] are envisioned to play a role in the design of memory devices with ultimate storage density (a more detailed discussion of this issue with some practical implementation mechanisms is presented in the Section 4.4, Chapter 4 of the present thesis). Another nice example is a single-molecule transistor based on a coordination compound, which exhibit either single-electron phenomena, such as Coulomb blockade, or the Kondo resonance [119,120]. Coordination bonds may be decisive in molecular recognition and offer an excellent means for the fabrication of surface-supported complex molecular arrangements: however, their exploration for surface supramolecular chemistry is yet in its infancy [121,122].

The second part of the present thesis (Chapter 4) focuses on the implementation of concepts of supramolecular coordination chemistry for surface-supported synthesis of novel metal-organic architectures. The principal advantage of using metal-ligand interaction as compared to hydrogen bonding lies in the increased strength of coordination bonds with respect to the weak coupling through hydrogen bonding. In

Supramolecular Coordination Chemistry

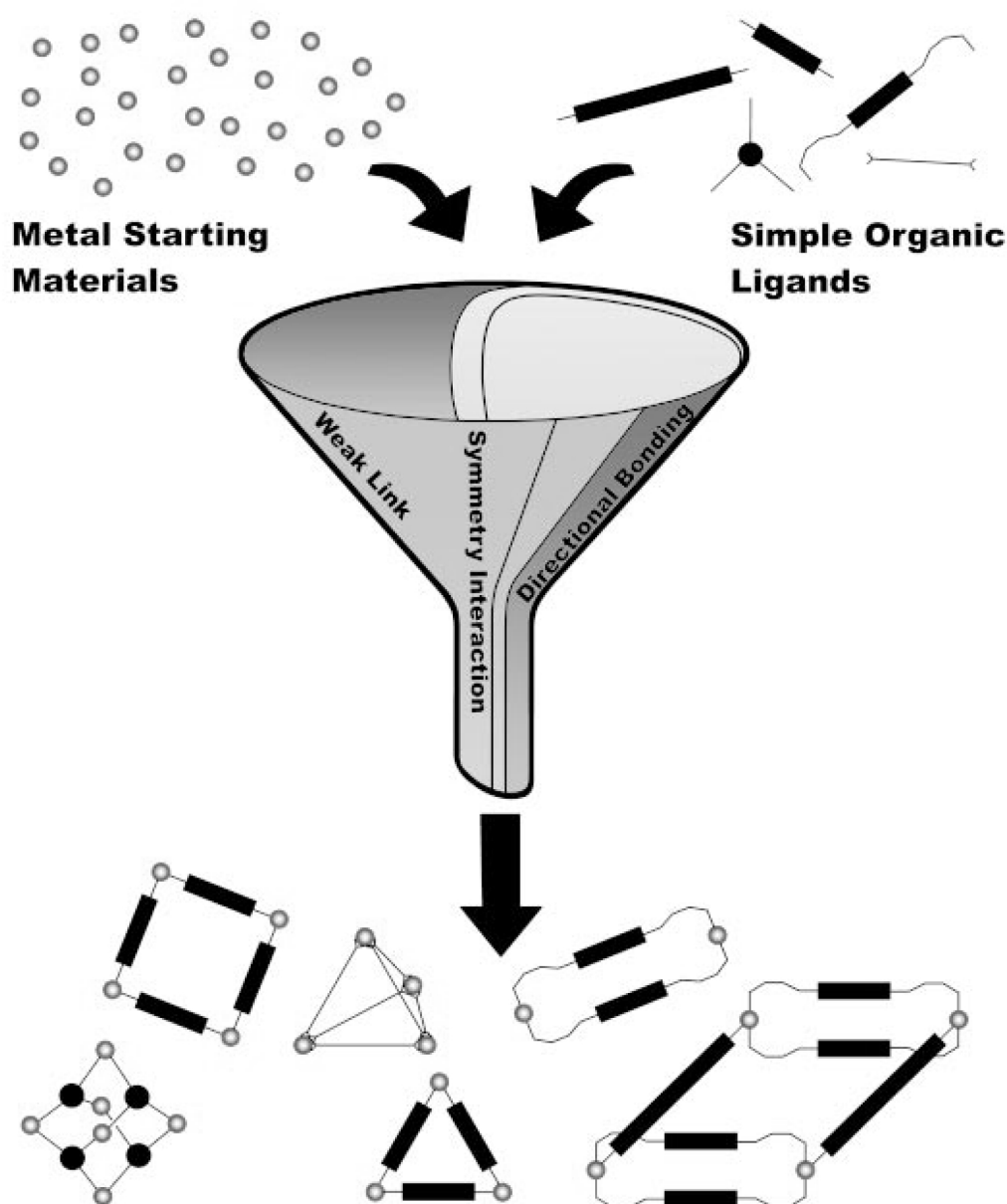


Figure 1.3: Figure 1.3: Principal idea behind supramolecular coordination chemistry: by passing starting materials - metals and functional organic molecules (ligands) through the 'melting bonding pot' of weak linkage formalism, employing symmetry interactions and directional bonding, we arrive at highly organized and predictable architectures. The dream of supramolecular engineering becomes a reality? (adopted from [86]).

solution and solid state chemistry this allows for intentional selection of either thermodynamic or kinetic reaction pathways through the judicious choice of ligands, transition metals, and reaction conditions. As suggested from general coordination chemistry, defective structures in this case can often be corrected or annealed to the desired product by adjusting reaction times and conditions. Thus a straightforward translation of coordination chemistry principles to surfaces is expected to provide an access to deliberate manipulation of highly directional metal-ligand interactions by the variation of reaction conditions (initial concentrations of constituents or substrate temperatures) or by post-annealing procedures to obtain distinct supramolecular architectures through transition metal mediated assembly. Moreover, using STM for high spatial resolution characterization allows real-space evaluation of some fundamental chemical structural concepts - like bonding geometry, chirality, hierarchical assembly etc.

As the model molecular linkers for probing metal-organic coordination two molecules were chosen - TMA and TMLA described above. Both species are known to be effectively involved in metal-organic complexation [123,124] and thus represent good exemplary organic species for evaluating mechanisms of surface-supported metal-organic coordination.

In the Chapter 4 the conceptual approach for the rational design of nanostructures at surfaces by metal-organic coordination is demonstrated.

In the following Sections examples of utilizing in situ formation of coordination bonding geometries is explored for the demonstration of selected fundamental concepts of chemistry at surfaces at the single molecule level. Each Section includes a short introduction into the particular area of solution or solid-state chemistry, where analogues to the described systems are briefly described.

The reaction between carboxylates of deprotonated TMAs and freely available surface copper adatoms results in the formation of coordination compounds, where single Cu centers coordinate four TMA ligands in square-planar geometry to form cloverleaf-shaped arrangement (Section 4.1). Single events of association and dissociation reactions involving rotation and diffusion in individual reactant and product species were followed one molecule at a time. From measured reaction rates the

corresponding energetics was quantified.

Utilizing Cu as metal center in surface-supported metal-organic architectures proved to be an exemplary strategy for the evaluation of the dynamics of coordination bonding. Choosing Fe atoms as metal centers for coordination provides an increased bond strength in the metal-organic complex and, in general, supplies more effective interaction of the adatoms with available organic ligands. I.e., when both Fe and Cu adatoms are present on the substrate (intrinsically available Cu adatom' gas on Cu(100) and deposited Fe single atoms), the competing interactions of organic ligands with both Fe and Cu results in a formation of stable complexes with Fe, whereas Cu-driven complexation is partially or completely hindered. In the same time, blocking of the step-edges by Fe adatoms also accounts for reduction of the amount of available copper adatoms on the surface. With the (Fe,Cu)/TMA system both Fe-TMA and Cu-TMA complexes can be observed under elevated temperatures, whereas the system (Fe,Cu)/TMLA does not produce any detectable Cu-TMLA complexation even in the absence of competing Fe adatoms. These complexation scenarios strongly suggest Fe providing a better chemical environment for metal-organic coordination reactions with carboxylates. An analogy with conventional solution coordination chemistry can be drawn here regarding the stability constants for various metal chelates - generally, the stability of these complexes is higher if Fe(III) ions are involved, compared to those formed with Cu and Fe(II) [125]. Thus the following examples of metal-organic architectures are relying exclusively on reactions involving Fe adatoms, deposited on copper substrates.

Section 4.2 describes the way chiral coordination compounds can be generated out of achiral components - molecules of TMA and Fe atoms. Following their sequential deposition on Cu(100), we show how the molecules react with the metal centers to chiral complexes stabilized by metal-ligand interactions. These results effectively demonstrate that a square-planar ML_4 complex can be chiral in two dimensions when symmetric bidentate ligands are employed which link to the metal atom (representing the stereogenic center) in an organized unidentate fashion.

Based on these observations in Section 4.3 a scenario for hierarchical assembly in two-dimensional systems is presented. The application of surface metal-organic

coordination to obtain a chirally functionalized surface is demonstrated.

Section 4.4 refers to the potential in molecular magnetism using metal-organic coordination hybrid supramolecular structures. The metal-ligand arrays are designed on the surface, where positioning of individual magnetic centers with high accuracy is achieved.

Finally, in Section 4.5 the principles of surface metal-organic complexation are utilized for the modular assembly of two-dimensional metal-organic coordination networks.

Chapter 2

Experimental

In this Chapter an introduction to the principles and theory of the experimental method used, namely scanning tunneling microscopy (STM), is given. The experimental set-up and sample preparation employed during the studies are discussed in Section 2.2 and Section 2.3, respectively.

2.1 Experimental Methods

Scanning Tunneling Microscopy

Tunneling phenomena are as old as quantum mechanics itself. Tunneling is an extremely important transport mechanism in bulk matter and ultra-thin-films. For instance, the Bardeen-Cooper-Schreiffer theory for superconductivity received decisive experimental support from investigations employing planar metal-oxide-metal tunnel junctions, pioneered by Giaever and coworkers in the early sixties [126]. Following "classical" electron tunneling experiments, scanning tunneling microscopy (STM) [127] was invented by Binnig and Rohrer in 1982 [46, 128]. The revolutionary advantage of STM was the ability to perform *tunneling experiments with spatial resolution at the atomic scale*.

Figure 2.1(a) shows the schematics of an STM. A tip, normally a sharpened metallic wire, is brought close to the conducting surface of a sample. The lateral tip position (x and y axis), as well as the tip-sample distance s are controlled with picometer precision by means of voltage signals applied to piezo-electric materials. If

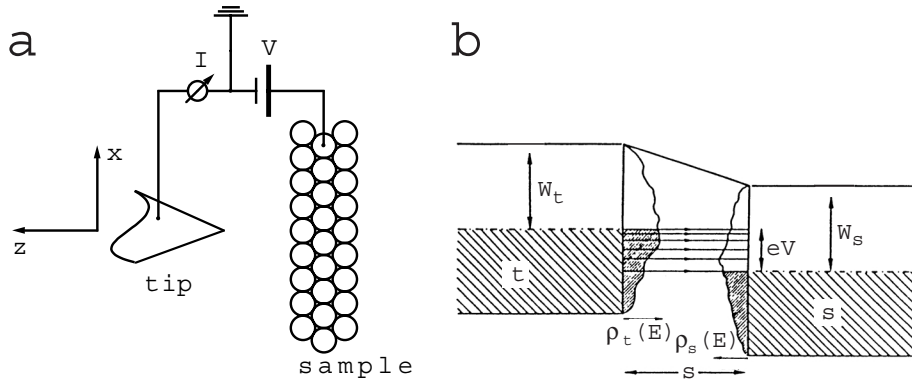


Figure 2.1: (a) Schematic of an STM. (b) Corresponding potential energy diagram.

the tip is brought close enough to the sample that the wave functions of the conduction electrons of tip and sample begin to overlap substantially, a measurable tunneling current I flows between the biased sample (potential V with respect to ground) and the tip (Fig. 2.1(b)). The tip-sample distance in typical tunneling experiments is about 5–10 Å. Since the tunneling current depends exponentially on the tip-sample distance, it mainly flows through the few atoms at the very apex of the tip. Thus the tunneling current is highly localized, leading to the atomic-scale resolution of STM. In the case of a positively biased sample (as in Fig. 2.1(b)) the net current comes from electrons tunneling from occupied states in the tip to unoccupied states of the sample. The current per energy unit, i , is represented by the density of horizontal arrows in Fig. 2.1(b). As can be seen i decreases with decreasing energy since the energetically lower lying states decay steeper in the vacuum barrier region. Whereas it is intuitively clear from Fig. 2.1(b) that the tunneling current will depend on the density of occupied and unoccupied states of tip and sample (ρ_t and ρ_s), respectively, the exact calculation of the tunneling current starting from the electronic structures of tip and sample is a difficult task. It is further complicated by the fact that the atomic structure and the chemical nature of the tip apex is normally not known.

To interpret STM data one may follow the widely used transfer Hamiltonian approximation introduced by Bardeen [129], where the tunneling current is given

by [130]:

$$I(V) = 2e \sum_{\mu,\nu} \frac{2\pi}{\hbar} |T_{\mu,\nu}|^2 \delta(E_\mu - eV - E_\nu) \times \\ \left(f(E_\mu - eV, T) [1 - f(E_\nu, T)] - f(E_\nu, T) [1 - f(E_\mu - eV, T)] \right). \quad (2.1)$$

Here the summation goes over all quantum states μ and ν of the unperturbed sample and tip, respectively, f is the Fermi–Dirac distribution function¹, T is the temperature and $T_{\mu,\nu}$ is given by

$$T_{\mu,\nu} = -\frac{\hbar^2}{2m_e} \int_{\Sigma} d\mathbf{S} (\Psi_\nu^* \nabla \Psi_\mu - \Psi_\mu \nabla \Psi_\nu^*), \quad (2.2)$$

which must be evaluated over a surface Σ within the barrier region and with the wave functions of the unperturbed sample and tip, Ψ_μ and Ψ_ν , respectively. The $T_{\mu,\nu}$ matrix elements depend roughly exponentially on the barrier width s .

To get beyond qualitative properties of the tunneling current one has to find good approximations for the matrix elements $T_{\mu,\nu}$. A simple STM theory is the s -wave approximation for tip wave functions introduced by Tersoff and Hamann [131], leading to the following expression for the tunneling current [132, 133]

$$I(V, T, x, y, s) \propto \int_{-\infty}^{\infty} dE \rho_s(E, x, y) \rho_t(E - eV) \times \\ \mathcal{T}(E, V, s) [f(E - eV, T) - f(E, T)], \quad (2.3)$$

where ρ_t is the density of states (DOS) of the tip, x and y characterize the lateral position on the sample and s the distance between tip and sample measured from a virtual plane passing through the uppermost atoms. ρ_s is the LDOS of the sample in this virtual plane. An often used expression for the tunneling transmission factor $\mathcal{T}(E, V, s)$ reads [133]:

$$\mathcal{T}(E, V, s) = \exp \left(-2s \sqrt{\frac{m_e}{\hbar^2}} \sqrt{W_s + W_t - 2E + eV} \right). \quad (2.4)$$

Here V is the electric potential of the sample with respect to the tip, W_s and W_t are the work functions of sample and tip, respectively (cf. Fig. 2.1).

¹Energies are given with respect to the Fermi level if not otherwise stated.

Although this is a crude simplification, the expressions in Eqs. (2.3) and (2.4) contain the essential and are a good starting point for qualitative and under certain conditions quantitative discussions.

All STM images presented in this thesis are taken in the so-called *constant-current imaging* mode [127]. In constant-current imaging the tunneling current I is compared to a preset current value I_0 . The difference signal $\Delta I = I - I_0$ is fed back to the voltage applied to the z -piezo so that the tip-sample distance is adjusted in order to minimize ΔI [134]. The surface is then scanned by the tip and the voltage applied to the z -piezo in order to keep the current constant is recorded. One thus obtains a so-called topograph $z(x, y)|_{I,V}$ which term is misleading because $z(x, y)|_{I,V}$ is rather a surface of constant local density of states (LDOS) at the Fermi energy (E_F) of the sample. Thus it reflects the electronic structure and *one has to be careful to interpret $z(x, y)|_{I,V}$ images in terms of surface topography*. The size, nature and chemical identity of the tip influence not only the resolution and shape of STM scan but also the electronic structure to be measured.

The interplay of topography and electronic structure becomes crucial when interpreting STM data obtained on molecular adsorbates. A well-known counterintuitive example is atomic oxygen chemisorbed on a metal surface, which appears as depression in STM images even if the atom is positioned above the metal surface layer [63]. STM patterns of molecules often show internal structure and details but the interpretation is not straightforward due to the fact that protrusions on the STM image do not necessarily represent actual lateral position of atoms.

Before the first successful STM experiments with clearly resolved organic molecules were reported [135–137] it appeared questionable whether “insulating” molecules can be imaged by STM at all. As stated above, the tunneling current is proportional to the sample LDOS near the Fermi level E_F within the framework of the s -wave theory of STM. Most organic molecules have a large energy gap between the highest occupied (HOMO) and the lowest unoccupied (LUMO) molecular orbital(s). If physisorbed on a metal surface, the molecule-related states are usually far away from the substrate Fermi energy. The HOMO- and LUMO- derived resonances are typically several eV below and above E_F , respectively. Therefore, the

molecule’s contribution to the LDOS near E_F is rather small and at a first glance one might expect organic molecules to be transparent for tunneling electrons at low bias voltage.

These findings are of general importance for the imaging of molecules adsorbed on metal surfaces. Nonresonant tunneling occurs and the contribution of the adsorbate to the current comes from tails of molecular orbital resonances crossing the Fermi level. These tails are usually rather small at the Fermi level, which explains why contributions from the substrate itself cannot be neglected, despite the rather important difference in height.

To interpret STM images of molecules the electronic structure of the adsorbate-substrate system can be calculated, whereby various levels of approximation are used ranging from effective Hückel to first-principles self-consistent methods based mainly on the density functional theory. Again, the tunneling current is frequently associated with the LDOS of the sample at the Fermi energy. In this approach the tip and the surface are treated separately, which neglects any interaction between them and is valid only in the limit of large tip-surface distances (similarly to the Tersoff-Hamann model, where the electrodes are treated separately and the result is derived for small voltages). Secondly, a severe approximation is made to the structure of the tip apex and any tip dependence of the image is lost. This can be accounted for by regarding p and d states as tip orbitals [138] or by describing the tip apex by a cluster of a small number of atoms [139, 140].

Another approach is the proper description of the interaction between sample and tip with a scattering theory formalism. The influence of tip-sample interactions becomes apparent in the imaging of adsorbed alkali metal atoms. Although they are known to substantially increase the LDOS at E_F , they are frequently transparent in STM data [141]. The basic idea of the scattering theory formalism is to consider the tunnel gap as a two-dimensional defect inserted between two semiinfinite periodic systems. The tunnel event is then viewed as a scattering process. An example is the electron scattering quantum chemical (ESQC) approach developed by Sautet and Joachim [142]. The tunnel junction is modeled by the approach of substrate and tip semiinfinite bulk solids. The adsorbate is chemisorbed on the substrate surface,

while the tip apex, attached to the second semiinfinite solid, is modeled by a cluster of 1-15 atoms. Coupling with the tip and substrate electron reservoirs is hence fully taken into account.

Aromatic molecules represent an important group of adsorbates, whose functionality can be exploited for building diverse molecular nanostructures at surfaces. Benzene was the first molecule of this class to be successfully imaged on a surface by high-resolution STM: coadsorbed with CO on Rh(111) [136], benzene molecules, which are bound at threefold substrate hollow sites as determined by LEED [143], appear as three lobes arranged in a triangle in STM topographs. The lobes are located near the middle of C-C bonds, in between underlying Rh substrate atoms as evidenced by ESQC [144]: the molecule appears to have 3-fold symmetry because molecular orbitals are hybridized with the rhodium substrate atoms below. As a consequence the STM image of benzene does not show positions of molecular C atoms but specific C-C bonds.

High-resolution STM studies, combined with calculations of LUMO and HOMO, were performed with more complex aromatic species in the early 90's. Particularly, a comparative study of naphthalene ($C_{10}H_8$) and azulene ($C_{10}H_8$) adsorption on Pt(111) evidences that a simple calculation methodology based on extended Hückel molecular orbital theory adequately predicts details of internal structure [145]. Electron and hole density plots show very good agreement with the actual STM data and enable the reliable identification of molecular species.

A detailed description of several theoretical approaches to the contrast mechanism of adsorbate imaging with the scanning tunneling microscope is given in a recent review by Sautet [146].

2.2 Experimental Set-up

All measurements presented in this thesis have been performed with the variable temperature UHV-STM setup, described and used in previous studies [147].

The *variable temperature* STM [149] is operational in the temperature range 40 K–800 K. It is incorporated into an ultrahigh vacuum (UHV) chamber (base pressure

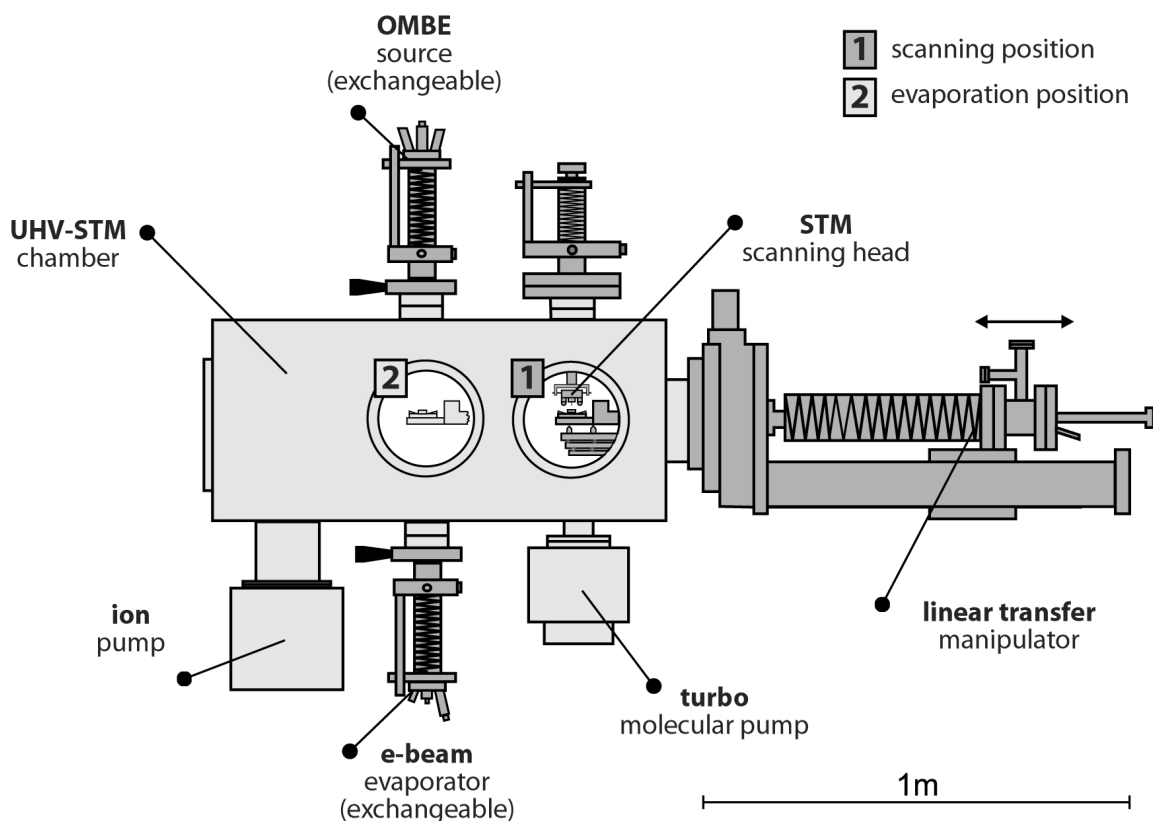


Figure 2.2: Schematic drawing of the UHV-STM system, employed in the experiments. Sample is transferred from the position, where STM measurements are performed, to the position, where organic molecules and metal atoms can be sequentially evaporated, by using a linear transfer manipulator. Both evaporators - organic molecular beam evaporator and e-beam metal evaporator - are mounted behind UHV valves to allow for an exchange of molecular species or metals for evaporation without breaking the vacuum of the main chamber. (Figure is adopted from Ref. [148], where a similar set-up was used).

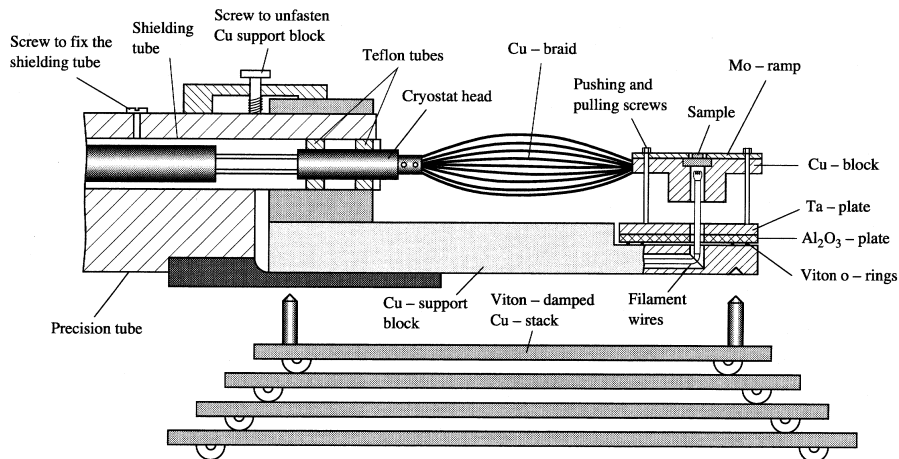


Figure 2.3: Side view of the manipulator and the sample holder. In the STM mode the copper support block is decoupled from the precision tube and rests on the viton-damped Cu-stack ([150]).

$\approx 2 \cdot 10^{-10}$ mbar), which is equipped with standard surface preparation and analysis tools (see Fig. 2.2 for schematic drawing). Several evaporators for metals and organic molecules can be added. The sample is tightly mounted on the sample holder, cooling is realized with a Helium flux cryostat via a Cu-braid and the sample can be heated radiatively or by electron bombardement (cf. Fig. 2.3).

During STM measurements the sample holder is decoupled from the precision tube and rests on the viton-damped Cu-stack (cf. Fig. 2.3); for low frequency vibration damping the whole UHV chamber is suspended by springs from the ceiling. The STM is a home-built “beetle type” STM (cf. Fig. 2.4).

For operation, the STM is simply placed on the sample holder and by applying proper voltage pulses to the outer piezo legs walks down the ramp. Once the STM is in tunneling range, scanning is effectuated through the inner piezo. The sample remains mounted to the manipulator during all operations, which throughout guarantees full temperature control. For a more detailed description, see [150].

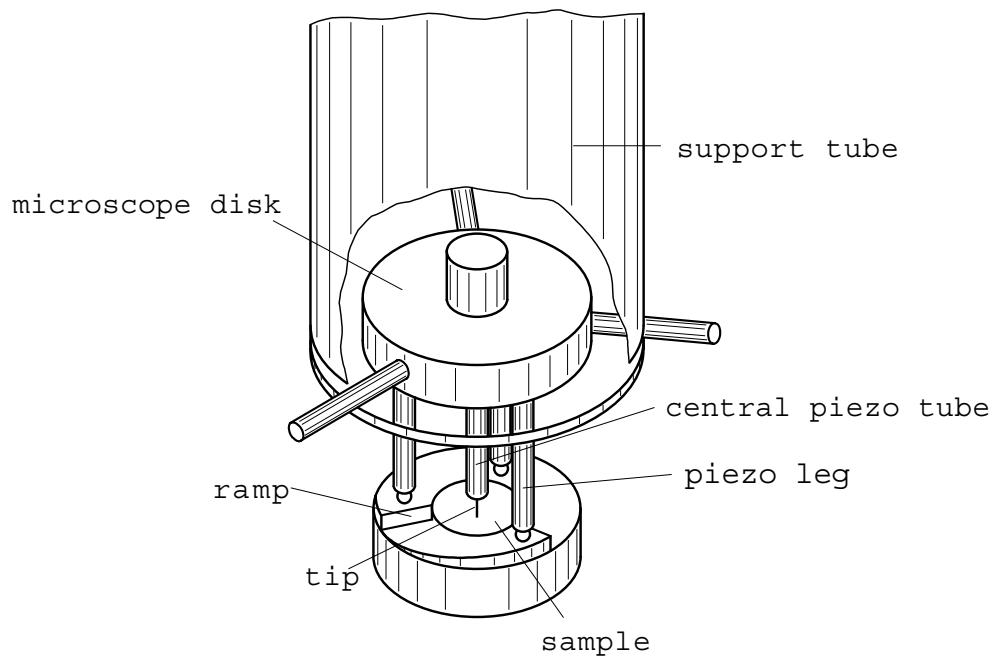


Figure 2.4: Principle of the “beetle-type” STM. The body of the STM, consisting of a microscope disk and three piezo legs, is placed onto a circular ramp. For the coarse approach between the tip and the sample the STM “beetle” - driven by a electrical signal provoking a “stick and slip” movement - walks down the circular ramp on the piezo legs. Once the STM is in the tunneling range scanning is effectuated through the central piezo, which is a single tube scanner. The STM “beetle” is lifted from the sample with the help of a support tube.

2.3 Sample Preparation

Crystal Preparation

All experiments described in the present thesis have been performed on the single crystal fcc Cu(100) surface. The crystal is hat shaped with a circular surface of 7 mm in diameter and a total thickness of 3 mm. It is supplied by MaTeck with an orientational misfit of better than 0.1° and mechanically polished (grain size < 30 nm). The sample was cleaned under UHV conditions by sequential cycles of Ar^+ sputtering at 300 K and subsequent annealing to 800 K. We typically used a $10.0 \mu\text{A}$ ion beam (as detected on the sample) of 500 eV energy and an incidence angle of 45° for sputtering. One sputter cycle typically lasted 20 min. Annealing was performed at a temperature of 800 K and during 1 min at 750 K for the very last cleaning cycle to provide smooth surface with low amount of impurities. The pressure while annealing was always below $3 \cdot 10^{-9}$ mbar.

This procedure resulted in atomically clean and flat surfaces with regions showing terraces of around 1000 Å width. For the prepared surface we observed a coverage of less than ≈ 0.05 % of a monolayer (ML) impurities.

Electron-Beam Heating Evaporation of Metals

Iron atoms were evaporated on a Cu(100) surface *in situ* using an e-beam heating evaporator (OMICRON). Coverage calibration was performed by area estimation using STM in submonolayer regime. One monolayer of Fe corresponds to 1 Fe atom per a_0^2 ($a_0^2 = 2.55$ Å, is the nearest-neighboring spacing of copper atoms of the Cu(100) surface). Depending on the needs of a particular experiment, Fe atoms were deposited on substrates, kept at low (100K), room- or elevated (450K) temperatures.

Organic Molecular Beam Epitaxy

Organic layers of TMA and TMLA have been prepared *in situ* under UHV conditions. Due to the molecules' high stability and moderate vapor pressure, a molecular beam can be generated by thermal evaporation under UHV conditions [151,152]. Thus both TMA and TMLA (purity 99+ percent, Sigma-Aldrich Chemie GmbH) have been

deposited by a conventional Knudsen-cell at background pressures of $\approx 1 \cdot 10^{-9}$ mbar. In Table 2.1 the temperatures of the crucible employed for the two different materials are given (corresponding flux: at the crucible temperatures employed one physical monolayer is formed within about 1 minute).

	TMA	TMLA
T (K)	460 - 463	410 - 412

Table 2.1: Evaporation temperatures.

One molecular monolayer is defined as the surface is fully covered by the flat lying molecule species: for TMA (or TMLA) this accounts to 0.046 molecule per a_0^2 . For very low coverages a lower evaporation temperature was chosen to obtain an evaporation time in the order of one minute.

Due to identical stoichiometry of the species the molecular mass of TMA and TMLA amounts to 210 amu. Using quadrupole mass spectroscopy analysis throughout evaporation tests shows characteristic peaks of evaporated species, which signals the presence of the species under investigation (193 amu for TMA and 148 amu for TMLA, respectively [153]). The main peak at 193 amu for TMA results from single ionized molecules and 148 amu for TMLA - from species dissociated in the mass spectrometer.

Chapter 3

Bonding and Ordering of Mellitic Acids on Cu(100)

A promising class of candidates to form supramolecular aggregates are molecular species comprising functional groups for hydrogen bond formation, which provide the possibility to benefit from the H-bond energetics and directionality to fabricate highly organized assemblies. Such species have been employed at surfaces, and the results demonstrate the successful use of organic molecules, e.g. with moieties for head-to-tail or lateral coupling, and suggest that in general species with functional groups providing geometrical (steric) or electronic complementarity can be employed.

The adsorption and supramolecular self-assembly of trimesic and trimellitic acid on Cu(100) [154] surface is discussed in this Chapter. The molecule trimesic acid (TMA) - 1,3,5-benzenetricarboxylic acid - represents a prototype material for supramolecular self-assemblies [155–158]. TMA is known to assemble in diverse supramolecular structures due to the trigonal exodentate functionality, and the most common motif identified therein is a planar honeycomb network structure formed

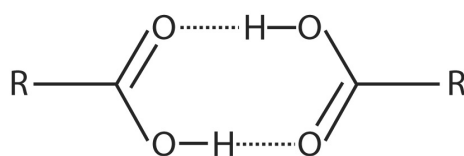


Figure 3.1: Hydrogen-bond mediated dimerization of the self-complementary carboxyl groups

through the dimerization of carboxyl groups, as depicted in Fig. 3.1. In the three-dimensional (3D) α -polymorph of the TMA crystal structure, these networks interpenetrate, i.e., the 14 Å diameter holes of the honeycombs are catenated. Moreover, the tendency of network formation in TMA is frequently employed for the fabrication of clathrates (inclusion complexes) [156–159].

Trimellitic acid (TMLA) - 1,2,4-benzenetricarboxylic acid - for the molecular structure refer to [160] and to Fig. 1.2(b)) - similarly belongs to the mellitic acid series. It is thermally and chemically robust carboxylic acid with exodentate functionality in two dimensions [161]. The reduced symmetry of TMLA, as compared to TMA, accounts for the existence of two 2D-chiral species upon confinement at a surface.

The ordering principles of trimesic and trimellitic acids at surfaces represent an exemplary model system in the understanding of supramolecular self-assembly at surfaces. In order to tackle this issue, we have performed variable temperature STM investigations on the adsorption and supramolecular ordering of TMA and TMLA on a *Cu*(100) substrate. Our results reveal that for the TMA / *Cu*(100) system at low temperatures (< 280 K) flat-lying TMA molecules form islands where the honeycomb motif prevails, similar to that identified in 3D supramolecular structures. This demonstrates that 3D ordering principles from organic crystals can be translated to the 2D scene. For the case of TMLA no particular ordering is detected for hydrogen-bonded arrangements at low-temperature substrate (200 K). It is demonstrated furthermore that due to the chemical activity of the *Cu* surface atoms, the low-temperature arrangements of TMAs irreversibly transform. The stripe-shaped supramolecular structures at higher substrate temperatures (around 300 K) are identified. This is associated with a deprotonation of the TMA molecules leading to carboxylate formation and an upright bonding geometry. By contrast, deprotonation of TMLAs is still hindered at room- and even elevated (450K) temperatures, and ordered structures develop only when the substrate is heated during deposition (450 K). The deprotonation of one of the TMLA's carboxylic group results in a nearly flat adsorption of the molecule (which contrasts with TMA case).

The results demonstrate how the adsorbate-substrate interaction can be exploited

to drive the transformation of supramolecular arrangements at surfaces.

3.1 Supramolecular Assemblies of Trimesic Acid on Cu(100)

The low-temperature phase with the two-dimensional honeycomb motif. The low-temperature phase of TMA was prepared with the temperature of the substrate held in the range 192 - 280 K for different experimental sets. In Fig. 3.2(a) an exemplary STM image (taken at 205K) of self-assembled TMA aggregates is depicted. In this experiment, the deposition took place at 240 K and subsequently the crystal was cooled down to the imaging temperature. In the insets the atomically resolved clean Cu(100) surface revealing the orientation of the high-symmetry [011] direction and a close view of the supramolecular structure are shown, respectively. The triangular appearance of the molecules with a characteristic side length of ~ 8 Å (which agrees with the dimensions of an individual TMA molecule [153]) strongly suggest a flat-lying adsorption geometry, i.e. molecules are oriented with their phenyl rings parallel to the substrate (cf. the molecular geometry of TMA in Fig. 1.2(a)). At low molecular coverages (in our experiments TMA up to 0.1 ML were studied) physically adsorbed π -systems are preferentially oriented parallel to the metal surface, which is associated with π -bonding to the substrate [43, 145, 162, 163]. In the case of TMA the planar adsorption geometry is reflected in the molecules' apparent height of ~ 1.5 Å in the STM images (cf. the STM contour line in Fig. 3.2(c)), which is a typical value for planar aromatic molecules with a π -system oriented parallel to the surface [137, 146, 164].

The data in Fig. 3.2 reveal moreover that TMA islands with smooth borders have formed at the surface decorating the atomic steps. This implies a preferred TMA adsorption at the step edges and an appreciable low-temperature diffusion rate, which allows TMA molecules to transport at the substrate (only for temperatures below 200 K the mobility is suppressed such that only randomly scattered molecules could be observed). Furthermore there must be edge mobility along island perimeters; otherwise the formation of fractal islands derived from a diffusion limited aggregation

scenario would be expected. Within the islands a honeycomb motif with a periodicity of ~ 20 Å prevails. This configuration (cf. the detailed view in the inset of Fig. 3.2(a)) is associated with supramolecular self-assembly through dimerization of carboxyl endgroups, similar to the network structures in 3D TMA crystals. However, hexagonally arranged mesh of TMA molecules is slightly distorted with respect to the honeycomb structure in bulk TMA crystal and two equivalent, but rotated by 90° in respect to the Cu(100) azimuths, meshes can be distinguished (compare the configurations in Fig. 3.2(b) and in the inset therein). The distorted honeycomb structural motif of TMA has TMA-TMA distances through the mesh center of 20.4 Å ($8a_0$) and 22.8 Å ($8.94a_0$) (shown in the corresponding cross-section profiles of Fig. 3.2(c)). The distortion is ascribed to the preferred adsorption of the molecules on a surface with corrugated potential energy. Preliminary results of *ab initio* calculations employing density functional theory with the generalized gradient approximation indicate that the molecules are preferentially bound at the fourfold hollow site of the substrate and bonding at top sites is unlikely (the energy difference is ~ 0.2 eV; three layers of Cu(001) with a (5x5) unit cell were used) [165]. This is a typical finding for adsorption of large organic molecules at metal surfaces and is in agreement with the fact that at temperatures below 160 K the adsorbed TMA molecules do not diffuse at the surface upon adsorption. To fulfill the requirement of the fourfold hollow site adsorption on Cu(100) surface a structural model for the distorted honeycomb motif is proposed in Fig. 3.2(d), which agrees with the STM data very well.

In the crystal structure of bulk alpha-polymorph trimesic acid a 14 Å diameter holes of the honeycomb exist, implying the TMA-TMA distance of 19.7 Å through the mesh center and the OH \cdots O bond length of 2.7 Å. With the present system the TMA-TMA distances through the mesh center are 20.4 Å and 22.8 Å, giving rise the average length of the OH \cdots O bond close to 3.7 Å which exceeds by ~ 1 Å the corresponding distance in the crystalline a-phase of TMA [155]. Similarly increased hydrogen bond lengths have been reported with other systems, where COH \cdots N bonding in supramolecular aggregates with 4-[trans-2-(pyrid-4-yl-vinyl)] benzoic acid at a Ag(111) surface was investigated. They are associated with the occupation of high-symmetry positions at the substrate and moreover possibly reflect H-bond relaxation

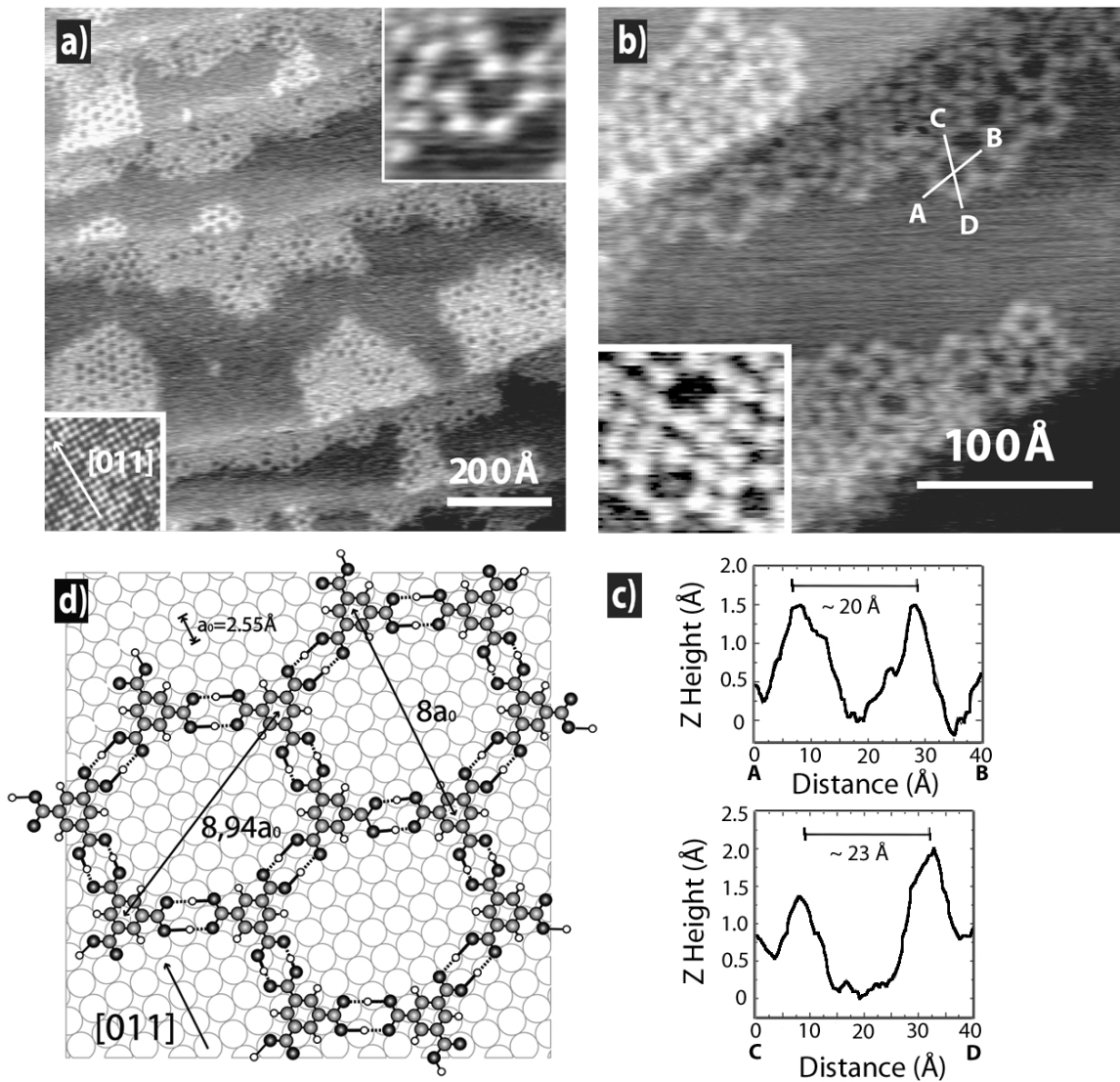


Figure 3.2: Low-temperature phase of TMA. **(a)** STM image of compact TMA islands at Cu(100) decorating atomic steps. ($100 \times 100 \text{ nm}^2$, deposited on 240 K Cu (100), image taken at 205 K, bias voltage $U_b=0.39 \text{ V}$, tunneling current $I_t=1.11 \text{ nA}$). In the islands a honeycomb motif is resolved which is associated with extensively hydrogen-bonded two-dimensional TMA networks. Insets: atomically resolved Cu (100) surface (lower left) and two meshes of the honeycomb structure (upper right). **(b)** STM image of honeycomb elements ($30 \times 30 \text{ nm}^2$, $U_b=0.511 \text{ V}$, $I_t=0.139 \text{ nA}$) with the corresponding height profiles (with lateral and height calibration performed) along the lines marked A-B and C-D are shown in **(c)**. Inset: 90° rotated honeycomb meshes, coexisting with close-packed TMA molecules. **(d)** Structural model for the honeycomb network with individual TMA centered at substrate hollow sites. Oxygen atoms are represented by dark circles, carbon atoms by light grey circles, hydrogen atoms - by white ones. The characteristic dimensions of the structure are indicated.

in the presence of the electron gas at the metal surface. The proposed supramolecular self-assembled configuration can thus be understood from the balance of two main factors: the TMA molecular geometry driving carboxyl group dimerization and the molecular π -orbital interaction with the copper surface, which suggests the most energetically favorable adsorption with the phenyl ring in the hollow site of the substrate. Note that for the network formation it must be assumed that within a single carboxyl group the H atom is free to transfer from one oxygen atom to the other in the adsorbed state, a behavior which is well known for related systems [166]. In the absence of this effect, eight different configurations for flat-lying TMA would exist.

Albeit the data in Fig. 3.2 clearly demonstrate that honeycomb structure prevails in the small islands, typically 20 nm by 20 nm in size, it was not possible to obtain a full layer or at least a large domain, consisting exclusively of this structure. In particular, close-packed TMA arrangements coexist with the honeycomb structures, as shown in inset on Fig. 3.2(b). And pentagonal meshes, comprising of 5 TMA molecules (which points out the absence of azimuthal alignment of individual molecules within these structures) are frequently found. The attempts to resolve superstructure patterns in LEED measurements were not successful. This lack of a long-range order is believed to associate with kinetic limitations and an appreciable substrate corrugation experienced by the adsorbed TMA. Efforts for equilibration to induce long-range order by increasing the substrate temperature destabilized the low-temperature phase and the honeycomb networks were irreversibly transformed and cooling down again does not lead to a restoration of the initial situation. Our STM observations reveal that with increasing temperatures the TMA honeycomb networks transform to a new regular phase at room temperature. Note that improved ordering can be achieved on the less corrugated substrate graphite [167].

Room-temperature phase: stripe structure. The room temperature phase can either be obtained upon annealing the low-temperature phase or directly upon molecular deposition with the substrate held at 300 K. Corresponding STM data are presented in Fig. 3.3. One can clearly distinguish elongated striped islands in four distinct orientations, i.e. along the $[03\bar{1}]$, $[0\bar{1}3]$, $[01\bar{3}]$ and $[013]$ crystallographic directions, respectively (cf. the atomic resolution inset in Fig. 3.3(a) for the high symmetry

directions of the pristine surface). This fact signals more pronounced adsorbate-substrate interaction as compared to the case of the low-temperature phase.

In the areas surrounding the islands, in the STM data at room temperature frequent spikes and dashes appear in single scanlines. Such findings are typical for isolated mobile adsorbates with hopping rates comparable to the x-scanning frequency (in our case typically ~ 4 Hz) [52]. A detailed analysis of the TMA surface diffusion was not performed. The observations demonstrate that at room temperature the surface is actually covered by a 2D crystalline phase (i.e., the islands) coexisting with a lattice gas. Only when TMA condensates in islands the individual molecules are at rest and can be entirely imaged by STM due to the intermolecular lateral attraction.

Upon detailed inspection of the stripe phase, further features become apparent. This is demonstrated by the STM image in Fig. 3.3(b), where a high-resolution image of a [013]-oriented island is presented. First, it can be seen that intermolecular distances (measured as a distance between the maxima of the bright features, which are associated with the individual TMA molecules, within the islands are markedly smaller (6.4 \AA - cf. the height profile on Fig. 3.3(c)) than the corresponding characteristic size of the flat adsorbed TMA identified in the low-temperature adlayer. The closer packing in the stripe phase is rationalized as a result from a bonding transition of adsorbed TMA. It is suggested that a reorientation of TMA from a flat-lying to an upright-standing conformation takes place as a result of carboxylate formation following deprotonation of TMA carboxyl groups due to the chemical activity of the copper substrate. The STM contour line along the islands reveal that the height of the upright species amounts to $1.3 - 1.5 \text{ \AA}$, which does not reflect that expected from molecular geometry. This is rationalized by the fact that the STM topograph reflects the electronic structure of the surface. For example, in the case of 4-[*trans*-2-(pyrid-4-yl-vinyl)] benzoic acid on Cu(111) the upright-standing molecule, 12.3 \AA in molecular geometry, only has a height of around 1.4 \AA in STM [147], which was assigned to a poor electric conductance along the molecular axis. The second interesting feature of the room-temperature phase is that the TMA molecules show exclusively spherical appearance in STM, independent of the bias voltage. Further studies reveal that under certain conditions the stripe phase can be transformed into a new one, in which

TMA molecules have a clear triangular shape, signaling a flat-lying geometry. Thus the spherical- shape TMA observed by STM does not contradict an upright-standing geometry. Carboxylate formation is a typical finding at Cu surfaces and analogous surface chemical bonds evolve upon thermal activation with simpler species containing a carboxyl group (e.g., benzoate/Cu(110) [168–171], acetate/Cu(110) [172], formate/Cu(100) and formate/Cu(110) [173, 174]). Benzoic acid, reported as an exemplary compound with a carboxylate group for copper-carboxylate bond formation (see - [170, 174] and references therein), initially adsorbs in a flat-lying benzoate configuration on Cu(110) and converts to the upright species close to saturation coverages, thus providing a reduced bonding area which allows more molecules to adsorb [174]. By contrast, studies of benzoate/Cu(111) system [170] evidence upright adsorption at very low coverages. With the present carboxylate the molecule’s anchoring at the substrate reflects the formation of a distinct chemisorption bond between substrate Cu atoms and the oxygen atoms of the carboxylate group. The corresponding gain in chemisorption energy with the upright geometry is expected to compensate for the loss of the p-bonding upon reorientation of the flat-lying species. For comparison, theoretical studies indicate a bonding energy of ~ 2 eV for formate (HCOO) at Cu(100) [175, 176].

The STM data in Fig. 3.3 reveal that each of the islands consists exclusively of an odd number of rows oriented in the stripe direction (we observed islands consisting of three, five, seven or even nine TMA rows running parallel), where the molecules are topographically inequivalent (cf. the STM contour line in Fig. 3.3(c)). We concentrate on the discussion of stripes with 5 row width. There the very central row is always imaged brighter. Furthermore the topographic height of neighboring rows alternates, i.e., the 2nd and 4th row are imaged slightly darker. Finally, within any row, the individual TMA do not perfectly follow a line in the stripe direction. Rather, they are arranged in a zigzag mode, whereby every second molecule in the 2nd and 4th row is imaged with a slightly reduced height. The different imaging heights of adjacent molecules (either within a row or in adjacent rows) are presumably related to different bonding configurations of TMA molecules at the substrate - possibly through either one or two deprotonated carboxyl groups available for carboxylate formation in

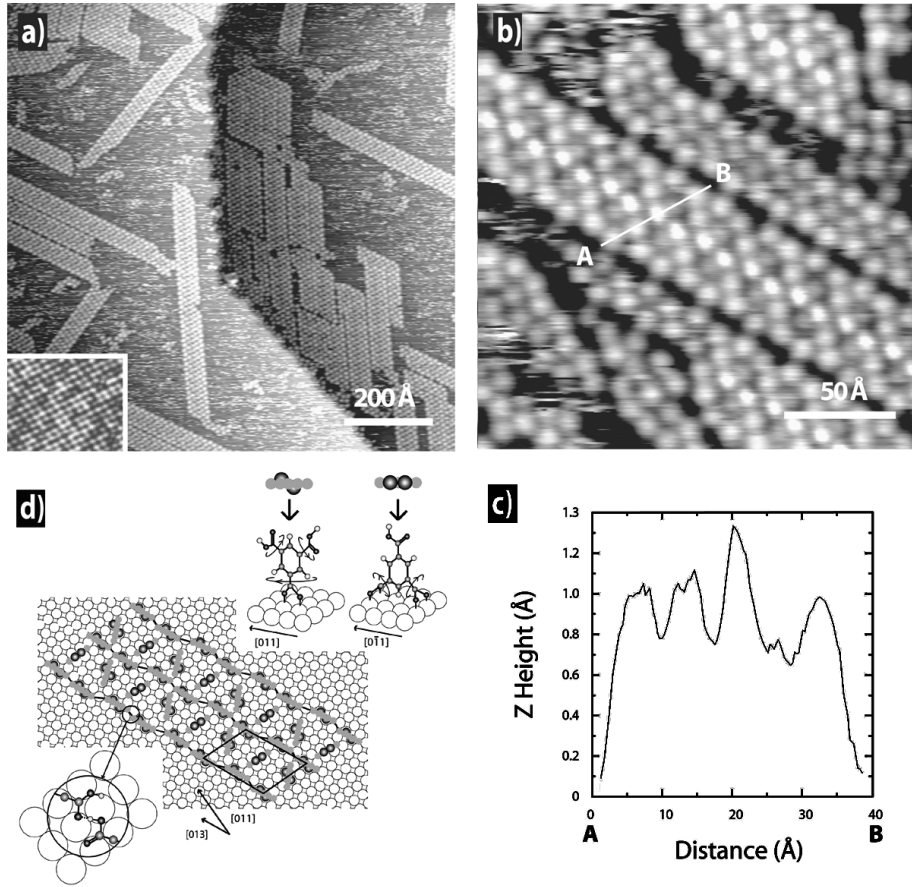


Figure 3.3: TMA/Cu(100) stripe phase evolving at room temperature. **(a)** STM image taken shortly after deposition at room temperature ($100 \times 100 \text{ nm}^2$, $U_b=0.752 \text{ V}$, $I_t=0.54 \text{ nA}$). Four distinct orientations of the islands can be seen (Inset : atomically resolved pristine Cu(100) surface). **(b)** Close view of a five-TMA-wide island ($20 \times 20 \text{ nm}^2$, $U_b=1.54 \text{ V}$, $I_t=0.2 \text{ nA}$) and **(c)** height profile along the line marked A-B revealing the different imaging contrast for adjacent TMA molecules and their intermolecular distances (Z-heights are given in a normalized scale and do not represent the absolute values) **(d)** Tentative structural model for the striped supramolecular arrangement consisting of five TMA rows running parallel - the stripe orientation and the Cu(100) azimuth are indicated. Within a stripe-shaped island molecules are represented schematically with an emphasis on the adsorption sites. In the upper right two possible anchoring geometries of TMA derived carboxylates are shown. The conformational rotation of carboxyl groups in respect to the C-C bond is assumed and shown by arrows. Oxygen atoms are shown in black, carbon atoms in light grey, hydrogen atoms - in white. In the lower left a possible H-bonding geometry along the stripe orientation is indicated. The unit cell of the structure is marked.

two different upright molecular orientations. Both calculations [175, 176] and experimental evidence [168–170, 172, 173] indicate that upright carboxylates have a strong preference for the short-bridge site occupation, where carbon atom lies midway between two next-neighbor copper surface atoms, with whom the oxygen atom form chemical bonds.

In the case of trimesic acid no experimental data or theoretical investigations concerning the carboxylate adsorption sites are available. However, our tentative adsorption scenario based on geometrical reasoning strongly favors a structural model of bidentate copper-carboxylate bonding where TMA can either be adsorbed through one carboxylate located at a short bridge site, or through two carboxylates, both centered at the short-bridge site and thus rotated in respect to the phenyl ring plane by 90° , with the molecule's center at a hollow site (a similar geometry was reported for phthalic anhydride adsorption on $\text{Cu}(110)$ [177]). These configurations are shown in Fig. 3.3(d). Preliminary investigations indicate that once the TMA molecule is bound in an upright-standing configuration, the further deprotonation of the remaining carboxylic groups is delayed or requires higher thermal energies, since they are no longer in direct contact with the copper substrate. A tentative model for a stripe phase island consisting of five molecular rows is reproduced in Fig. 3.3(d). This arrangement is believed to be stabilized by H-bond formation between the intact carboxyl groups within the first, third and fifth row in the direction of the island orientation (a similar weaving of molecules within the rows via hydrogen bonding is proposed for tartaric acid molecules adsorbed on $\text{Cu}(110)$ [64]). TMA bound at short-bridge sites account for the zigzag arrangement in the odd-numbered rows. The second and the fourth row, where STM revealed periodic changes in the imaging height, are believed to comprise two bonding configurations. In both cases, hydrogen bonding to the odd-numbered rows can be achieved when a ladder-type network is assumed. Hence, the TMA ordering in the stripe phase is presumably related to the formation of a supramolecular ladder-type structure. The edges of the ladders only consist of short bridge site adsorbed TMAs, while every second interlink within the ladder is a hollow-site adsorbed molecular species. By analogy, the one-dimensional islands of three TMA rows constitute single ladders, those of five TMA rows double ladders,

and so forth. In our model, the hollow-site adsorbed TMA molecules are constrained in space by their four-point attachment to the surface via two carboxylate groups, which imparts the rigid and well-defined adsorption geometry. For short bridge site adsorbed TMA, we make use of the fact that carboxylates can freely rotate around the C-C bond (an analogy can be drawn with thiophene carboxylic acid adsorption on Cu(110) [178], where the rotation of the molecular plane is attributed to the intermolecular interaction) and thus the molecular plane (defined by the aromatic ring) can be rotated to optimize the hydrogen-bonding configuration. The different contrast in the STM images for the neighboring rows can be deduced directly from the structural model, where short bridge site adsorbed TMAs give brighter contrast than hollow site adsorbed ones.

3.2 Trimellitic Acid on Cu(100)

The deposition of TMLA molecules on a low temperature substrate (100-200 K) does not result in any ordered structures. Presumably hydrogen-bonding dominates the resulting assemblies (a typical STM topograph is presented in Figure 3.4), however no particular ordering is detected. The analysis with x-ray photoemission spectroscopy (XPS, [179]) evidences that the molecular species are fully protonated, nevertheless no extended ordered H-bonding mediated structures are developing, which are presumably obstructed by reduced symmetry of the molecule as compared to the case of TMA. The mobility of molecular species at low temperature is high enough for the aggregation of TMLA, which is associated with H-bonding. Presumably supramolecular ordering can occur on a less corrugated/reactive substrate. In the inset of Figure 3.4 one can distinguish individually resolved randomly oriented TMLAs as four-lobe protrusions.

With appreciable TMLA concentrations (coverage exceeding 0.6 ML), deposited on the Cu(100) substrate held at elevated temperature (400 K), well-defined molecular layers are developing. Figure 3.5(a) shows a typical STM topograph of $1.05\ \mu\text{m} \times 1.4\ \mu\text{m}$ surface region. Remarkably wide surface terraces have formed, effectively alternating with bunches of narrow ones. Due to the scanner spacial limitations, the

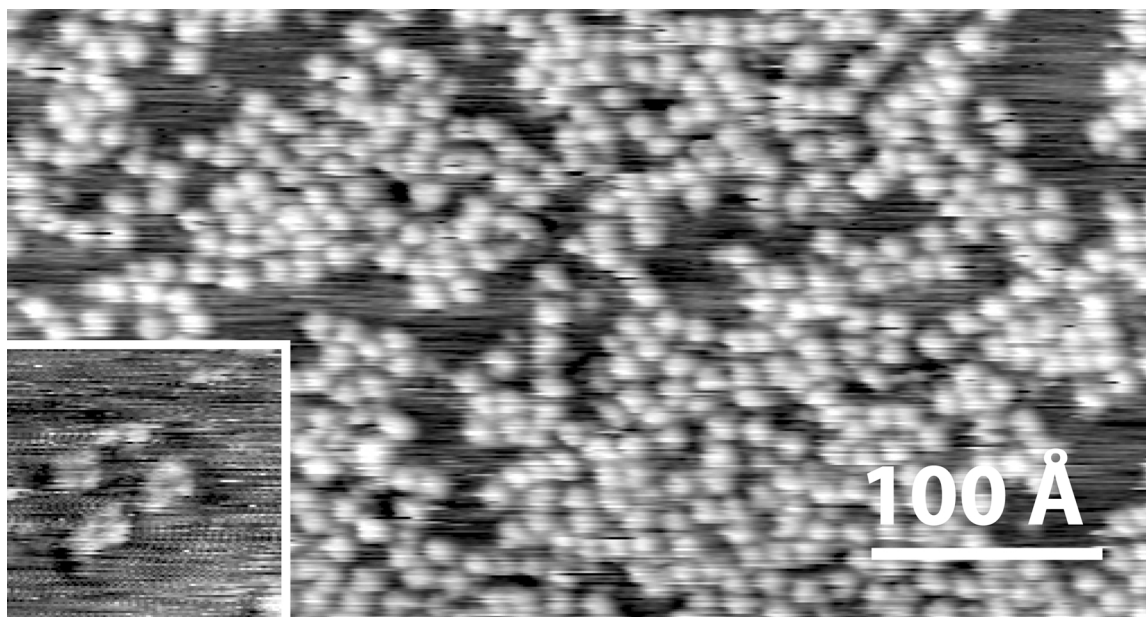


Figure 3.4: Disordered arrangements of TMLAs upon deposition at 100 K substrate. Imaging at 170 K. Inset - sub-molecular resolution of TMLA molecules with four-lobe appearance of individual species.

ultimate length of individual terraces cannot be identified unambiguously, however, within accessible region of max $2.37 \mu\text{m}^2$ ($1.54 \mu\text{m} \times 1.54 \mu\text{m}$) most of the 'wide' terraces run continuously. Continuous terraces can reach 290 nm in width, and the most frequently encountered width for this type (estimated from the analysis of several large-scale topographs) falls in the range of 100-200 nm, whereas within the bunches the width of narrow terraces amounts 10 nm and less. The step-terrace reconstruction of the surface covered with the organic layer is thus clearly distinct from that of the pristine surface, where no step-bunching is encountered and terraces are usually smaller and more regularly ordered.

Massive copper surface mass transport, accompanying the domain formation resulting from considerable substrate-adsorbate interaction, is expected to be responsible for the TMLA-induced terrace width distribution in the final arrangements. Previous reports evidence strong noble metal surface modification upon adsorption of organic species [48,180,181], resulting in step edge faceting and bunching [182,183]. An analysis of the STM data with submonolayer coverages of TMLA (coverages below 0.5 ML) shows substantial modifications of the step-edge shape in the terraces,

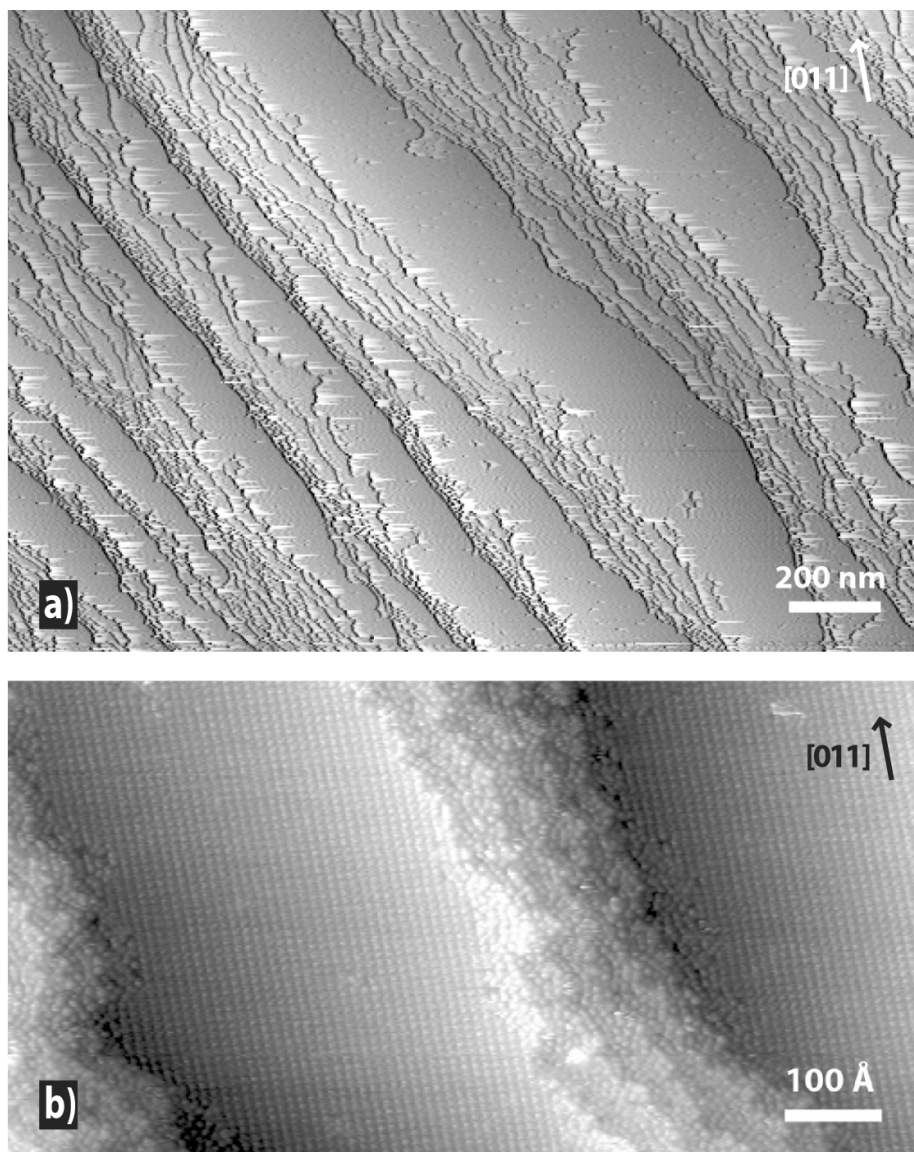


Figure 3.5: Extended TMLA domains on Cu(100) surface. **(a)** Large scale view on the surface, reshaped by the presence of the TMLA organic adlayer. Terraces with very large widths result from the deposition of TMLA molecules on the substrate held at 400K. Cu[011] azimuth is shown. **(b)** Molecular structure of the adlayer - well-ordered TMLA domains, oriented along the Cu[011] azimuth can be seen in the large terraces. Individual TMLA molecules within the domain are imaged as oval dots. On the bunches of narrow terraces no regular order of TMLA exists.

where ordered domains start to develop. The smooth shape of the terrace termination and the preferential width of the terraces, where organic island are present, indicate step-flow growth and prove the presence of strong TMLA-Cu interactions reshaping underlying surface.

The temperature of the substrate during deposition is a crucial parameter for the formation of these ordered domains. While room-temperature deposition of TMLA at lower coverages (< 0.5 ML) never leads to the formation of ordered structures (subsequent annealing also does not promote the domain formation) - deposition in the range of 350 K - 450 K results in the observed morphology with a good reproducibility. A detailed experimental (XPS, NEXAFS) and theoretical (using density functional theory) analysis of this phase is currently performed [179] and suggests that the domain consists of molecules with their aromatic ring slightly tilted out of the surface plane and merely one carboxylic acid group per molecule in the form of a carboxylate.

In view of the chemical reactivity of the substrate and the elevated temperature employed in the preparation, it is suggested that one of the molecules' carboxylic group is deprotonated upon deposition, analogous to findings for other carboxylic acids on Cu surfaces under comparable conditions and the case of TMA, described in the previous Sections.

In the present case at the elevated substrate temperatures the deprotonation of individual carboxyle groups in low-coverage TMLA is presumably hindered (which is reflected in the absence of the ordered domain structure formation upon simple annealing), and for the initiation of this process additional energy or specific inter-molecular interactions are needed. The latter idea is supported by the observation at high molecular coverages (at 0.9 ML or upon multilayer deposition at low substrate temperatures, followed by annealing at 450K for at least 30 min) the domain structure locally develops [179]. In the pure organic layer thus a two-dimensional arrangement of reactive carboxylates (with one out of three functional groups deprotonated) is needed for the ordered structure development.

We associate the striking difference in molecular monolayer behavior at different temperatures with deprotonation of carboxylic groups of TMLA species, followed by

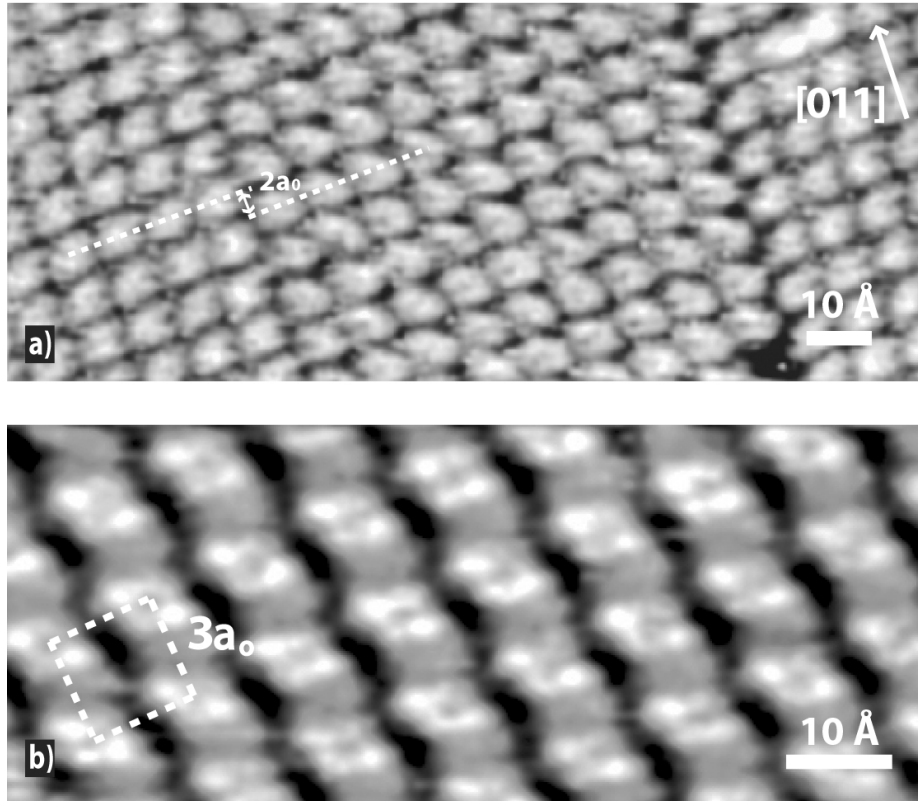


Figure 3.6: Molecular arrangement in ordered TMLA domains. **(a)** The rare case of boundaries between two homochiral domains. The boundary, coinciding with the Cu[011] azimuth, represents the mirror symmetry axis. TMLAs in neighboring domains are shifted by $2a_0$ in the direction of the marked copper azimuth. ($a_0=2.55\text{\AA}$ is the Cu(100) nearest-neighbor distance). **(b)** Submolecular resolution of individual TMLAs, comprised in the domain. Molecules are resolved as four-lobe features by STM. The (3×3) superstructure unit cell is indicated by a dashed-line square with a side length of 7.6\AA (corresponding to $3a_0$).

the drastic increase in the substrate-adsorbate interaction and initiation of the surface mass transport, which results in a non-equilibrium terrace evolution.

A further zoom into the structure of the organic layer on the 'wide' terraces is shown in Figure 3.5(b). Well-ordered two-dimensional domains with a superstructure oriented along the Cu(100) high-symmetry directions are developing on all 'wide' terraces, separating them topologically from those in the bunches, where an ordered molecular structures are never observed (cf. Figure 3.5(b)). Ordered domains extend over the entire terraces and are (3 x 3) commensurate with the underlying Cu substrate.

Due to the nearly flat-lying bonding of TMLAs at the Cu surface (geometry supported by NEXAFS investigation of the organic adlayer [179]), the surface acts as a symmetry breaking agent for the molecules, which are prochiral in three dimensions (cf. molecular geometry of TMLA in Figure 1.2(b)). The effect of chirality induction by the surface and the formation of enantiomorphous structures from racemic mixtures upon their two-dimensional confinement [184,185] (or even imparting pseudochirality to originally achiral species [186–188]) is a well documented phenomenon. In the case of TMLA, the chiral signature upon flat adsorption drives the formation of extended homochiral domains. Effectively that means that the 2D chirality of TMLA, arising upon two-dimensional confinement, drives chiral recognition and mesoscopic enantiomeric separation, reflected in the vast micrometer-sized homochiral domains formation. Accordingly, the translation of the chiral information from single molecules to the micrometer scale domains is achieved.

Moreover, domain boundaries in the organic overlayer structure are extremely rare and can be identified only at relatively small molecular coverages, when two distinct mirror symmetric domain phases are simultaneously developing on the same terrace (Figure 3.6(a)). Within the domain individual TMLAs are imaged as four-lobe protrusions, as shown in Figure 3.6(b).

Chapter 4

Modular Assembly of Coordination Architectures at Surfaces: Novel Design Principles for Low-Dimensional Supramolecular Systems

The principles of coordination chemistry, introduced by Alfred Werner towards the end of the 19th century, are recognized as being a key element in molecular recognition and an excellent strategy for the fabrication of three-dimensional supramolecular arrangements. Self-assembly in coordination chemistry offers a valuable means to design in a rational and highly selective way architectures whose structural complexity approaches that common in biology [86, 189]. Supramolecular self-assembly has been applied in deliberate positioning of functional molecular species at suitable substrates [47, 52, 53, 74], aiming to establish design routes for novel low-dimensional molecular materials and devices [15, 17, 21, 28, 66]. However, to date, surface supramolecular self-assembly relies mainly on hydrogen bonding or electrostatic intermolecular coupling. These interactions bear the disadvantage of low thermal and mechanical stability. Thus there is a strong current demand to introduce a new concept for the construction of more rigid surface self-assembled supramolecular

architectures [121, 122]. The implementation of coordination chemistry principles to control surface supramolecular self-assembly provides a new concept for deliberate design of durable and versatile functional nanoarchitectures at surfaces.

Chapter 4 presents the conceptual approach of implementing coordination chemistry to metal surfaces aiming at the rational design of functional supramolecular architectures. In order to gain direct insight into the nature of coordination compounds at surfaces, STM was used to analyze the mechanism of metal complexation with organic ligands and to develop recipes for deliberate construction of metal-organic architectures. Since both molecular ligands and metal centers are provided by vacuum deposition of organic molecules/metals from molecular beam evaporators onto an atomically clean single crystal Cu(100) surface (see Section 2.3, Chapter 2 for details of experimental procedures), we gain precise control of both absolute and relative concentrations of the respective constituents.

The general mechanism of coordination at surfaces is discussed in details in Section 4.1. The energetics of the particular metal-ligand interactions under investigation are in a range where reaction rates actually permit direct elucidation by imaging methods of evolution and dynamics of such interactions on surfaces at ambient temperature. Using STM direct insight into the principles of complexation of organic molecules and transition metal centers can be gained. Single complexation reaction events, involving TMA ligands and Cu atoms, were monitored and quantified to understand the general coordination mechanism.

The versatility of metal-organic supramolecular engineering at metal surfaces is demonstrated in the following Sections.

In Section 4.2 direct observations of chiral mononuclear metal-organic complexes of TMA and Fe are presented. Using metal-organic coordination on surface the generation of two-dimensional chirality in supramolecular assembly of achiral components is exemplified.

Based on this the hierarchical assembly of homochiral supramolecular motifs on a Cu(100) surface is described in Section 4.3. The chiral functionalization of the substrate by homochiral supramolecular motifs forming nanoporous networks built from the same components (TMA and Fe adatoms) is achieved and characterized by

STM.

Section 4.4 deals with synthesis of hybrid molecular nanostructures with potential magnetic properties. 'Print boards' of magnetic Fe atoms, incorporated in a matrix of organic TMLA ligands are discussed.

Finally, in Section 4.5 the application of the concept of surface metal-organic coordination for the modular assembly of two-dimensional metal-organic coordination networks in the system TMLA/Fe on Cu(100) is demonstrated.

4.1 Coordination Reactions Followed in Real-Time

For the present investigation conducted at an atomically clean surface we took advantage from ligand systems based on carboxylic acids and transition metals whose characteristics are well understood [190]. Specifically, we address metal-ligand bonding of trimesic acid (TMA) and Cu atoms. Its complexation was observed on Cu(100) in ultrahigh vacuum at temperatures in the range 250 - 300 K following deposition at room temperature. Under these conditions the carboxylic groups of TMA are completely deprotonized such that three reactive COO^- ligands per TMA exist [154]. The deprotonation in this case is presumably related to the availability of Cu adatoms at the surface, which are known to exist on Cu(100) at the employed temperature range. The reason behind the presence of Cu adatoms is their continuous evaporation from atomic step edges, which accounts for the presence of a two-dimensional lattice gas at the surface. This process can be understood in analogy to the coexistence of gas and condensed phases in bulk systems described by the vapor pressure of a substance. Due to their high surface mobility at room temperature individual Cu adatoms cannot be resolved in STM images.

At appreciable coverages individual molecules appear as equilateral triangles in STM images (cf. Figure 4.1(a)), which reflects a flat-lying geometry where the molecule is bound with its phenyl ring parallel to the substrate. As shown earlier (Chapter 3.1, Section 3.1), upon deposition on low-temperature substrate TMA molecules undergo the transformation of adsorption orientation. That is, adsorbed

in a flat conformation at low temperatures (100 - 200K), TMAs experience partial deprotonation and change their adsorption geometry to the up-right standing when the substrate is brought to room temperature. However, with time evolution all three carboxylic groups deprotonate, which results in the molecules reorientation once again: this time stronger interaction of flat-adsorbed phenyl ring dominates over the bonding of carboxylates to the substrate atoms, resulting in TMAs reorientation from up-right standing to flat-lying conformation.

The symmetry and characteristic side length of approximately 8 Å agrees well with the shape and dimensions of TMA [154]. Four distinct orientations with respect to the substrate lattice were found with one of the triangle's corners always pointing along a high symmetry direction, $[011]$ or $[0\bar{1}1]$, of the Cu(100) surface. This situation is understood as a consequence of the occupation of high-symmetry hollow sites at the substrate atomic lattice. The data reveal, moreover, that the molecules tend to be arranged in a complementary manner, that is, neighboring TMA molecules are oriented antiparallel, and, as such, the close packing at the surface can be explained as a consequence of the space-filling principle. However, this rule is not generally obeyed and arrangements occur where four TMA form a cloverleaf structure with a bright protrusion at the center. The formation of the cloverleaf structure is directly related to the density of the Cu adatom lattice gas. The decisive role of atom evaporation from steps could be proven in the present case by the following experiments. In the first case, step mobility was limited by step decoration with carbon monoxide which significantly delayed compound formation. In the second case, compound formation could be triggered by co-deposition of Cu or by raising the temperature. Thus cloverleaf configuration is associated with a central Cu adatom which is coordinated by the carboxylate ligands from the four surrounding molecules and is hence designated $[\text{Cu}(\text{TMA})_4]^n$.

A close inspection of the STM image in Figure 4.1(a) reveals that the TMA carboxylate ligands do not point straight towards the central protrusion in the compound. This demonstrates that the oxygen atoms in the respective COO^- moieties are not equivalent, indicating an unidentate coordination of the Cu atom as illustrated by the model in Figure 4.1(b). If it is assumed that TMA molecule is in an unrelaxed

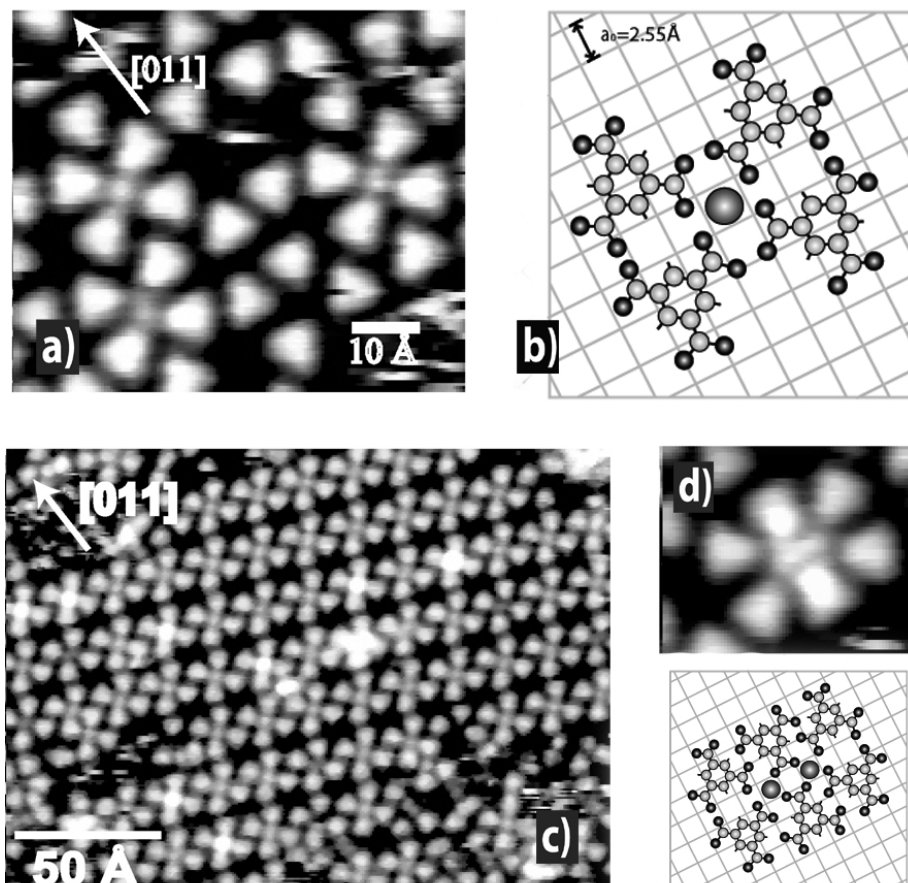


Figure 4.1: (a) STM topograph of trimesic acid adsorbed on a Cu(100) surface at 300 K. The triangular shape reflects a flat-lying adsorption geometry. protrusion represent $[\text{Cu}(\text{TMA})_4]^{n-}$ coordination compounds. (b) Model for the $[\text{Cu}(\text{TMA})_4]^{n-}$ configuration with a central Cu atom coordinated by four carboxylate ligands, where carbon atoms are in light gray, oxygen atoms in black, and Cu adatoms in dark grey; phenyl ring hydrogens are omitted for clarity; the Cu substrate is depicted by the light-grey lattice, where $a_0 = 2.55 \text{ \AA}$. In agreement with the tunneling data the TMA triangles do not point straight to the central site, which indicates a unidentate coordination of the Cu adatom. (c) Regular array of $[\text{Cu}(\text{TMA})_4]^{n-}$ complexes. (d) STM image and model of the $[\text{Cu}_2(\text{TMA})_6]^{n-}$ coordination compound with four unidentate and two *syn, syn* coordination bonds.

geometry, the Cu \cdots O distance is estimated to be 3 Å, which is substantially larger than the characteristic Cu \cdots O distance of ~ 2 Å encountered in three-dimensional copper carboxylates [190]. This Cu \cdots O distance relaxation is attributed to the role of substrate atomic lattice, which energetically favors high-symmetry adsorption sites. Moreover, the nature of the coordination bond itself is expected to be modified in the presence of the electrons from the Cu conduction band. Similar effects were encountered in hydrogen-bonded assemblies [52, 57]. Finally the STM topograph shown in Figure 4.1(c) demonstrates that a regular array of $[\text{Cu}(\text{TMA})_4]^{n-}$ cloverleaves can be obtained.

The square shape of the $[\text{Cu}(\text{TMA})_4]^{n-}$ configuration with its fourfold coordination is characteristic of Cu^{II} complexes [191, 192]. Thus the cloverleaf arrangement *per se* should be considered formally as $[\text{Cu}^{II}(\text{TMA})_4]^{10-}$ ion. However, it is important to note that the charge on both the Cu adatoms and the adsorbed TMA molecules is strongly affected by the presence of the electrons of the metal surface, which effectively screen any charged adsorbate. A deprotonated TMA molecule at the surface should thus not be considered as $(\text{TMAad})^{3-}$, but rather as neutral TMA/Cu(100) complex. As an important consequence the oxidation state of the central Cu atoms in the $[\text{Cu}(\text{TMA})_4]^{n-}$ configuration cannot be determined unambiguously. This contrasts the situation encountered with isolated compounds in three dimensions, where the charge is usually balanced by counterions.

Extended one-dimensional or two-dimensional networks, where more than one carboxylate ligand per TMA participates in coordination bond formation, were not formed. This is again associated with the influence of the substrate atomic lattice, which pins the positioning and orientation of the reactive species at the surface. However, a second compound could be identified close to saturation of the TMA monolayer, where two Cu atoms are bound by six TMA molecules. An analysis of corresponding STM data (cf. Figure 4.1(d)) reveals that with this $[\text{Cu}_2(\text{TMA})_6]^{n-}$ configuration four unidentate and two *syn, syn* coordination bonds are present.

The mechanism for the formation of the $[\text{Cu}(\text{TMA})_4]^{n-}$ compounds could be directly followed by STM measurements at room temperature (real-time STM movies showing the formation and decay of the coordination compounds in real space are

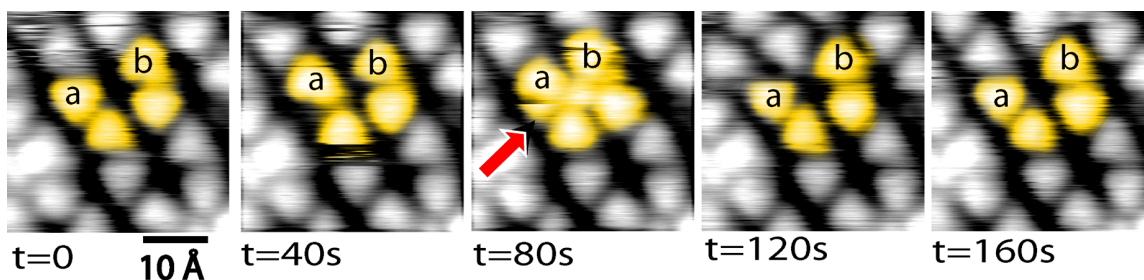


Figure 4.2: Molecular rotors working as dynamical atom trap: Sequence of STM images revealing the molecular mobility during the association and dissociation of a $[\text{Cu}(\text{TMA})_4]^{n-}$ cloverleaf over a 160-second time interval. After rotational motions and displacements of TMA molecules ($t = 40$ s), a Cu adatom is captured and the coordination compound is formed ($t = 80$ s). A TMA molecule which rotated while the image was recorded is marked by red arrow. The coordination bond is subsequently disrupted and the Cu atom disappears again ($t = 120$ s).

available at [http://www.mpi-stuttgart.mpg.de/kern/Res act/supmat 2.html](http://www.mpi-stuttgart.mpg.de/kern/Res%20act/supmat%202.html)). The formation of single chemical bonds has been shown before, however in these studies the bonding was typically induced by manipulating the reactants with the tip of a scanning tunneling microscope at very low temperatures [193,194]. In striking contrast, with the present observations the reaction proceeds under equilibrium conditions. As a consequence the natural path of a multicomponent chemical reaction could be characterized: The thermal rotations of single TMA molecules can be monitored as surface diffusion is restricted by space limitations. This is illustrated by the sequence of images in Figure 4.2, which have been taken over a time interval of 160 s. In the initial frame, the TMA molecules marked **a** and **b** change orientation and position, revealing rotation and hopping of single molecules. The characteristic spikes along the scanning direction are caused by TMA motions occurring while the data were recorded; for example, in the image taken at 80 s molecule **a** switched its orientation, from pointing upwards to pointing downwards (marked by the arrow). Both **a** and **b** are aligned antiparallel with respect to their neighbors at $t=0$ so as to achieve close packing. Neither of them was in a correct position or orientation for the cloverleaf arrangement. In the second (40 s) and third frame (80 s) **a** and **b** switched orientations, respectively, and the cloverleaf configuration with a central protrusion evolved. This effect is understood to be a result of the capturing of a copper atom diffusing on

the surface, which forms coordinative bonds with the carboxylate ligands of the TMA molecules, i.e., an association reaction leading to a $[\text{Cu}(\text{TMA})_4]^{n-}$ complex took place. The Cu atom can exclusively be resolved when it is held by four carboxylate ligands, otherwise its high surface mobility makes STM imaging impossible. The subsequent frame ($t = 120$ s) reveals that the dissociation reaction readily takes place under the same conditions, indicating that thermal motions or collisions with other molecules suffice to disrupt the metal-ligand bond. These observations reveal that molecular rotors (namely, the spinning TMA molecules) with functional endgroups can operate as a dynamical trap for diffusing Cu adatoms. The compound formation is exclusively feasible when four TMAs switch to the adequate mutual orientation and snatch a Cu atom passing by at the crucial moment. In marked contrast to $[\text{Cu}(\text{TMA})_4]^{n-}$, the $[\text{Cu}_2(\text{TMA})_6]^{n-}$ species was found to be stable at the employed conditions.

Quantitative information on the lifetime and formation of the compounds was obtained from the measurements made at low concentrations, where both Cu adatoms and individual TMA molecules are highly mobile at the surface. Accordingly, no isolated species can be observed. However, as demonstrated by the STM image in Figure 4.3(a), single or small groups of compounds can be readily resolved. That is, the $[\text{Cu}(\text{TMA})_4]^{n-}$ configuration is stationary and can be imaged until it eventually dissociates. The lifetime of the cloverleaf arrangements depends strongly on the local environment. For instance, with two compounds neighboring each other (ellipse in Figure 4.3(a)) the average lifetime is typically more than three times longer than that of an isolated species (circle in Figure 4.3(a)). This observation suggests two species have different reactivity, that is, two neighboring species are more stable than isolated ones. Since both measurements were made simultaneously at the same temperature this is associated with steric effects. As indicated in Figure 4.3(a) (TMA marked by arrows) the movement of adjacent molecules in neighboring complexes is impeded so that they experience higher energy barriers for rotation or migration. This hindering effect thus indirectly reduces the probability of dissociation. Similarly increased lifetimes were observed for compounds at step edges, where the steps act as the hindrance. In the extreme case a $[\text{Cu}(\text{TMA})_4]^{n-}$ compound in a regular array, as shown in Figure 4.1(c), has never been observed to dissociate during our measurements, that

is, over 5 h. Lifetimes of the $[\text{Cu}(\text{TMA})_4]^{n-}$ compounds in different environments are compiled in Table 4.1.

	Isolated on terrace	At step-edge	Two neighboring $[\text{Cu}(\text{TMA})]^{n-}$	Saturated layer
lifetime [s]	34 ± 5	87 ± 5	120 ± 5	> 18000

Table 4.1: Average lifetime of $[\text{Cu}(\text{TMA})_4]^{n-}$ complexes in different local chemical environments at 300 K.

The average lifetime of an isolated cloverleaf was determined from an analysis of STM sequences with 100 frames recorded at room temperature with high scanning velocities (9 second per frame) to be 34 ± 5 s. The inverse of this value corresponds to the mean dissociation rate. In a similar way dissociation rates at reduced temperatures have been determined; the entire result is plotted in the Arrhenius representation in Figure 4.3(b). The data points fall on a straight line whose slope corresponds to the energy barrier for dissociation of the coordination compound (E_d). The linear fit of the data yields $E_d = 0.31 \pm 0.08$ eV. With the present system, the determined energy is a convolution from the contributions associated with coordination bond formation and the repositioning of the involved elements (note that value of the present energy barrier is smaller than the binding energy of related coordination compounds in the gas phase. The higher stability of the $[\text{Cu}_2(\text{TMA})_6]^{n-}$ configuration is understood as a consequence from the increased number of coordination bonds involved and possibly an increased barrier for molecular rotations in this more densely packed arrangement (steric hinderance).

Our results show that single-molecule investigations can provide comprehensive insight into the evolution of coordination compounds, where several reacting species are involved. In view of the rich potential and wide application of metal-ligand interactions, it is suggested that such insight will be valuable in the future search for nanoscale elements on templates. More generally speaking, the observations reveal that the natural path of a multicomponent chemical reaction can be directly characterized and the corresponding energetics can be quantified.

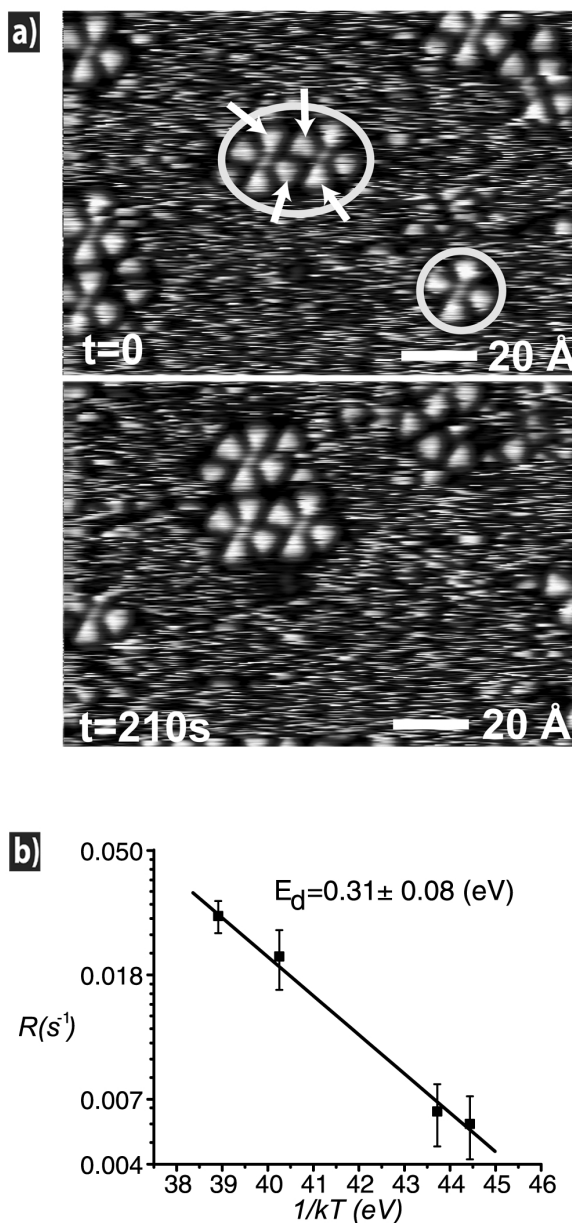


Figure 4.3: (a) Observation of both isolated and small aggregates of $[\text{Cu}(\text{TMA})_4]^{n-}$ complexes for low coverages at room temperature. Freely transporting and spinning TMA molecules coexist on the surface with copper adatoms, which were not imaged by STM. The characteristic spikes along the scanning direction were caused by those moving TMA molecules, while the dark shadows surrounding the stationary $[\text{Cu}(\text{TMA})_4]^{n-}$ compounds are areas where free molecules are not present. The lifetime of the isolated compounds (marked by a circle) was determined by sequential imaging of the same area. Aggregates of several compounds such as that marked by the ellipse have increased lifetime because of the hindered motion of neighboring molecules (marked by arrows). (b) Arrhenius representation of the dissociation rate (R) for isolated $[\text{Cu}(\text{TMA})_4]^{n-}$ compounds derived from analysis of STM data for low coverages at temperatures in the range 260–300 K. The corresponding energy barrier is determined to be $E_d = 0.31 \pm 0.08$ eV.

4.2 Direct Insight Into Mononuclear Chiral Compounds

As an example of using the surface metal-organic coordination for the investigation of fundamental phenomena in organic chemistry at surfaces, direct observation of chiral metal-organic complexes assembled on a Cu(100) surface are discussed in this Section.

A rich variety of chemical and physical systems occur in two forms distinguished solely by being mirror images of each other - a phenomenon, known as chirality. The discovery by Louis Pasteur - his milestone experiment of 1848 on the manual separation of enantiomorphous crystals of sodium ammonium tartrate [195] - laid the foundations of modern stereochemistry, which was placed on an absolute basis one century later by works of Bijvoet et al. [196]. Chiral specificity plays a fundamental role in chemistry, biology and pharmacology [98]. It is encountered at different levels, from single molecules and supramolecular assemblies to living organisms [36,197,198]. In fact, terrestrial life utilizes exclusively the *L*-enantiomers of amino acids - a striking fact, known as the 'homochirality of life', which stimulated long-standing efforts to understand its origin [199,200].

One hundred years after the formulation of the theory of metal-organic coordination, stereochemical considerations are of central interest in the development of the chemistry of coordination compounds [201–203]. In conventional solution chemistry chiral coordination compounds are obtained either by stereoselective synthesis using chiral species [204] or by spontaneous resolution upon crystallization in the absence of any chiral auxiliary [205–207]. The spontaneous resolution, which yields racemic mixtures of enantiopure agglomerates (crystals), is usually associated with chirally discriminative interactions from coordination and/or hydrogen bonds.

Besides its importance in life sciences, chiral asymmetry is fundamental in surface processes - heterogeneous asymmetric catalysis applications for their almost enzymatic specificity demand asymmetrically active substrates [208,209]. The surface, acting as a symmetry breaking agent, can induce formation of enantiomorphous domains from racemic mixtures [184,185] or even impart pseudochirality to achiral

molecules [186,187].

Recent studies revealed that by STM detailed insight into chirality phenomena at surfaces can be gained, including chiral recognition and chirality determination of single molecules, supramolecular assemblies, and extended enantiomerically pure overlayers [54, 56, 57, 64, 75, 210, 211]. Many of these studies have shown that surfaces can be used to induce enantiomeric separation or enantiomorphic ordering in supramolecular assemblies produced by deposition of a racemate, prochiral or achiral molecules [56, 57, 64, 75, 211–213].

In this Section single-molecule level STM observations of chiral complexes generated by the assembly of achiral components at a metal surface are presented. Following codeposition of iron atoms and TMA molecules on Cu(100), the molecules react with the metal centers to form chiral complexes stabilized by metal-ligand interactions.

Small amounts of iron atoms and TMA were sequentially deposited at 100 K. Further thermal annealing to 300 K accounts for deprotonated carboxylic acid groups of TMA molecules, which lie flat on the surface and are resolved as equilateral triangles (cf. preceding Section). Thus three carboxylate ligands per molecule are available, which on the pure Cu (cf. the previous Section) leads in the presence of Cu adatoms evaporated from substrate steps to the formation of Cu-TMA coordination compounds. In the presence of coadsorbed Fe, this process is obstructed and the TMA molecules rather readily react with coadsorbed Fe atoms.

As shown in the STM image in Figure 4.4(a), flower-shaped arrangements where a central protrusion is decorated by four TMA molecules were fabricated by deposition of Fe and TMA at low concentrations. These structures are thermally stable and appear exclusively in the presence of Fe on the surface. Their proportion initially increases for a given TMA coverage with the Fe dose, as illustrated by the plot in Figure 4.4(b). When both reactants are present in a 1 Fe : 4 TMA ratio, they almost exclusively assemble in the flower-shaped structures, which are consequently identified as compounds from a central Fe atom surrounded by four TMA molecules (designated $\text{Fe}(\text{TMA})_4$). Figure 4.4(a) also reveals that all complexes are aligned exclusively in two orientations at the surface, whereby a statistical analysis demonstrates that the

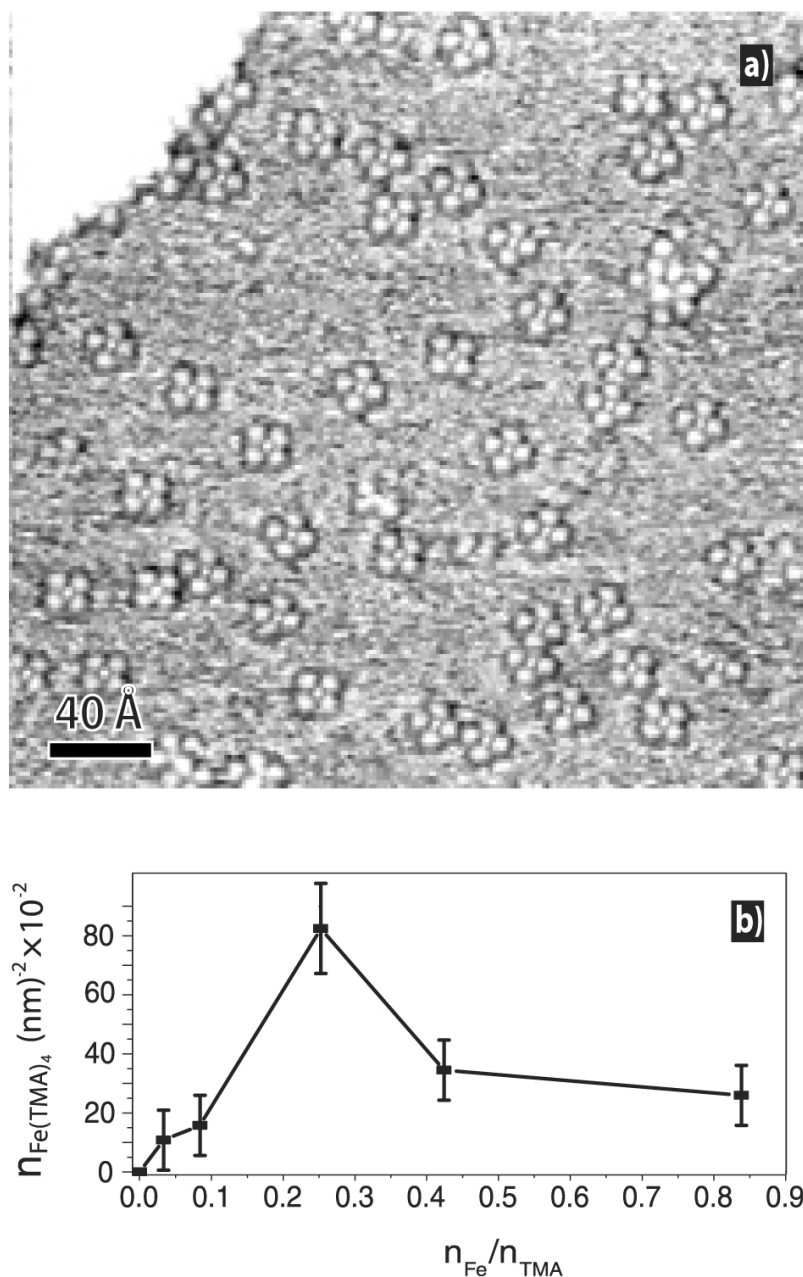


Figure 4.4: (a) Flower-shaped Fe(TMA)₄ complexes predominate on the Cu(100) surface following codeposition of Fe and TMA in a 1 : 4 ratio at low coverages. (b) The evolution of the complex concentration as a function of the Fe-TMA concentration ratio (with the TMA coverage constant at 0.63 molecules per nm²) has a marked peak at the ideal stoichiometry, where about 40 percent of the available reactants form Fe(TMA)₄ complexes.

two orientations are equal in occurrence.

A close inspection of the high-resolution STM image reproduced in Figure 4.5(a) reveals that the angle between the high-symmetry [011] direction of the substrate and the principal axis of the complexes (arbitrarily defined from the connection of the centers of two opposing TMA molecules, marked as dashed lines) is $+75^\circ$ or -75° . Furthermore it can be seen that in a complex the TMA molecules do not point straight towards the center Fe. Rather, their triangular envelope is rotated by 22.5° clockwise or counterclockwise with respect to the principal axes of the compound. This is associated with a unidentate Fe-carboxylate bond, where one of the oxygen atoms of the carboxylate group involved in the bonding comes significantly closer to the central Fe atom than the other. Moreover it is found that there is a strict correlation of the rotation for every TMA molecule in a given complex. In a complex rotated by $+75^\circ$ (-75°) relative to the substrate [011] direction each individual TMA molecule rotates counterclockwise (clockwise). As a consequence of this symmetry break the two resulting species, labelled *R* and *S*, cannot be superimposed onto each other by translation or rotation on the surface. They are mirror-symmetric configurations with respect to the [011] direction of the substrate and thus represent two $\text{Fe}(\text{TMA})_4$ enantiomers on $\text{Cu}(100)$.

A model for the enantiomers based on high-resolution STM data is depicted in Figure 4.5(b). It reveals that the unidentate bonding in conjunction with the correlated rotation accounts for a compact arrangement of the molecules in the complexes. Possibly the packing is assisted by hydrogen bond formation between the oxygen atoms of the carboxyle moiety, which do not directly couple to the Fe center, and the phenyl ring of the neighboring molecule - similar to the mechanism of achiral ligand locking in a chiral conformation, known from conventional stereochemistry [205, 214]. From the modeling the O-Fe bonding distance is estimated to fall below 2 Å, which agrees well with the typical value of Fe-carboxylate bonds in three-dimensional compounds [215] (note that for the analogous Cu-TMA compound, described in the earlier Section, the O-Cu distance amounts to $\simeq 3$ Å, which signals a substantially increased metal-carboxylate bond strength in the O-Fe case). Also, the square-planar geometry is frequently encountered in metal-carboxylates. Similarly

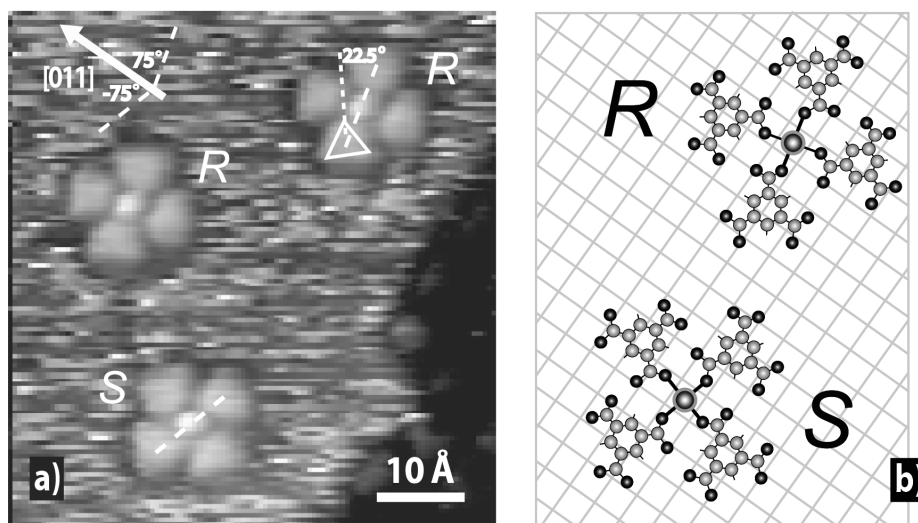


Figure 4.5: (a) High-resolution image showing the two $\text{Fe}(\text{TMA})_4$ 2D enantiomers, labeled R and S representing mirror-symmetric species with respect to the [011] substrate direction. (b) Corresponding geometrical model. Carbons are shown in light grey, oxygens - in black, phenyl ring hydrogens are omitted). There is a unidentate coordination of the carboxylate ligands to the central Fe atom (shown in dark grey and placed on the hollow site) with a bond length of about 2 Å (black lines). The corresponding rotation of the carbon backbone is strictly correlated for all TMA molecules in a given complex. The resulting symmetry break accounts for the chirality of the complexes.

with the previously discussed case of Cu-TMA complexation, the oxidation state of the Fe in the $\text{Fe}(\text{TMA})_4/\text{Cu}(100)$ compound cannot be determined unambiguously in view of screening effects mediated by substrate electrons.

Notably, as mentioned earlier in Introduction, $\text{Fe}(\text{TMA})_4$ complexes can coexist with analogous $\text{Cu}(\text{TMA})_4$, however, the latter possess limited stability and transform to more stable $\text{Cu}_2(\text{TMA})_6$ arrangements (Section 4.1 of the present Chapter). Nevertheless, $\text{Fe}_2(\text{TMA})_6$ complexes were never observed under experimental conditions employed (extended Fe-TMA structures, comprising 16 TMA and 9 Fe can develop at elevated Fe coverage - see Section below). This suggests that, in general, the energy barrier for the formation of the M_2TMA_6 exists.

Our results demonstrate that surface metal-organic complexation can be at the origin of two-dimensional chirality generation, which can be explored at a single-molecule level. Generally speaking, it is shown that a square-planar ML_4 complex can be chiral in two dimensions when symmetric bidentate ligands are employed which link to the metal atom (representing the stereogenic center) in an organized unidentate fashion. In principle this intriguing example for stereoisomerism can be similarly encountered for three-dimensional octahedral compounds of the general form MXYL_4 when the bidentate ligands lie in the same plane.

4.3 Hierarchical Self-Assembly

Organizational hierarchies are abundant in biological systems and biomaterials such as proteins, viruses or biogenic crystals [216–218]. In a similar way distinct levels of structural hierarchies and complexity are encountered in artificial supramolecular systems stabilized by non-covalent chemical bonds [219, 220]. An intriguing issue where our current understanding is rather limited concerns the *aufbau* of highly organized supramolecular architectures, i.e., the principles governing the transition between the primary (molecular) building blocks and the final mesoscale systems. The steering of the corresponding processes will be paramount for the development of novel supramolecular functional materials [221–229]. Particularly interesting are low-dimensional chiral assemblies in view of their intrinsic relation to

the biological world [230] and their importance in heterogeneous asymmetric catalysis, chemical sensing, enantioselective antibody recognition and host-guest chemistry [34, 64, 209, 231–235].

In this Section we report single-molecule level observations on the hierarchical assembly of homochiral nanocavity arrays at a metal surface by employing principles of surface metal-organic coordination, described earlier. Figure 4.6 schematically shows key findings : The primary building blocks TMA molecules and Fe atoms assemble in the form of secondary mononuclear chiral complexes, which are stabilized by metal-ligand interactions. The secondary complexes in turn are antecedents for tertiary polynuclear nanogrids representing the dissymmetric motifs which in a final stage are organized in mesoscale networks comprising a regular arrangement of homochiral nanocavities. These nanocavities present identically shaped ~ 1 nm diameter hosts, equally spaced by ~ 3.5 nm from each other and functionalized by eight carboxylate groups in a well-defined arrangement. The precise positioning of the molecules and the metal centers at the surface opens up new possibilities for the bottom-up fabrication of complex functional nanomaterials.

As shown in the previous Section, at 300 K the carboxylate ligands readily react with the adsorbed Fe atoms leading to the initial formation of chiral $\text{Fe}(\text{TMA})_4$ complexes where a central Fe atom is surrounded by four organic molecules. Since *R* and *S* enantiomers are homogeneously distributed at the surface this 'cloverleaf phase' represents a racemic mixture. A further, albeit metastable type of secondary structure is a Y-shaped complex made out of a single Fe atom coordinating three TMA molecules (marked by the white circles in Figure 4.7(a)). At 300 K the Y-shaped complexes are unstable at the surface and can only be observed at appreciable coverages in the vicinity of the immobile $\text{Fe}(\text{TMA})_4$ complexes or at step edges, where their lifetime is locally increased due to steric hindrance of decay and lateral motion, by the analogy with the similar effect where $\text{Cu}(\text{TMA})_4$ are employed (Section 4.1). This implies in particular that in addition to the material in the stable coordination compounds, mobile iron atoms and TMA molecules are present at the surface.

The next level of structural complexity is encountered upon annealing of the cloverleaf phase to 350 K. Polynuclear assemblies form which typically consist of 16

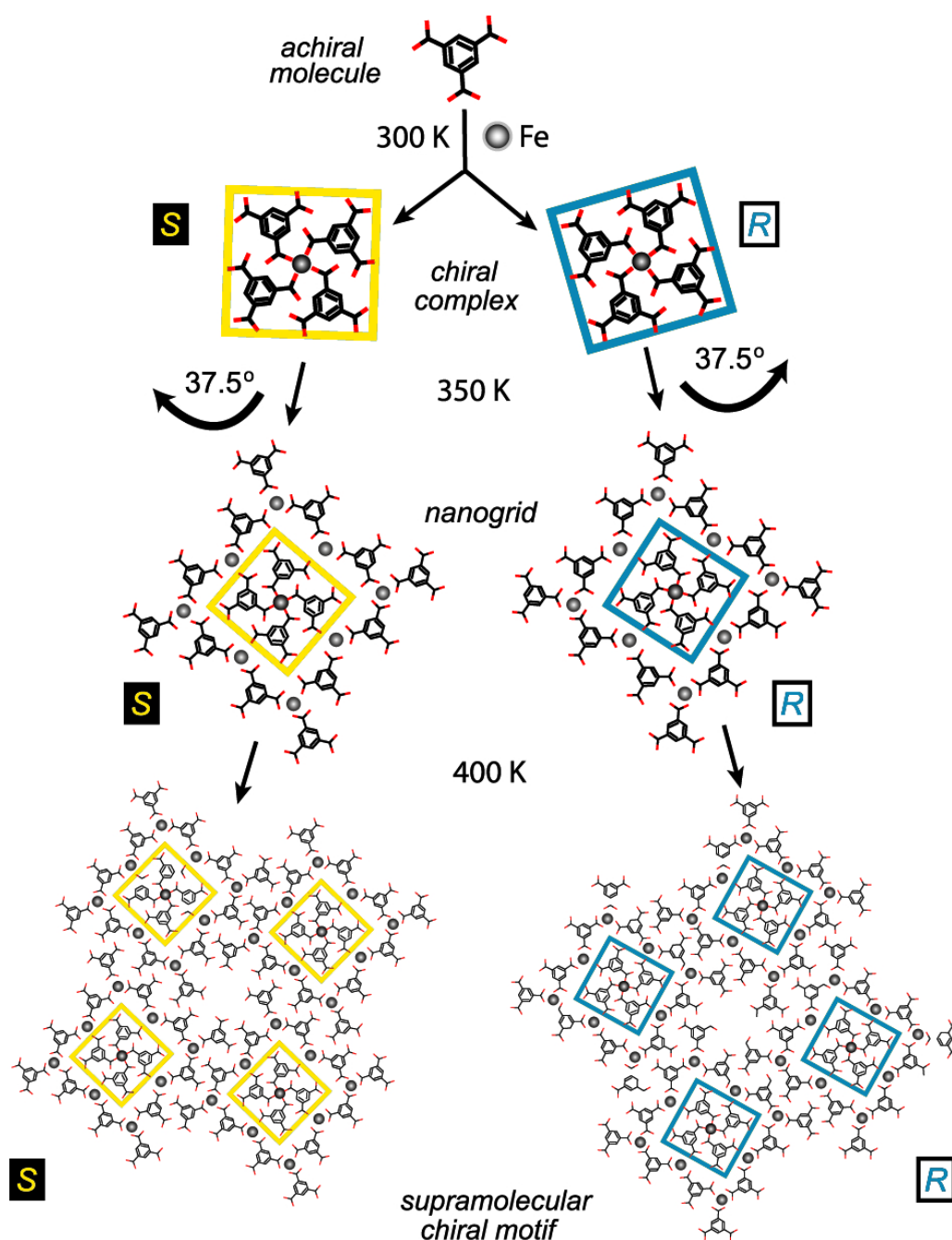


Figure 4.6: *Aufbau* of dissymmetric supramolecular motifs mediated by hierarchical assembly of simple achiral species. Molecules of trimesic acid (oxygen atoms are shown in red) and Fe atoms (light grey spheres) represent the primary units which are employed for the formation of secondary chiral mononuclear ($\text{Fe}(\text{TMA})_4$) complexes. The complexes are antecedents for tertiary polynuclear nanogrids which are in turn the supramolecular motifs for the assembly of homochiral nanocavity arrays. The respective mirror-symmetric configurations (labeled *S* and *R*) are indicated with yellow or blue frames.

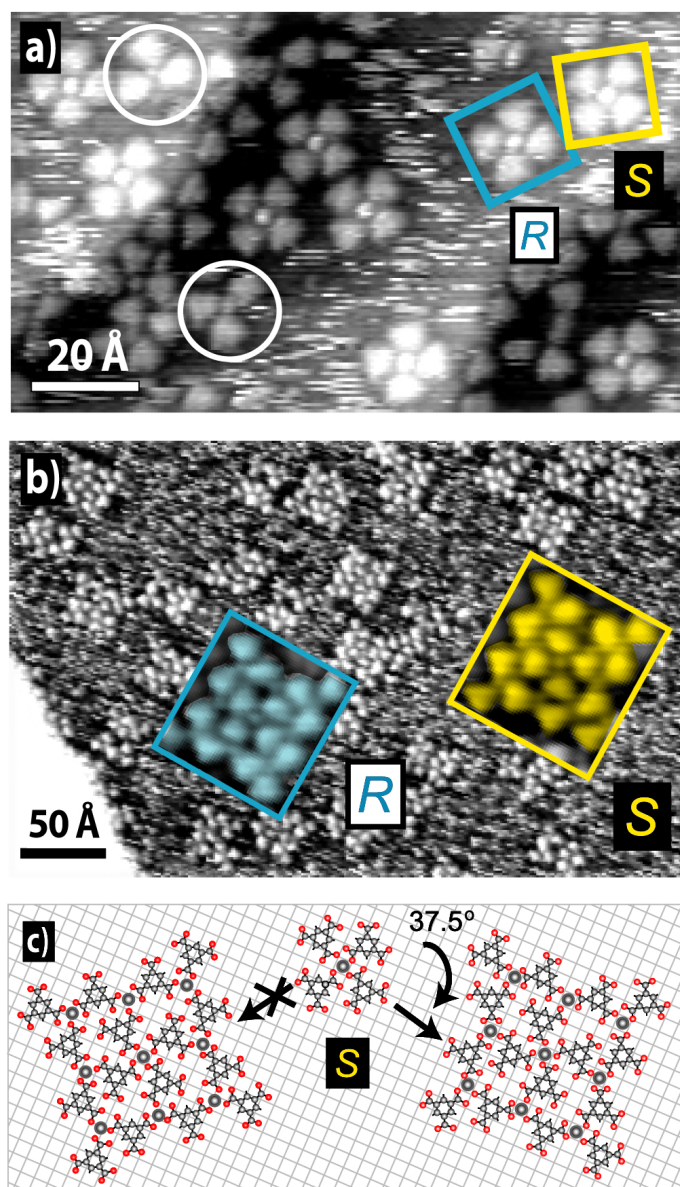


Figure 4.7: Hierarchical assembly of metal-organic architectures monitored by STM. (a) Secondary structures formed at 300 K. Blue and yellow squares indicate two different enantiomers of cloverleaf-shaped $\text{Fe}(\text{TMA})_4$ complexes (representation following Figure 4.6). White circles mark metastable Y-shaped $\text{Fe}(\text{TMA})_3$ complexes. (Fe coverage: 0.06ML; TMA coverage: 0.8ML). (b) Assembly of tertiary stage : square-shaped polynuclear nanogrids evolve upon annealing at 350 K. The insets reveal that the respective core units of the dissymmetric metal-organic motifs are related to the chiral secondary $\text{Fe}(\text{TMA})_4$ compounds (color coding as in Figure 4.6). (Fe coverage: 0.02ML; TMA coverage: 0.4ML). (c) Assembly of ideal polynuclear *S* nanogrid based on STM topography. A 37.5° clockwise rotation of the $\text{Fe}(\text{TMA})_4$ cloverleaf core unit is necessary to allow for hollow-site adsorption of all Fe atoms (light grey) involved.

TMA molecules arranged in square-like molecular 4×4 nanogrids (see Figure 4.7(b)), which are always oriented along the high symmetry directions of the Cu(100) substrate. High-resolution STM images (e.g., Figure 4.7(b) insets) reveal that the core unit of each nanogrid is a $\text{Fe}(\text{TMA})_4$ complex, which is surrounded by four Y-shaped arrangements. This configuration suggests that the mononuclear complexes in the cloverleaf phase represent antecedents for the nanogrids. In the simplest picture this can be viewed as resulting from an attachment of four Y-shaped complexes to the corners of a $\text{Fe}(\text{TMA})_4$ complex mediated by incorporation of further Fe atoms forming a second coordination shell (cf. Figure 4.6). However, a closer inspection of the data reveals that the central cloverleaf complexes are additionally rotated by an angle of 37.5° in the nanogrids' development whereby their chiral nature persists (the rotation must be clockwise for *S* and counterclockwise for *R* species, respectively). This rearrangement is associated with the easier positioning of second shell Fe atoms at the energetically preferred substrate hollow-sites (note that in an ideal tertiary nanogrid a total of nine Fe atoms are included, but second shell Fe atoms seem to be missing in some cases). As shown in Figure 4.7(c), for a hypothetical *S* nanogrid made from an *S* complex in an unrelaxed geometry without rotation (model at the left side) only the central Fe atom maintains a hollow site position while the others adsorb at unfavorable bridge or top sites of the Cu(100) surface. The 37.5° clockwise rotation (for the *S* species) allows for the positioning of all Fe atoms at hollow sites. The chiral arrangement of the secondary core units induces dissymmetric tertiary nanogrids. I.e., there is a chirality proliferation in the nanogrid assembly. Accordingly no translation or rotation in two dimensions would allow for a superposition of the mirror-symmetric configurations labeled *R* or *S* as depicted in Figure 4.6 and Figure 4.7. Similar with the mononuclear complexes in the cloverleaf phase the *R* and *S* nanogrids are found to be homogeneously distributed on the surface forming a racemic mixture.

The final stage of complexity at the mesoscopic scale is achieved upon further annealing of the substrate to 400 K leading to the formation of extended regular metal-organic superstructures. The STM image reproduced in Figure 4.8(a) depicts the corresponding two-dimensional coordination networks with a square ($3.5 \text{ nm} \times 3.5 \text{ nm}$)

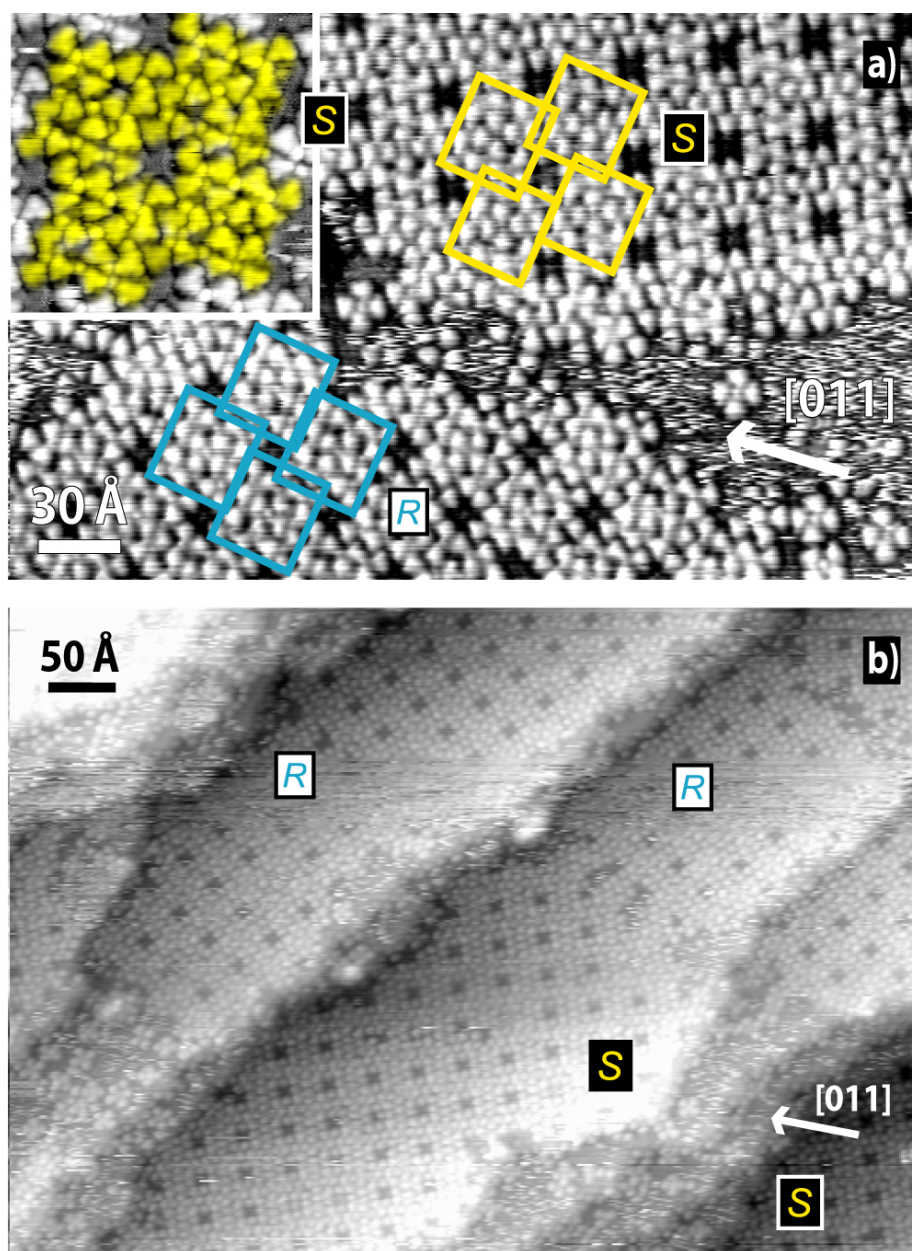


Figure 4.8: Hierarchical assembly of metal-organic architectures monitored by STM. **(a)** Formation of extended nanocavity arrays triggered by 400 K annealing. Two homochiral domains are assembled consisting of pure enantiomers (marked by blue or yellow rectangles, coding as in Figure 4.7). The inset is a high-resolution image of a *S*-type nanocavity, which is surrounded by eight TMA molecules. (Fe coverage: 0.06ML; TMA coverage: 0.8ML). **(b)** Highly organized homochiral domains cover the entire surface at saturation coverage. Enantiopure domains labeled *R* and *S* comprise homochiral nanogrids. (Fe coverage: 0.06ML; TMA coverage: 0.8ML).

unit cell comprising a regular arrangement of nanocavities. The tertiary nanogrids are identified as the underlying supramolecular motifs. Accordingly a close inspection of the data (cf. inset in Figure 4.8(a)) reveals that the shape of the individual ~ 1 nm diameter nanocavity is defined by the interlocking of four nanogrids. The interlocking nanogrids are of the same chirality, which is associated with the fact that exclusively homochiral species match. In contrast, there is no smooth joining of *R*- and *S*-type nanogrids; it is obstructed by the tilt angle between the mirror-symmetric species implying a geometric mismatch (in analogy to stereochemistry-driven hydrogen-bonded homochiral supramolecular assemblies [57, 75]). As a striking consequence chirality is bestowed to the entire nanocavity arrays. Accordingly, as shown in Figure 4.8(a) two domains exist on the surface which are mirror images of each other, whereby the symmetry axis is given by the high symmetry [011] direction of the Cu(100) substrate (marked by the arrow in Figure 4.8(a)). The assembly of the nanocavity arrays is thus *chiroselective* or *chiroinductive*, i.e., in their evolution only the building blocks with the appropriate chirality are assembled or alternatively the chiral signature of the incorporated material is induced by already existing arrangements. The net result is in either case that enantiopure domains evolve with a distinct higher level of organization as the preceding racemic mixture of isolated nanogrids. Large scale STM data (cf. Figure 4.8(b)) reveal that at saturation coverage a well-ordered layer comprising the supramolecular motif readily covers the entire surface. The respective homochiral single domains were found to be robust (thermal stability up to 450 K) and to be up to 50 nm wide extending over entire substrate terraces. As expected there is an equal distribution of *R*- and *S*-type domains.

The inset in Figure 4.8(a) demonstrates furthermore that each nanocavity is enclosed by eight TMA molecules, which account for an opening with an inner diameter of ~ 1 nm. Since each TMA vertex carries a carboxylate group, in total eight COO^- ligands surround a single cavity. A tentative model of the nanocavities is shown in Figure 4.9 (the orientation of the carboxylate groups cannot be conclusively determined on the basis of STM data, and they may rotate out of the molecular plane). The distinct size, shape and chemical functionality make the nanocavity arrays a promising candidate to be employed as host system for the selective adsorption of

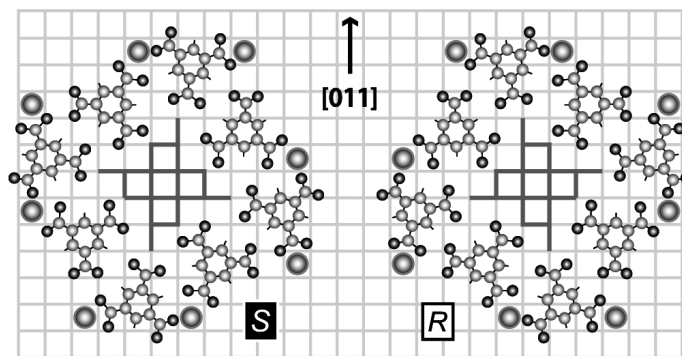


Figure 4.9: Tentative model of nanocavities from STM topography, where the *S* (*R*) nanocavity is assembled from *S* (*R*) motifs. The central opening (where the underlying copper grid is colored darker to mark the chiral nature of the cavity) is functionalized by the eight surrounding carboxylate groups. It represents a chiral host for chiroselective adsorption of guests and enantioselective heterogeneous catalytic processes.

molecular guests. In addition to its chemical functionality the homochiral nature of the nanocavities is of great interest for enantioselective recognition and asymmetric catalysis.

Our observations demonstrate that the hierarchic assembly of robust metal-organic architectures at surfaces can be followed at the single molecule level and provides a novel rationale for the fabrication of highly organized supramolecular materials. This extremely versatile approach implies the potential to construct surface-supported nanocavity coordination arrays with programmed size, shape and functionality by the appropriate choice of the employed constituents. Moreover, the distinct arrangement of metal centers and organic molecules in these systems accounts for multifunctional nanostructured templates.

4.4 Print Boards of Magnetic Centers

The last decade brought numerous breakthroughs in the area of molecule-based magnetic materials. Molecular architectures of varying dimensionality, containing magnetic centers, are recognized having unique magnetic properties unavailable in conventional metal/intermetallic and metal-oxide magnets [103, 104, 236, 237]. Moreover, collective magnetic behavior is a common phenomena in 3D metal-organic sys-

tems, where magnetic centers are effectively coupled through organic linkers. The flexibility in the rational design of such hybrid molecular materials provides the prospects of manipulating their basic electronic and magnetic properties by changing the system topology [238]. Notably, supramolecular chemistry offers a great potential in developing new strategies for the generation of novel molecule-based structures that are magnetically active [112] or magnetic components of reduced dimensionalities [103, 113, 239].

In the present Section we exploit the potential of surface metal-organic coordination for the construction of a 2D molecular-based 'print board' - a regular arrangement of magnetic centers - Fe atoms, rigidly positioned on the substrate. Distinct coordination complexes, similar to those described in the preceding Sections, are formed by the complexation of TMLA molecules with Fe. This results in the formation of extended arrays of densely packed metal-organic structures with the core of individual Fe atoms, which are arranged in a square-type lattice. The decisive precursor structure, needed for the print board structures to develop, the well-ordered organic layers of TMLAs, was described above (Section 3.2, Chapter 3).

Since TMLA molecules in the precursor layers are adsorbed flat (with a slightly tilted molecular plane) and comprise functional groups to react with deposited Fe adatoms, the formation of metal-organic architectures is expected by analogy with the previously described systems. At small Fe concentrations (Fe coverages amount around 0.03 ML) ordered arrays of individual compact arrangements develop, as shown on Figure 4.10, when deposition is made on the substrate held at 450K. These arrays evolve on the basis of ordered TMLA domains and tend to preserve the previous surface morphology: wide terraces contain well-ordered structures, while on narrow ones only randomly scattered aggregates are encountered (cf. Figure 4.10(a)). The STM image in Figure 4.10(b) reveals the high ordering in the array. One can distinguish individual cloverleaf-shaped arrangements, packed together to form a well-ordered extended array, strictly (6 x 6) commensurate with the underlying Cu substrate. Similar with the $\text{Fe}(\text{TMA})_4$ complexes described previously, these assemblies are identified as a complex of four molecular species, coordinated in a square-planar fashion by the central transition metal atom. I.e., upon deposition of small amounts

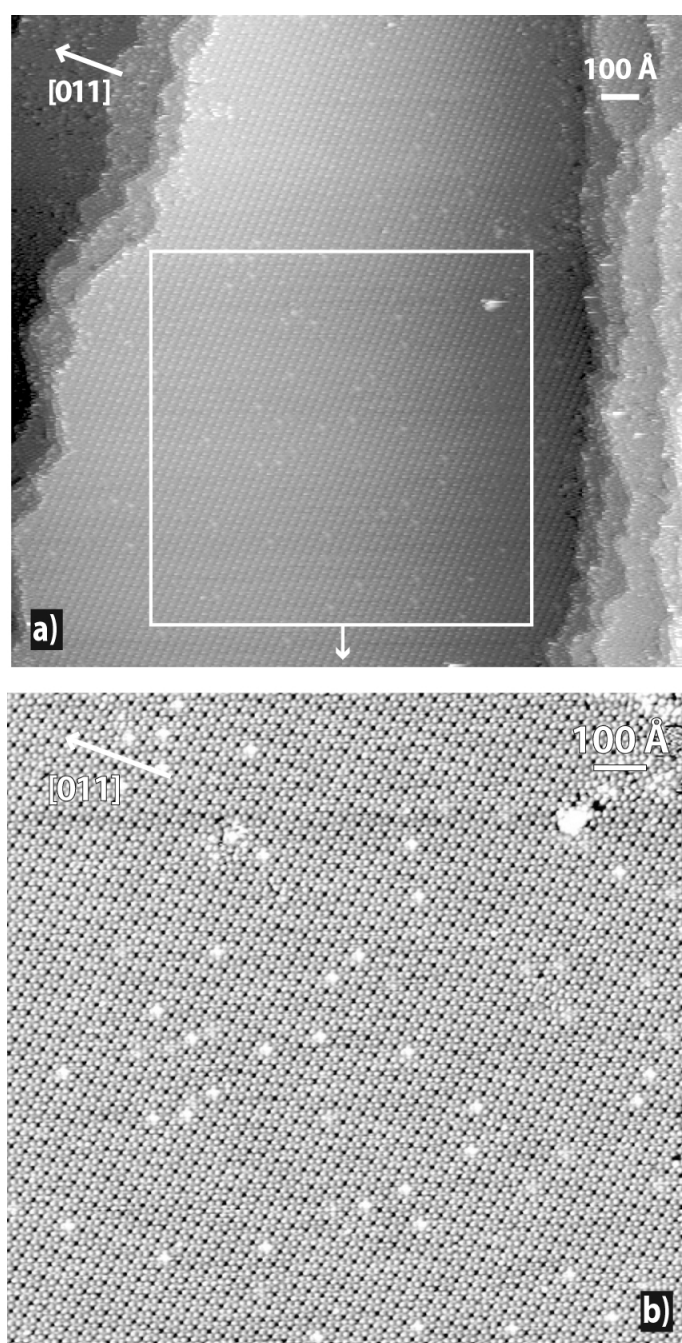


Figure 4.10: Print board of Fe centers: array of $\text{Fe}(\text{TMLA})_4$ metal-organic complexes, providing a rigid arrangement of magnetic Fe centers on the surface. **(a)** Overview on the surface morphology. The region, zoomed in (b), is outlined by a white rectangle. **(b)** Regular array of $\text{Fe}(\text{TMLA})_4$ complexes, seen as cloverleaf-shaped entities. Cu[011] azimuth is shown for reference.

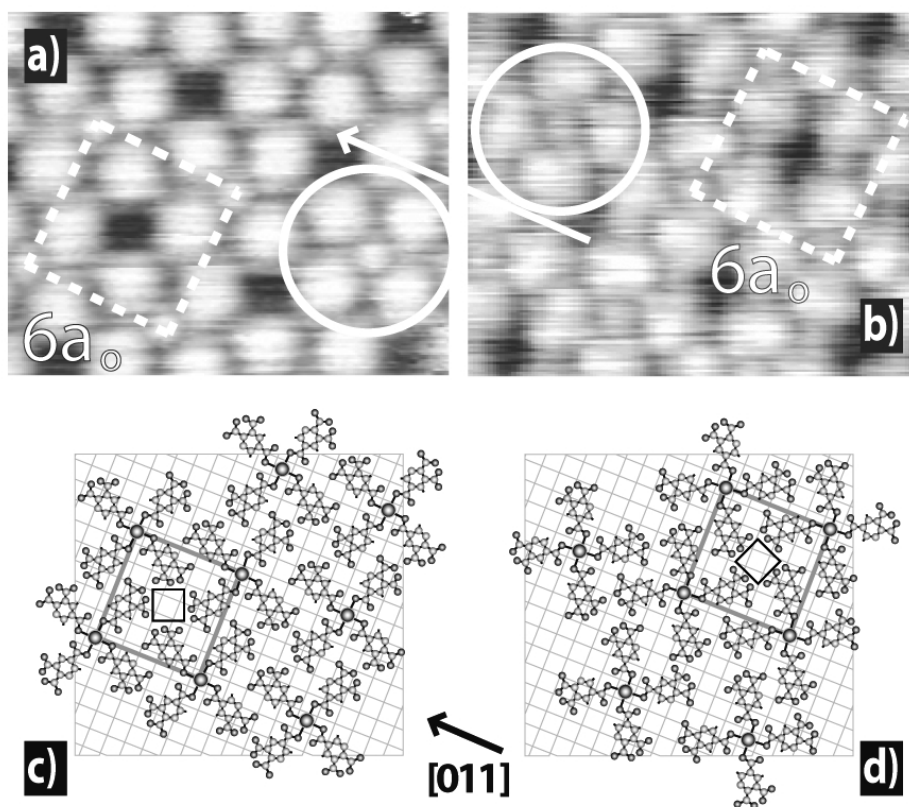


Figure 4.11: Molecular arrangement and packing of cloverleaf-shaped complexes. Two enantiomers, forming similar ordered arrangements are shown in (a) and (b) respectively. The Cu[011] mirror symmetry axis is indicated by an arrow. The lattice unit cell is in both cases identical and dashed in white. (c, d) Tentative geometric model for the compact arrangement of $\text{Fe}(\text{TMLA})_4$. Chiral folding of individual complexes results in formation of enantiopure arrays, where complexes of only one handedness coexist. The lattice, formed by Fe magnetic centers is represented by a (6x6) unit cell, marked in grey. Functional cavities, formed by packing of four complexes are indicated by a square. C are shown in light grey, O in dark grey, H are omitted for clarity.

of Fe onto the organic precursor layer, the carboxyle groups react with the transition metal adatoms and metal-organic $\text{Fe}(\text{TMLA})_4$ complexes are formed. However, in marked contrast to the previously described cases, the presence of the precursor layer promotes an extended array size with the regularly arranged individual $\text{Fe}(\text{TMLA})_4$ metal-organic complexes, whence a well defined positioning of magnetic centers is achieved.

The detailed structure of the complexes is revealed by the data in Figure 4.11(a, b). Each individual complex comprises a central Fe atom and four surrounding TMLA

molecules. The distance between the centers of neighboring complexes (measured as the distance between central Fe atoms) amounts to $6a_0$ (a_0 stands for Cu nearest-neighbor distance and equals 2.55\AA) in both principal directions. Moreover, two distinct types of $\text{Fe}(\text{TMLA})_4$ complexes within different arrays are encountered. The comparison of Figure 4.11(a) and Figure 4.11(b) evidences the presence of two enantiomeric species - i.e. folded in opposite directions (clockwise and anti-clockwise) and non-superimposable upon in-plane rotation or translation. Thus one type represents the mirror image of the other one with respect to the Cu $[011]$ azimuth (shown by the white arrow in Figure 4.11(a, b)), and thus each single array of packed complexes with only one handedness (as the one presented on Figure 4.10) is effectively homochiral.

A close inspection of two arrays with different chirality (cf. Figure 4.11(a, b)) shows that the chirality of individual complexes in this case does not lead to a significant difference in the ordering of the entire array - central Fe atoms are spaced by 6 Cu surface lattice constants (2.55\AA) along $[011]$ and $[0\bar{1}1]$ directions in both types of arrays. In the tentative geometric model, presented for both enantiomers in Figure 4.11(c, d) the details of the structural arrangement are illustrated: The complexes are sterically packed to form an extended regular topology with the individual $\text{Fe}(\text{TMLA})_4$ interacting with their neighbors possibly through hydrogen bonding or weak electrostatic forces. The compact openings of the underlying Cu substrate between the complexes, imaged in STM as dark features, represent, in fact, chiral cavities, functionalized by surrounding TMLA ligands. Their functionality as hosts for molecular inclusion interactions can be potentially addressed (for a more detailed discussion of the functionality of similar cavities, frequently encountered in surface-supported metal-organic architectures, c.f. Section 4.3, or the following Sections).

The positioning of individual Fe centers in nm-sized regular arrays potentially leads to collective magnetic behavior of atomic spins. The system Fe/Cu(100) is a classic example for the study of magnetism in ultrathin layers, which exhibit a strong dependence of magnetic behavior on the film structure (see [240] and ref. therein). For transition metal systems of even lower dimensionality, magnetic ordering is detected in one- and zero-dimensional topologies [241–243]. With the present TMLA / Fe system individual identical metal-organic coordination complexes form an extended array.

Since the coordination does not propagate in any particular direction, individual magnetic moments (if any) of $\text{Fe}(\text{TMLA})_4$ complexes are kept unperturbed, keeping the overall magnetic moment of the system randomly fluctuating over time, averaged by the fluctuation of individual moments of each complex. However, finite-sized magnetic particles and single transition metal atoms are known to develop giant magnetic anisotropy [243]. Similar effects can be expected here, which could be interpreted in terms of paramagnetic nature of the formed metal-organic arrays: Upon applying external magnetic fields anisotropic magnetization is expected to develop, which, normally, would not persist if the external field is removed. However, the role of the underlying substrate in mediating a collective magnetic behavior of the system can not be decisively ruled out [244]. These issues will be clarified by means of x-ray magnetic circular dichroism (XMCD) or other measurements with magnetic sensitivity.

4.5 Metal-Organic Coordination Networks

Metal-organic coordination networks (MOCN) are widely studied examples of molecular architectures with well-defined shape and geometry that have been obtained using transition metal centers and concepts from coordination chemistry [86, 189, 245]. MOCNs have been realized with specific topologies and a high structural stability [34, 114, 235, 246–253]. They may exhibit intriguing properties, including molecular recognition, functionalities for heterogeneous asymmetric catalysis, inclusion phenomena, etc. [222, 239, 254–260].

This Section addresses the application of the concept of metal-organic coordination for the rational design of surface-supported MOCNs with tunable topologies at a well-defined metal surface. The sequential deposition of TMLA molecules and Fe atoms on a clean Cu(100) substrate gives rise to the formation of 2D surface-supported open networks, stabilized by relatively strong lateral metal-organic coordination bonds. The precise control of the concentration ratio of the components allows for the assembly of distinct architectures. With this approach new possibilities for the bottom-up fabrication of low-dimensional functional materials is successfully

demonstrated.

The necessary precursors for surface-supported MOCNs as described in a previous Section 3.2 are organic layers of a well-defined TMLA phase obtained by deposition of submonolayer TMLA on the Cu(100) substrate. Upon deposition of Fe atoms onto the TMLA layer, the carboxyle groups readily react with the transition metal adatoms. The STM image reproduced in Figure 4.12(a) reveals the formation of an extended regular network oriented along the principal directions of the substrate at the Fe coverage of one Fe to one TMLA molecule. The network single domains are oriented along a substrate high-symmetry direction and are up to $100 \times 100 \text{ nm}^2$ in size, frequently covering entire substrate terraces (areas with compact islands, presumably from Fe aggregation, and other defects account for approximately 20 percent of the total surface). The MOCN contains anisotropic cavities and can be found in two 90° -rotational domains, reflecting the symmetry of the substrate.

The high-resolution STM image depicted in Figure 4.12(b) allows distinguishing the individual TMLA with the characteristic four-lobe features, similar to the molecular resolution in the pure organic layer. This indicates that the flat adsorption geometry is preserved. Paired molecular rows running along the $[011]$ direction have formed under the influence of the incorporated Fe atoms. The paired rows are interconnected by individual molecules oriented in the direction perpendicular to the rows. Thus this structure is designated 'double-row MOCN'. At the points of intersection bright protrusions are resolved, which are associated with the deposited Fe atoms, similar to the STM imaging of metal atoms in related compounds formed at Cu(100) and described earlier in the present Chapter. The relative orientation of the molecules with respect to the metal atoms indicates that the TMLA carboxyle groups point to the Fe, which is associated with the formation of a lateral coordination bond. Consequently, the entire structure can be understood as an open network-type Fe-carboxylate arrangement stabilized by metal-ligand interactions.

A tentative geometrical model for the double-row MOCN based on an analysis of STM data is presented in Figure 4.12(b). We assume that both Fe atoms and phenyl rings reside at the energetically preferential hollow sites of the substrate. The Fe atoms in the double-row MOCN form ladders with a square $4a_0 \times 4a_0$ repeat unit ($a_0 =$

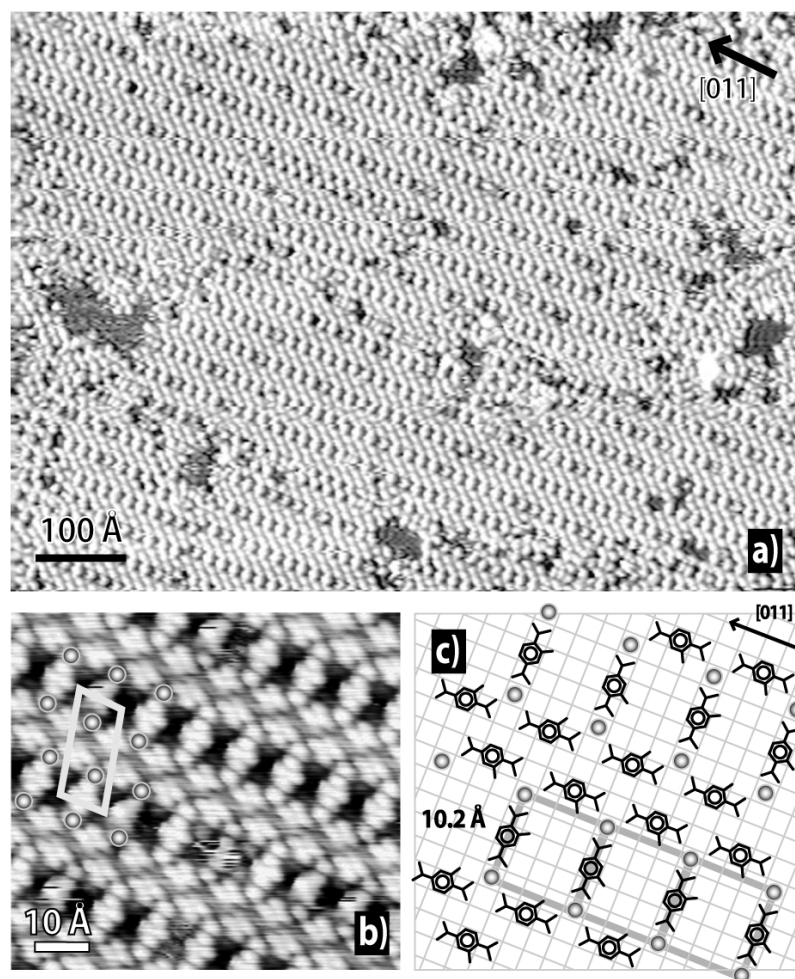


Figure 4.12: ‘Double-row MOCN’ assembled upon tuning the coverage ratio to one Fe atom per TMLA molecule. (a) Large-scale STM topography showing the regularly ordered network structure comprising anisotropic cavities. (b) High-resolution STM image revealing the four-lobe molecular structure. Single protrusions at the network’s points of intersection are associated with Fe atoms, laterally coordinated by TMLA carboxylato moieties. The unit cell of the network is marked in grey and Fe atoms around are highlighted by the grey circles. (c) Tentative model for the double-row Fe-carboxylate MOCN. The side carboxylate groups are assumed to be oriented perpendicular to the surface. Fe atoms (light grey) are arranged in a ladder-type structure with a 10.2 Å x 10.2 Å repeat unit, as indicated.

2.55 Å is the surface lattice parameter of Cu(100)). Each Fe atom interacts with three TMLA: The data signal a unidentate linkage to the two neighboring molecules from the double row and a bidentate coupling to the isolated species in the perpendicular orientation. This arrangement implies a distorted four-fold coordination for each Fe atom, a configuration frequently encountered in three-dimensional square-planar metal-carboxylates [190]. However, it is important to note, that as in the previous described cases for surface metal-organic coordination, with the present system the charge on both adsorbed TMLA molecules and Fe atoms is strongly affected by the electrons of the metal surface, which effectively screen the adsorbates and in particular prevent from the determination of the Fe oxidation state. In the model we assume that a too close rapprochement of the laterally non-coordinated carboxylate groups at the o-position is avoided by their 90° rotation out of the surface plane. This behavior is suggested from described earlier theoretical analysis of TMLA bonding in the organic layer, and is also a well-known conformational adaptation for carboxylic acids in solution chemistry. Furthermore the o-position side groups are placed randomly since we found that they do not influence the primary frame structures of the MOCNs ¹. The effective cavity envelope is $\sim 3 \times 10 \text{ Å}^2$ as estimated from high resolution STM data. The stoichiometric Fe : TMLA ratio in the model structure is determined to 0.66, which falls below the necessary 1:1 ratio required for the network formation ².

A second network type designated 'single-row MOCN' is obtained upon increasing the adsorbate coverage ratio to 2 Fe atoms per TMLA molecule. As demonstrated by the STM image reproduced in the Figure 4.13, MOCNs with different topology are formed which follow again the high-symmetry directions of the substrate and grow in extended islands. Two types of structures comprising different cavities can be discerned, which are designated α - and β -phase, respectively. These structures

¹In fact, using 1,4-benzenedicarboxylic acid (TPA), a molecule with two carboxylic groups at *para*-positions, exactly the same MOCN structures can be fabricated, which proves that the side group does not play a significant role in the MOCN formation.

²This difference is attributed to the effective loss of Fe atoms in other surface chemical processes. I.e., not the entire amount of deposited Fe is employed in the coordination network formation. Decoration of substrate step-edges, and in particular Fe island formation are frequently suggested from inspection of STM topographs. Also a small percentage of the Fe atoms might be lost in substrate atom exchange processes.

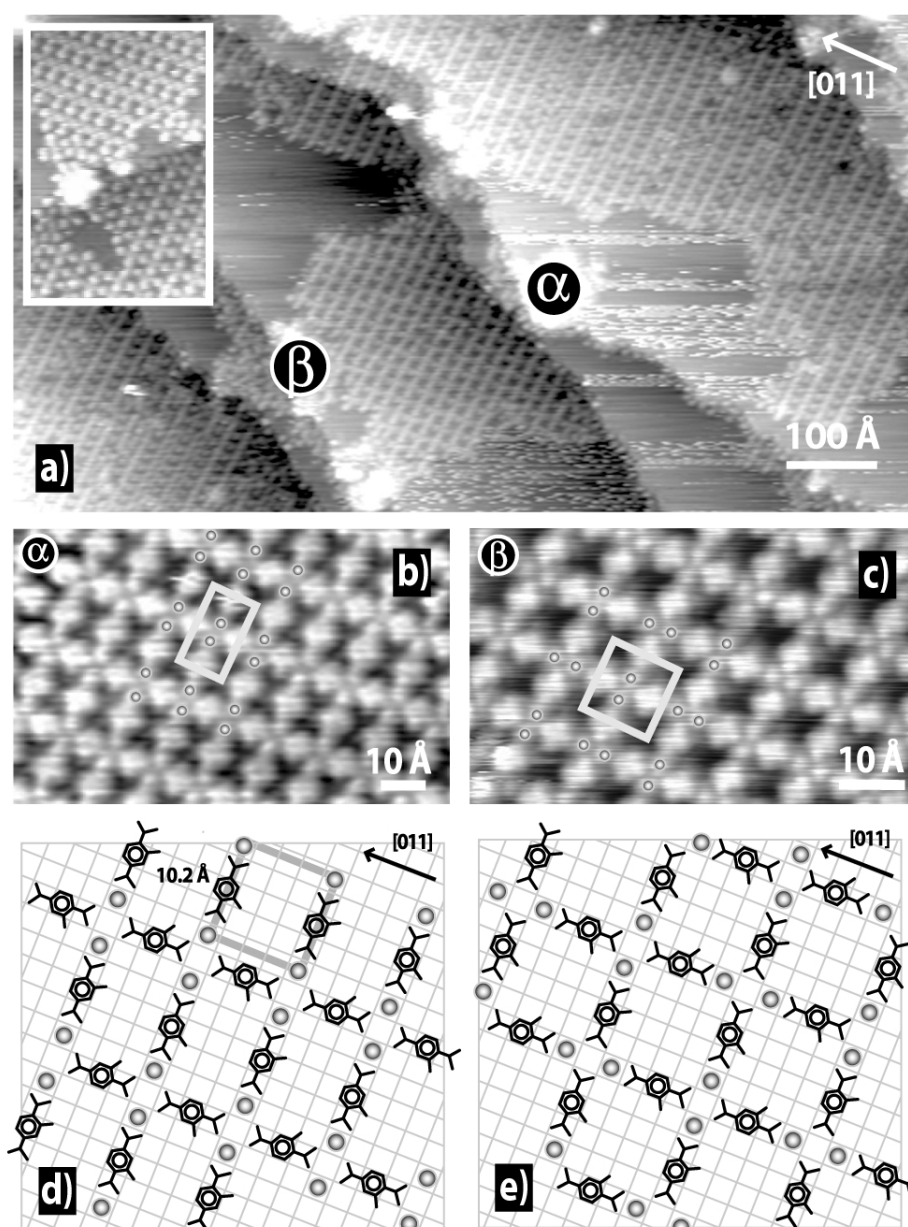


Figure 4.13: 'Single-row MOCN' assembled upon tuning the coverage ratio to two Fe atoms per TMLA molecule. (a) Overview STM topography showing two species of regularly ordered networks designated α - and β -phase. In the inset both 90° rotational domains of the α -phase are depicted. (b, c) In high-resolution STM data the detailed arrangement of Fe and TMLA in both α - and β -phase is resolved. A rectangular and square unit cell is characteristic for the networks of α - and β -phase, respectively (shown in grey, surrounding Fe atoms are highlighted). (d, e) The tentative models α - and β -phase are identified as MOCN isomers (Fe atoms shown in grey). While in both phases the same stoichiometry is encountered and Fe atoms have identical coordination environments, their geometrical arrangement is different.

always develop simultaneously, which signals that they are close in composition and energy. In the corresponding high-resolution STM data shown in Figures 4.13(b, c) the positioning of the constituents is revealed. The networks consist of a sequential arrangement of individual TMLA molecules and Fe atoms, which are identified by their respective imaging characteristics, similar to those in the double-row MOCN. In the α -phase (cf. Figure 4.13(b)) a rectangular unit and a cavity of similar shape and size as that in the double-row MOCN is identified. However, the cavity density is increased now since in the α -phase the cavities are separated by single TMLA molecules in contrast to the double-row structures where the cavities are separated by pairs of TMLA molecules (cf. Figure 4.12). Because of its anisotropic shape two 90° rotational domains are found in the α -phase (cf. inset in Figure 4.13(a)). In the β -phase (cf. Figure 4.13(c)) a square unit comprising cavities of concave edges is found in a continuous two-dimensional Fe-carboxylate network. The essential difference between the α - and β -phases consists in the symmetry of the Fe-carboxylate linkage in the MOCNs' points of intersection. While it is always identical in the α -phase, for the β -phase an alternating orientation of the Fe pairs present at each intersection is found. This is illustrated by the corresponding models depicted in Figures 4.13(d, e), which also show that the integral coordination of each Fe atom is equivalent for both phases. However, in the α -phase a given TMLA molecule either has two bidentate or four unidentate linkages to two Fe atoms, whereas in the β -phase for every given molecule both bidentate and unidentate bonding are encountered at its extrema. Apparently the energy change associated with this subtle difference is small, which is understood as the reason for the simultaneous evolution of both phases under the employed conditions. Thus the two phases of the single-row MOCNs are closely related and can be regarded as structural isomers, which is a common finding for metal-organic frameworks [34]. In analogy with the double-row MOCN the stoichiometric coverage ratio of Fe : TMLA of 1:1 for the ideal single-row MOCNs falls below the actual 2:1 value required for the network formation³.

With the present system only the carboxylate groups in the *para* position seem

³Similar to the case of double-row MOCN this fact can be rationalized as a result of effective loss of Fe atoms in various surface processes.

to be decisive for the formation and the final topology of the encountered MOCNs, whereas the remaining side group is not directly involved in metal-organic complexation. Unfortunately the detailed positioning of side groups in the various network structures cannot be unambiguously determined at the basis of the STM data obtained, which is associated with the distortion of the molecules upon adsorption and the weak contribution of this moiety to the tunneling current. Note that the presence of the side group will nevertheless be important for the functionality of the cavity. E.g., it may result in the formation of two mirror-symmetric MOCN cavities since TMLA is a two-dimensional chiral species.

It is interesting to address the potential functionality of the obtained MOCNs. Firstly, the single- and double-row structure contain magnetic atoms which are periodically arranged. It is expected that the organic linkers mediate magnetic coupling between the Fe atoms, similar to effects in related metal-organic magnetic structures, developed recently [112,261–263]. The ladder-type and two-dimensional metal-organic linkage in the double-row and single-row MOCNs thus represent nanoscale magnetic arrangements with distinct symmetry. On the other hand, the obtained networks provide a regular arrangement of cavities with well-defined shape and chemistry. Finally, the MOCNs are of potential use as templates for three-dimensional molecular architectures, such as nanoporous lattices.

Chapter 5

Outlook

In the present thesis novel design principles for supramolecular systems at metal surfaces were developed. Whereas hydrogen-bonded two-dimensional assemblies have been investigated in recent years to probe the general principles of self-assembly of molecular species at metal substrates, the concept of surface metal-organic coordination was introduced here and exploited for the formation of distinct surface-supported supramolecular architectures. Using scanning tunneling microscopy we elucidated the basic mechanisms in surface metal-organic coordination by monitoring real-time complexation reaction events and evaluating associated reaction rates and energies. Fundamental phenomena, such as chirality and hierarchical self-assembly, as well as supramolecular design concepts for open-network-type architectures were successfully probed and explored. Moreover, a first step towards magnetic nanosystems with ultimately high density of magnetic centers was accomplished: The *in situ* fabrication of a metal-organic matrix to position individual Fe atoms in extended two-dimensional arrays.

Naturally, two principle ways can be envisioned for the further development of the expounded strategy. On the one hand the continuation of structural studies, where the enormously rich arsenal of organic ligands and metals, accumulated by conventional solution and solid state metal-organic chemistry, can be explored to construct supramolecular architectures, up to now unimagined at surfaces. This opens multiple pathways for the design of novel nanostructured functional materials. A systematic development of the genuine bottom-up strategy for the fabrication of

novel metal-organic architectures presented here, is expected to provide subtle control over the resulting versatile topologies at the nanoscale.

Furthermore a deeper understanding of the nature of surface coordination bonding can be obtained using *ab initio* density functional theory calculations. Our first results in this direction evidence the possibility to determine the electronic structure, associated energies and exact coordination geometries for low-dimensional metal-organic architectures [264].

The development of the principal ideas, outlined in this thesis, potentially may help in particular to overcome the traditional problem in 3D crystal engineering - the lack of predictive power when designing supramolecular solid state systems. Expanding the strategy to a wide range of nanoscale topologies will allow to address specific issues of nanochemistry. In fact it is expected that the final topology of surface supported metal-organic supramolecular structure can be steered by the symmetry and chemical properties of the substrate, ligand functionality and coordinating transition metal. The dimensionality reduction at the surface provides well-defined reaction conditions, where the mobility of the reactants is constrained by the surface atomic lattice, providing simultaneously a template for the metal-organic architecture.

On other hand, the *functionality* of the fabricated and envisioned surface-supported metal-organic structures needs to be investigated. Regarding the architectures demonstrated in the present thesis, several ways can be envisioned. Probing the functionality for selective host-guest interactions of chiral nanocavities (Section 4.3, Chapter 4) requires their interaction with the truly 3D chiral molecular species, which potentially can display selective adsorption. Good candidates for that would certainly be simple aminoacids (e.g. glycine), which can be easily evaporated *in situ* and are of comparable size with the preformed functional pores. The magnetic properties of designed "magnetic print-boards" (Section 4.4, Chapter 4) can be elucidated by means of surface-sensitive x-ray magnetic circular dichroism measurements (XMCD) using synchrotron radiation. Previous results indicate that this technique is sensitive for extremely small amounts of magnetic centers, positioned on the surface [241,243]. Thus it is suitable for probing potential cooperative magnetic behavior in diverse metal-organic architectures. Local probes, like scanning tunneling spectroscopy and

inelastic STS (STIS) can be as well employed to investigate the effects of dimensionality and the nature of the ligands on the magnetic behavior of transition metal coordination centers. Applications for nanocatalysis can be envisioned with the present systems since the catalytic functionality of mono- and di-iron centers is essential in biological enzymatic reactions [265, 266]. Moreover, the availability of Fe centers in chiral configuration can eventually lead to the exploration of phenomena related to asymmetric nanocatalysis. Finally, the functionality of open-network structures for reversible guests accommodation can be addressed by tuning the topology of the coordination network (e.g. changing the pore size and configuration). First results in this direction suggest that metal-organic coordination networks and their derivatives indeed function as host-guest systems, where accommodation and desorption of the guest species can be achieved while keeping intact the structure of the host porous network [267]. The potential of the porous network to function as nanoreactors, providing a well-defined nanoscale chemical environment within individual pores is similarly appealing.

In conclusion, the introduced novel conceptual approach for the fabrication of surface-supported supramolecular architectures is expected to broaden our understanding of fundamental concepts of surface supramolecular self-assembly phenomena and is envisioned to be a versatile and effective tool for the rational design of functional supramolecular nanosystems.

Bibliography

- [1] Editorial, *Nature Mat.* **2**, 127 (2003).
- [2] J. D. Watson and F. H. C. Crick, *Nature* **171**, 737 (1953).
- [3] R. P. Feynman, *Eng. Sci.* **23**, 22 (1960).
- [4] G. E. Moore, *Int. Elec. Devices Mtg (IEDM) Technical Digest* (IEEE, Piscataway, New Jersey, 1975), Vol. 75, p. 11.
- [5] M. Schulz, *Nature* **399**, 729 (1999).
- [6] D. A. Müller *et al.*, *Nature* **399**, 758 (1999).
- [7] *Science* **299**, 1683 (2003).
- [8] V. Balzani, A. Credi, F. M. Raymo, and J. F. Stoddart, *Angew. Chem. Int. Ed.* **39**, 3348 (2000).
- [9] M. Schliwa and G. Woehlke, *Nature* **422**, 759 (2003).
- [10] N. C. Seeman, *Nature* **421**, 427 (2003).
- [11] C. M. Niemeyer and M. Adler, *Angew. Chem. Int. Ed.* **41**, 3779 (2002).
- [12] J. Hasty, D. McMillen, and J. J. Collins, *Nature* **420**, 224 (2002).
- [13] C. M. Niemeyer, *Angew. Chem. Int. Ed.* **40**, 4128 (2001).
- [14] T. A. Taton, *Nature Mat.* **2**, 73 (2003).
- [15] *Introduction to Molecular Electronics*, edited by M. C. Petty, M. R. Bryce, and D. Bloor (Oxford University Press, New York, 1995).

- [16] J. Tour, M. Kozaki, and J. Seminario, *J. Am. Chem. Soc.* **120**, 8486 (1998).
- [17] R. L. Carroll and C. B. Gorman, *Angew. Chem. Int. Ed.* **41**, 4378 (2002).
- [18] A. Aviram and M. A. Ratner, *Chem. Phys. Lett.* **29**, 277 (1974).
- [19] K. Stokbro, J. Taylor, and M. Brandbyge, *J. Am. Chem. Soc.* **125**, 3674 (2003).
- [20] A. Nitzam and M. A. Ratner, *Science* **300**, 1384 (2003).
- [21] C. Joachim, J. K. Gimzewski, and A. Aviram, *Nature* **408**, 541 (2000).
- [22] C. P. Collier *et al.*, *Science* **285**, 391 (1999).
- [23] H. W. C. Postma *et al.*, *Science* **293**, 76 (2001).
- [24] T. Rueckes *et al.*, *Science* **289**, 94 (2000).
- [25] Y. Luo *et al.*, *ChemPhysChem* **3**, 519 (2002).
- [26] D. I. Gittins, D. Bethell, D. J. Schiffrin, and R. J. Nichols, *Nature* **408**, 67 (2000).
- [27] C. P. Collier *et al.*, *Science* **289**, 1172 (2000).
- [28] J. Chen, M. A. Reed, A. M. Rawlett, and J. M. Tour, *Science* **286**, 1550 (1999).
- [29] J. S. Lindsey, *New Journal of Chemistry* **15**, 153 (1991).
- [30] G. M. Whitesides, J. P. Mathias, and C. T. Seto, *Science* **154**, 1312 (1991).
- [31] M. M. Conn and J. J. Rebek, *Chem. Rev.* **97**, 1647 (1997).
- [32] M. C. T. Fyfe and J. F. Stoddart, *Coord. Chem. Rev.* **183**, 139 (1999).
- [33] G. R. Desiraju, *Crystal Engineering: The Design of Organic Solids* (Elsevier, Amsterdam, 1989).
- [34] B. Moulton and M. J. Zaworotko, *Chem. Rev.* **101**, 1629 (2001).
- [35] J.-M. Lehn, *Science* **227**, 849 (1985).
- [36] J.-M. Lehn, *Supramolecular Chemistry* (VCH, Weinheim, 1995).

- [37] F. Vögtle, *Supramolecular Chemistry* (Wiley, New York, 1991).
- [38] *Comprehensive Supramolecular Chemistry*, edited by J. L. Atwood *et al.* (Pergamon, New York, 1996).
- [39] P. Ball, *Nature* **381**, 648 (1996).
- [40] *Science* **295**, 2400 (2002).
- [41] D. S. Lawrence, T. Jiang, and M. Levett, *Chem. Rev.* **95**, 2229 (1995).
- [42] G. R. Desiraju, *Nature* **412**, 397 (2001).
- [43] S. Chiang, *Chem. Rev.* **97**, 1083 (1997).
- [44] G. S. MacCarty and P. S. Weiss, *Chem. Rev.* **99**, 1983 (1999).
- [45] J. K. Gimzewski and C. Joachim, *Science* **283**, 1683 (1999).
- [46] G. Binnig and H. Rohrer, *Helvetica Physica Acta* **55**, 726 (1982).
- [47] T. Yokoyama *et al.*, *Nature* **413**, 619 (2001).
- [48] F. Rosei *et al.*, *Science* **296**, 328 (2002).
- [49] M. Schunack *et al.*, *Phys. Rev. Lett.* **86**, 456 (2001).
- [50] T. A. Jung, R. R. Schlittler, and J. K. Gimzewski, *Nature* **386**, 696 (1997).
- [51] K. W. Hipps, L. Scudiero, D. E. Barlow, and J. M. P. Cooke, *J. Am. Chem. Soc.* **124**, 2126 (2002).
- [52] J. V. Barth *et al.*, *Angew. Chem. Int. Ed.* **39**, 1230 (2000).
- [53] M. Böhrringer *et al.*, *Phys. Rev. Lett.* **83**, 324 (1999).
- [54] G. P. Lopinski, D. J. Moffatt, D. D. Wayner, and R. A. Wolkow, *Nature* **392**, 909 (1998).
- [55] M. Böhrringer, W.-D. Schneider, and R. Berndt, *Angewandte Chemie Int. Ed.* **39**, 792 (2000).

- [56] A. Kühnle, T. R. Linderoth, B. Hammer, and F. Besenbacher, *Nature* **415**, 891 (2002).
- [57] J. V. Barth *et al.*, *J. Am. Chem. Soc.* **124**, 7991 (2002).
- [58] G. A. Somorjai, *J. Phys. Chem. B* **106**, 9201 (2002).
- [59] M. Dürr *et al.*, *Science* **296**, 1838 (2002).
- [60] X.-C. Guo and R. J. Madix, *J. Phys. Chem. B* **107**, 3105 (2003).
- [61] G. S. MacCarty and P. S. Weiss, *J. Phys. Chem. B* **106**, 8005 (2002).
- [62] W. Ho, *J. Chem. Phys.* **117**, 11033 (2002).
- [63] T. Zambelli, J. V. Barth, J. Wintterlin, and G. Ertl, *Nature* **390**, 495 (1997).
- [64] M. O. Lorenzo, C. Baddeley, C. Muryn, and R. Raval, *Nature* **404**, 376 (2000).
- [65] *Transition Metals in Supramolecular Chemistry*, edited by J.-P. Sauvage (John Wiley & Sons, Chichester, England, 1999).
- [66] D. Philp and J. F. Stoddart, *Angew. Chem. Int. Ed.* **35**, 1154 (1996).
- [67] G. A. Jeffrey and W. Saenger, *Hydrogen bonding in biological systems* (Springer, Berlin, 1991).
- [68] *Comprehensive Supramolecular Chemistry*, edited by J. L. Atwood *et al.* (Pergamon, New York, 1996), Vol. 4.
- [69] G. A. Jeffrey, *An Introduction to Hydrogen Bonding* (Oxford Univ. Press, New York, 1997).
- [70] L. J. Prins, D. N. Reinhoudt, and P. Timmerman, *Angew. Chem. Int. Ed.* **40**, 2382 (2001).
- [71] T. Steiner, *Angew. Chem. Int. Ed.* **41**, 48 (2002).
- [72] J.-H. Fournier *et al.*, *J. Am. Chem. Soc.* **125**, 1002 (2003).
- [73] T. Kawai, H. Tanaka, and T. Nakagawa, *Surface Science* **386**, 124 (1997).

- [74] M. Furukawa *et al.*, Surface Science **445**, L58 (2000).
- [75] J. Weckesser *et al.*, Physical Review Letters **87**, 096101 (2001).
- [76] J. N. O'Shea *et al.*, J. Phys. Chem. B **105**, 1917 (2001).
- [77] T.-Q. Nguen, M. L. Bushey, L. E. Brus, and C. Nuckolls, J. Chem. Phys. **89**, 3331 (1988).
- [78] A. McNutt, S. Haq, and R. Raval, Surf. Sci. **531**, 131 (2003).
- [79] G. R. Desiraju, Angew. Chem. Int. Ed. **34**, 2311 (1995).
- [80] G. Frenking and N. Fröhlich, Chem. Rev. **100**, 717 (2000).
- [81] L. A. Finney and T. V. O'Halloran, Science **300**, 931 (2003).
- [82] R. H. Fish and G. Jaouen, Organometallics **22**, 2166 (2003).
- [83] *Bioinorganic chemistry: Transition metals in biology and their coordination chemistry*, edited by A. X. Trautwein (Wiley-VCH, Weinheim, Germany, 1997).
- [84] *Comprehensive Supramolecular Chemistry*, edited by J. L. Atwood *et al.* (Pergamon, New York, 1996), Vol. 5.
- [85] *Comprehensive Supramolecular Chemistry*, edited by J. L. Atwood *et al.* (Pergamon, New York, 1996), Vol. 7.
- [86] B. J. Holliday and C. A. Mirkin, Angew. Chem. Int. Ed. **40**, 2022 (2001).
- [87] A. Werner, Z. Anorg. Chem. **3**, 267 (1893).
- [88] *Comprehensive Coordination Chemistry*, edited by G. Wilkinson, R. D. Gillard, and J. A. McCleverty (Pergamon, Oxford, 1987).
- [89] J.-C. Chambron, C. Dietrich-Buchecker, and J.-P. Sauvage, in *Comprehensive Supramolecular Chemistry*, edited by J. L. Atwood *et al.* (Pergamon, New York, 1996), Vol. 9, Chap. 2, p. 43.

- [90] D. B. Amabilino, F. M. Raymo, and J. F. Stoddart, in *Comprehensive Supramolecular Chemistry*, edited by J. L. Atwood *et al.* (Pergamon, New York, 1996), Vol. 9, Chap. 3, p. 85.
- [91] B. Olenyuk, J. A. Whiteford, A. Fechtenkötter, and P. J. Stang, *Nature* **398**, 796 (1999).
- [92] M. Fujita, *Chem. Soc. Rev.* **27**, 417 (1998).
- [93] M. Fujita, in *Comprehensive Supramolecular Chemistry*, edited by J. L. Atwood *et al.* (Pergamon, New York, 1996), Vol. 9, Chap. 7, p. 253.
- [94] P. Baxter, in *Comprehensive Supramolecular Chemistry*, edited by J. L. Atwood *et al.* (Pergamon, New York, 1996), Vol. 9, Chap. 5, p. 165.
- [95] E. C. Constable, in *Comprehensive Supramolecular Chemistry*, edited by J. L. Atwood *et al.* (Pergamon, New York, 1996), Vol. 9, Chap. 6, p. 213.
- [96] R. Vilar, *Angew. Chem. Int. Ed.* **42**, 1460 (2003).
- [97] D. Braga, F. Grepioni, and G. R. Desiraju, *Chem. Rev.* **98**, 1375 (1998).
- [98] J. M. Brown and S. G. Davies, *Nature* **342**, 631 (1989).
- [99] C. Copéret, M. Chabanas, R. P. Saint-Arroman, and J.-M. Basset, *Angew. Chem. Int. Ed.* **42**, 156 (2003).
- [100] P. Serp and P. Kalck, *Chem. Rev.* **102**, 3085 (2002).
- [101] F. R. Hartley, *Supported Metal Complexes: A New Generation of Catalysts* (Kluwer Academic Publishers, Dordrecht, Holland, 1999).
- [102] A. D. Pomogailo, *Catalysis by Polymer-Immobilized Metal Complexes* (Gordon and Breach Science Publishers, Amsterdam, Holland, 1996).
- [103] *MRS Bull.*, special issue: Molecular-Based Magnets (J. S. Miller and A. J. Epstein, guest editors) **25(11)**, (2000).
- [104] O. Kahn, *Molecular Magnetism* (VCH, Weinheim, 1993).

- [105] D. Gatteschi and R. Sessoli, *Angew. Chem. Int. Ed.* **42**, 268 (2003).
- [106] M. Affronte *et al.*, *Phys. Rev. B* **66**, 064408 (2002).
- [107] J. R. Friedman, M. P. Sarachik, J. Tejada, and R. Ziolo, *Phys. Rev. Lett.* **76**, 3830 (1996).
- [108] J. Bera and K. R. Dunbar, *Angew. Chem. Int. Ed.* **41**, 4453 (2002).
- [109] K. Tanaka *et al.*, *Science* **299**, 1212 (2003).
- [110] R. Lescouëzec *et al.*, *Angew. Chem. Int. Ed.* **42**, 1483 (2003).
- [111] O. Waldmann *et al.*, *Phys. Rev. Lett.* **78**, 3390 (1997).
- [112] B. Moulton *et al.*, *Angew. Chem. Int. Ed.* **41**, 2821 (2002).
- [113] E. Coronado, J. R. Galán-Mascarós, C. J. Gómez-García, and V. Laukhin, *Nature* **408**, 447 (2000).
- [114] S. R. Batten and R. Robson, *Angew. Chem. Int. Ed.* **37**, 1460 (1998).
- [115] M. M. Turnbull and C. P. Landee, *Science* **298**, 1723 (2002).
- [116] G. J. Halder *et al.*, *Science* **298**, 1762 (2002).
- [117] Y. Sunatsuki *et al.*, *Angew. Chem. Int. Ed.* **42**, 1614 (1999).
- [118] O. Kahn and C. J. Martinez, *Science* **279**, 44 (1998).
- [119] J. Park *et al.*, *Nature* **417**, 722 (1999).
- [120] W. Liang *et al.*, *Nature* **417**, 725 (2001).
- [121] A. Semenov *et al.*, *Angew. Chem. Int. Ed.* **38**, 2547 (1999).
- [122] D. G. Kurth, N. Severin, and J. P. Rabe, *Angew. Chem. Int. Ed.* **41**, 3681 (2002).
- [123] C. R. Evanko and D. A. Dzombak, *Environ. Sci. Technol.* **32**, 2846 (1998).
- [124] D. E. Giammar and D. A. Dzombak, *J. Sol. Chem.* **27**, 89 (1998).

- [125] *NIST Standard Reference Database No. 46: Critical Stability Constants of Metal Complexes*, edited by A. E. Martell and R. M. Smith (National Institute of Standards and Technology, Gaithersburg, MD, 1994).
- [126] I. Giaever, *Phys. Rev. Lett.* **5**, 147 (1960).
- [127] C. J. Chen, *Introduction to Scanning Tunneling Microscopy* (Oxford University Press, New York, 1993).
- [128] G. Binnig, H. Rohrer, C. Gerber, and E. Weibel, *Phys. Rev. Lett.* **49**, 57 (1982).
- [129] J. Bardeen, *Phys. Rev. Lett.* **6**, 57 (1961).
- [130] E. L. Wolf, *Principles of Electron Tunneling Spectroscopy* (Oxford University Press, New York, 1985).
- [131] J. Tersoff and D. R. Hamann, *Physical Review Letters* **50**, 1998 (1983).
- [132] A. Selloni, P. Carnevali, E. Tosatti, and C. D. Chen, *Phys. Rev. B* **31**, 2602 (1985).
- [133] N. D. Lang, *Physical Review B* **34**, 5947 (1986).
- [134] S. Park and R. C. Barrett, in *Scanning Tunneling Microscopy.*, edited by J. Stroscio and W. Kaiser (Academic Press, San Diego, 1993).
- [135] J. K. Gimzewski, E. Stoll, and R. R. Schlittler, *Surf. Sci.* **181**, 267 (1987).
- [136] H. Ohtani, R. J. Wilson, S. Chiang, and C. M. Mate, *Physical Review Letters* **60**, 2398 (1988).
- [137] P. H. Lippel *et al.*, *Physical Review Letters* **62**, 171 (1989).
- [138] C. J. Chen, *Journal of Vacuum Science & Technology A* **9**, 44 (1991).
- [139] M. Tsukada *et al.*, *Surface Science Reports* **13**, 265 (1991).
- [140] M. Tsukada, H. Kageshima, N. Isshiki, and K. Kobayashi, *Surface Science* **266**, 253 (1992).

- [141] G. Doyen *et al.*, Physical Review B **48**, 1738 (1993).
- [142] P. Sautet and C. Joachim, Physical Review B **38**, 12238 (1988).
- [143] R. F. Lin, G. S. Blackmann, M. A. V. Hove, and G. A. Samorjai, Acta Cryst. B **43**, 368 (1987).
- [144] P. Sautet and C. Joachim, Chemical Physics Letters **185**, 23 (1991).
- [145] V. Hallmark, S. Chiang, K.-P. Meinhart, and K. Hafner, Phys. Rev. Lett. **70**, 3740 (1993).
- [146] P. Sautet, Chemical Reviews **97**, 1097 (1997).
- [147] J. Weckesser, Ph.D. thesis, Ecole Polytechnique Fédérale de Lausanne (EPFL), Switzerland, 2000.
- [148] D. Peterka, Ph.D. thesis, Ecole Polytechnique Fédérale de Lausanne (EPFL), Switzerland, 2002.
- [149] H. Brune, H. Röder, K. Bromann, and K. Kern, Thin Solid Films **264**, 230 (1995).
- [150] B. Fischer, Ph.D. thesis, Ecole Polytechnique Fédérale de Lausanne (EPFL), Switzerland, 1998.
- [151] E. Umbach, M. Sokolowski, and R. Fink, Applied Physics A **63**, 565 (1996).
- [152] S. R. Forrest, Chemical Reviews **97**, 1793 (1997).
- [153] *NIST Chemistry WebBook, NIST Standard Reference Database No. 6: IR and Mass Spectra*, edited by P. J. Linstrom and W. G. Mallard (National Institute of Standards and Technology, <http://webbook.nist.gov>, Gaithersburg, MD, 2001).
- [154] A. Dmitriev *et al.*, J. Phys. Chem. B **106**, 6907 (2002).
- [155] D. Duchamp and R. Marsh, Acta Crystallographica Sect. B **25**, 5 (1969).
- [156] F. H. Herbstein, Physical Review Letters **66**, 2911 (1991).

- [157] F. H. Herbstein, in *Comprehensive Supramolecular Chemistry*, edited by J. L. Atwood *et al.* (Pergamon, New York, 1996), Vol. 6, p. 61.
- [158] S. Kolotuchin *et al.*, Chem. Eur. J. **5**, 2537 (1999).
- [159] S. Chatterjee, V. Pedireddi, A. Ranganathan, and C. Rao, Journal of Molecular Structure **520**, 107 (2000).
- [160] F. Takusagawa, K. Hirotsu, and A. Shimada, Bull. Chem. Soc. Jap. **46**, 2960 (1973).
- [161] K. Biradha *et al.*, J. Am. Chem. Soc. **12**, 11894 (1998).
- [162] J. Stöhr, *NEXAFS Spectroscopy*, Vol. 25 of *Springer Series in Surface Sciences* (Springer-Verlag, Heidelberg, 1991).
- [163] A. Lee *et al.*, J. Phys. Chem. B **104**, 11729 (2000).
- [164] J. Weckesser, J. V. Barth, and K. Kern, Journal of Chemical Physics **110**, 5351 (1999).
- [165] A. Seitsonen, private communication (unpublished).
- [166] Hydrogen Transfer: Experiment and Theory. In *Ber. Bunsen-Ges. Phys. Chem.*; H.-H. Limbach and J. Manz, Eds.; **102**, 289, (1998).
- [167] S. Griessl *et al.*, Single Mol. **3**, 25 (2002).
- [168] B. Frederick, M. Ashton, and N. Richardson, Surf. Sci. **292**, 33 (1993).
- [169] B. Frederick *et al.*, Surf. Sci. **394**, 1 (1997).
- [170] C. C. Perry, S. Haq, B. G. Frederick, and N. V. Richardson, Surface Science **409**, 512 (1998).
- [171] Q. Chen *et al.*, Surf. Sci. **446**, 63 (2000).
- [172] K.-U. Weiss *et al.*, Phys. Rev. Lett. **69**, 3196 (1992).
- [173] D. Woodruff, C. McConville, and A. Kilcoyne, Surf. Sci. **201**, 228 (1988).

- [174] B. G. Frederick, F. M. Leibsle, S. Haq, and N. V. Richardson, *Surf. Rev. Lett.* **3**, 1523 (1996).
- [175] M. Casarin, G. Granozzi, M. Sambi, and E. Tondello, *Surf. Sci.* **307-309**, 95 (1994).
- [176] M. Sambi *et al.*, *Surf. Sci.* **315**, 309 (1994).
- [177] S. Haq, R. Bainbridge, B. Frederick, and N. Richardson, *J. Phys. Chem.* **102**, 8807 (1998).
- [178] B. Frederick *et al.*, *Surf. Sci.* **352-354**, 238 (1996).
- [179] A. Dmitriev *et al.*, in preparation (2003).
- [180] S. Haq and F. M. Leibsle, *Surf. Sci.* **355**, L345 (1996).
- [181] X. Zhao, *J. Am. Chem. Soc.* **122**, 12584 (2000).
- [182] F. S. Tautz *et al.*, *Surf. Sci.* **502-503**, 176 (2002).
- [183] X. Zhao *et al.*, *Surf. Sci.* **424**, L347 (1999).
- [184] C. J. Eckhardt *et al.*, *Nature* **362**, 614 (1993).
- [185] P. Nassoy, M. Goldmann, O. Bouloussa, and F. Rondelez, *Phys. Rev. Lett.* **75**, 457 (1995).
- [186] R. Viswanathan, J. A. Zasadzinski, and D. K. Schwartz, *Nature* **368**, 440 (1994).
- [187] F. Charra and J. Cousty, *Phys. Rev. Lett.* **80**, 1682 (1998).
- [188] S. J. Sowerby, W. M. Heckl, and G. B. Petersen, *J. Mol. Evol.* **43**, 419 (1996).
- [189] G. F. Swiegers and T. J. Malefetse, *Chem. Rev.* **100**, 3483 (2000).
- [190] R. C. Mehrotra and R. Bohra, *Metal Carboxylates* (Academic Press, London, 1983).
- [191] A. Doyle *et al.*, *Polyhedron* **19**, 2621 (2000).

- [192] P. R. Raithby, G. P. Shields, F. H. Allen, and W. D. S. Motherwell, *Acta Cryst. B* **56**, 444 (2000).
- [193] J. Lee and W. Ho, *Science* **286**, 1719 (1999).
- [194] S.-W. Hla, L. Bartels, G. Meyer, and K.-H. Rieder, *Phys. Rev. Lett.* **85**, 2777 (2000).
- [195] L. Pasteur, *C.R. Hebd. Seances Acad. Sci* **26**, 535 (1848).
- [196] J. M. Bijvoet, A. F. Pederman, and J. A. V. Bommel, *Nature* **168**, 271 (1951).
- [197] R. Noyori, *Asymmetric Catalysis in Organic Synthesis* (John Wiley & Sons, New York, 1994).
- [198] G. Palyi, C. Zucchi, and L. Caglioti, *Advances in Biochirality* (Elsevier, Oxford, 1999).
- [199] D. B. Cline, *Physical Origin of Homochirality in Life* (AIP Press, Woodbury, New York, 1996).
- [200] M. Avalos *et al.*, *Chem. Rev.* **98**, 2391 (1998).
- [201] A. D. Buckingham, in *Inorganic Biochemistry*, edited by G. L. Eichhorn (Elsevier, Amsterdam, 1997), Vol. 1, p. 3.
- [202] A. von Zelewsky, *Stereochemistry of Coordination Compounds* (John Wiley & Sons, Chichester, 1996).
- [203] C. Provent and A. F. Williams, in *Transition Metals in Supramolecular Chemistry*, edited by J.-P. Sauvage (John Wiley & Sons, Chichester, UK, 1999), Chap. 4, p. 135.
- [204] U. Knof and A. von Zelewsky, *Angew. Chem. Int. Ed.* **38**, 302 (1999).
- [205] L. Pérez-García and D. B. Amabilino, *Chem. Soc. Rev.* **31**, 342 (2002).
- [206] M. Lahav and L. Leiserowitz, *Angew. Chem. Int. Ed.* **38**, 2533 (1999).
- [207] I. Katsuki *et al.*, *J. Am. Chem. Soc.* **124**, 629 (2002).

- [208] A. Baiker and H.-U. Blaser, in *Handbook of Heterogeneous Catalysis*, edited by G. Ertl, H. Knözinger, and J. Weitkamp (Wiley-VCH, Weinheim, 1997), p. 2422.
- [209] H.-U. Blaser, *Tetrahedron: Asymmetry* **2**, 843 (1991).
- [210] H. Fang, L. C. Giancarlo, and G. W. Flynn, *J. Phys. Chem. B* **102**, 7311 (1998).
- [211] M. Böhringer, K. Morgenstern, W.-D. Schneider, and R. Berndt, *Angew. Chem. Int. Ed.* **38**, 821 (1999).
- [212] S. D. Feyter *et al.*, *Angew. Chem. Int. Ed.* **37**, 1223 (1998).
- [213] D. G. Yablon, D. Wintgens, and G. W. Flynn, *J. Phys. Chem. B* **106**, 5470 (2002).
- [214] E.-Q. Gao, S.-Q. Bai, Z.-M. Wang, and C.-H. Yan, *J. Am. Chem. Soc.* **125**, 4984 (2003).
- [215] *Encyclopedia of Inorganic Chemistry*, edited by R. B. King (Wiley, Chichester, 1994).
- [216] Z. R. Tian, J. L. J. A. Voigt, B. Mckenzie, and H. Xu, *Angew. Chem. Int. Ed.* **42**, 413 (2003).
- [217] *Self-Assembling Architecture*, edited by J. E. Varner (Alan R. Liss, New York, 1988).
- [218] A. J. Cann, *Principles of Molecular Virology* (Academic Press, San Diego, 2001).
- [219] M. C. T. Fyfe and J. F. Stoddart, *Acc. Chem. Res.* **30**, 393 (1997).
- [220] S. R. Seidel and P. J. Stang, *Acc. Chem. Res.* **35**, 972 (2002).
- [221] W. A. Lopes and H. M. Jaeger, *Nature* **414**, 735 (2001).
- [222] M. Eddaoudi *et al.*, *Science* **295**, 469 (2002).
- [223] J.-M. Lehn, *Science* **295**, 2400 (2002).

- [224] O. Ikkala and G. ten Brinke, *Science* **295**, 2407 (2002).
- [225] D. N. Reinhoudt and M. Crego-Calama, *Science* **295**, 2403 (2002).
- [226] M. D. Hollingsworth, *Science* **295**, 2410 (2002).
- [227] Y. Huang, X. Duan, Q. Wei, and C. M. Lieber, *Science* **291**, 630 (2001).
- [228] A. Hatzor *et al.*, *J. Am. Chem. Soc.* **120**, 13469 (1998).
- [229] P. Yang *et al.*, *Science* **282**, 2244 (1998).
- [230] W. A. Bonner, *Orig. Life Evol. Biosph.* **25**, 175 (1995).
- [231] N. Bowden *et al.*, *Angew. Chem. Int. Ed.* **121**, 5373 (1999).
- [232] J. M. Rivera, T. Martín, and J. R. Jr., *Science* **279**, 1021 (1998).
- [233] M. Geva, F. Frolow, M. Eisenstein, and L. Addadi, *J. Am. Chem. Soc.* **125**, 696 (2003).
- [234] M. E. Davis, *Nature* **417**, 813 (2002).
- [235] Y. Cui *et al.*, *Angew. Chem. Int. Ed.* **41**, 1159 (2002).
- [236] E. Coronado, P. Delhas, D. Gatteschi, and J. S. Miller, *NATO ASI Series* (Kluwer, Dordrecht, 1996).
- [237] E. Coronado, F. Palacio, and J. Veciana, *Angew. Chem. Int. Ed.* **42**, 2570 (2003).
- [238] H. Srikanth, R. Hajndl, B. Moulton, and J. Zaworotko, *J. Appl. Phys.* **93**, 7089 (2003).
- [239] S. S.-Y. Chui *et al.*, *Science* **283**, 1148 (1999).
- [240] J. Shen and J. Kirschner, *Surf. Sci.* **500**, 300 (2002).
- [241] P. Gambardella *et al.*, *Nature* **416**, 301 (2002).
- [242] S. D. Bader, *Surf. Sci.* **500**, 172 (2002).

- [243] P. Gambardella *et al.*, Science **300**, 1130 (2003).
- [244] N. Knorr *et al.*, Phys. Rev. B **65**, art. no. 115420 (2002).
- [245] S. Leininger, B. Olenyuk, and P. J. Stang, Chem. Rev. **100**, 853 (2000).
- [246] J. Lu *et al.*, Inorg. Chem **38**, 2695 (1999).
- [247] P. J. Stang, N. E. Persky, and J. Manna, J. Am. Chem. Soc **119**, 4777 (1997).
- [248] D. Venkataraman, G. B. Gardner, S. Lee, and J. S. Moore, J. Am. Chem. Soc. **117**, 11600 (1995).
- [249] M. Fujita, Y. J. Kwon, S. Washizu, and K. Ogura, J. Am. Chem. Soc. **116**, 1151 (1994).
- [250] L. R. MacGillivray, R. H. Groeneman, and J. L. Atwood, J. Am. Chem. Soc **120**, 2676 (1998).
- [251] M. Eddaoudi *et al.*, Acc. Chem. Res. **34**, 319 (2001).
- [252] K. Yamamoto *et al.*, Science **300**, 470 (2003).
- [253] M. Oh, G. B. Carpenter, and D. A. Sweigart, Angew. Chem. Int. Ed. **42**, 2026 (2003).
- [254] J. S. Seo *et al.*, Nature **404**, 982 (2000).
- [255] G. B. Gardner, D. Venkataraman, J. S. Moore, and S. Lee, Nature **374**, 792 (1995).
- [256] O. M. Yaghi, G. Li, and H. Li, Nature **378**, 703 (1995).
- [257] B. Chen *et al.*, Science **291**, 102 (2001).
- [258] C. J. Kepert, T. J. Prior, and M. J. Rosseinsky, J. Am. Chem. Soc **122**, 5158 (2000).
- [259] R. Kitaura *et al.*, Science **298**, 2358 (2002).
- [260] N. L. Rosi *et al.*, Science **300**, 1127 (2003).

- [261] E. Breuning *et al.*, Angew. Chem. Int. Ed. **39**, 2504 (2000).
- [262] J. R. Galán-Mascarós and K. R. Dunbar, Angew. Chem. Int. Ed. **42**, 2289 (2003).
- [263] D. Maspoch *et al.*, Nature Materials **2**, 190 (2003).
- [264] N. Lin *et al.*, in preparation (2003).
- [265] D. C. Rees and J. B. Howard, Science **300**, 929 (2003).
- [266] L. D. Slep and F. Neese, Angew. Chem. Int. Ed. **42**, 2942 (2003).
- [267] S. Stepanow *et al.*, in press (2003).

Acknowledgments

I want to thank Professor Klaus Kern, the director of my thesis, for giving me the bright opportunity to work in his group and by his guidance (with motivating optimism, energy and care in the same time) make this thesis to be accomplished.

I would like to express my deepest gratitude to Nian Lin, who supervised this thesis work and was directly involved in planning and realization of experiments, giving the fruitful ideas and helping them to come into reality. His wise and calm guidance is invaluable for my formation as a researcher, and I hope I can follow the attitude learnt from him in future.

My sincere gratitude also to Johannes Barth, who followed the projects, presented here, from the very beginning, being closely involved in the exchange of ideas. He was bringing invaluable contribution to data evaluation and fresh views on formulating the whole conceptual approach. I truly appreciate as well his careful reading of the manuscript and giving useful comments and general ideas.

I would like to express my hearty thanks to the people I worked with closely and who also largely contributed to this thesis project. Jens Weckesser, who, by side with Nian Lin, introduced me into the world of STM, full of magic and astonishment, and helped to start seeing atoms on an everyday basis. Hannes Spillmann, who was explaining me with patience (and in his calm and confident way) also the basics of chemistry. Mathieu Abel, who helped me to understand lots of things (and not necessarily directly related to our molecules) and with whom we've spent old good times, travelling around (et aller-retour) et j'en suis sûr encore plus à venir. Harold Zandvliet, whose short stay was a very nice time for us all, also travelling together to Schloss Ringberg. Sebastian Stepanow, who is to continue what we've started here and who is the super fun person to spend time in some dark places like synchrotrons

(wir sind alle nur Kaffee Maschinen, you know). Magalí Lingenfelder, who widened my personal imagination of motivation and a hard work - and in the same time created this relaxing southern atmosphere having 'Mate' in the lab on winter evenings. Dietmar Payer, who is a fun person to work (have lunch) with and a warrior to force experimental setup to run properly.

I also want to thank the members of the jury: Prof. K. Wandelt, Prof. E. Meyer and Prof. H. Brune for judging this thesis.

I would like to thank Ari Seitsonen who is carrying out (on his strong shoulders) the DFT calculations on the organic and metal-organic systems presented here - although not included in the present thesis, his calculations greatly contributed in understanding the fundamentals of the investigated systems.

I also thank the colleagues in Uni Bochum (Lehrstuhl für Physikalische Chemie I, Ruhr-Universität Bochum), particularly Thomas Strunskus, for their help in conducting synchrotron measurements (XPA and NEXAFS) on organic and metal-organic systems in BESSY II in cool city of Berlin . The gained knowledge helped a lot in understanding the chemistry of our systems and allowed us to look at them from different perspective (from the 'platform', actually).

I want to thank of course all the people from our department, who were around for the last three years and still are (and those who already left for now). Dear friends, you make working here a great pleasure! Hey, guys, I can't name you all - you are all great! And that's you who make our department a fantastic place. Special thanks to Ralf Vogelgesang and Roman Sordan though for helping me fighting with MikTeX and, actually, - we won (if you can read this).

To those who are the closest to me. Rosie Friemann, the angel of my life, for making me feel happy and being with me through all beautiful and hard times. Älskar dig! My Mom and Dad (mama Olya i papa Vova) for raising me like you did and convincing me to pursue the way (swarschikom-to byut prosto, esli i tak uje vse swarschiki vokrug - spasibo with love!), and Zoya and Inga - privet semye. It's a pity our grandmother (nasha babushka) can't see this - she always believed I'm kind of unserious.

Curriculum vitae

Name:	Alexandre Dmitriev
Date of Birth:	October 12, 1975
Nationality	Russian
1982 - 1992	Specialized Physical and Mathematical High School in Rostov on Don, Russia
1992 - 1997	Master studies in physics at the Rostov State University, Rostov on Don, Russia
June 1997	Master thesis under the supervision of Prof. V. Torgashev in the Department of Crystal Physics and Structure Analysis, Faculty of Physics, Rostov State University: “Structure of Interphase Boundaries in Silica”
February 1999 - October 1999	Research assistant in the group of Prof J. C. de Lima at the Departamento de Fisica, Universidade Federal de Santa Catarina, Florianopolis, Brasil
November 1999 - June 2000	Research and engineering assistant at Swiss-Norwegian Beam Lines at ESRF, Grenoble, France
2000 - 2003	Research assistant in the group of Prof. K. Kern - Department of Nanoscale Science at the Max-Planck-Institut für Festkörperforschung in Stuttgart, Germany
September 2003	PhD thesis: “Design Principles for Low-Dimensional Supramolecular Systems at Metal Surfaces”

Publications

J.C. de Lima, V. dos Santos, T. Grandi, P. C. D’Ajello, A. Dmitriev, “Thermodynamic considerations about the formation of alloys by mechanical alloying”, *Phys. Rev. B* **62**, 8871 (2000).

A. Dmitriev, N. Lin, J. Weckesser, J.V. Barth, and K. Kern, “Supramolecular Assemblies of Trimesic Acid on a Cu(100) Surface”, *J. Phys. Chem. B* **106**, 6907 (2002).

N. Lin, A. Dmitriev, J. Weckesser, J.V. Barth, and K. Kern, “Real-Time Single-Molecule Imaging of the Formation and Dynamics of Coordination Compounds”, *Angew. Chem. Int. Ed.* **24**, 4779 (2002).

P. Messina, A. Dmitriev, N. Lin, H. Spillmann, M. Abel, J.V. Barth, and K. Kern, “Direct Observation of Chiral Metal-Organic Complexes Assembled on a Cu(100) Surface”, *J. Am. Chem. Soc.* **124**, 14000 (2002).

J.V. Barth, J. Weckesser, N. Lin, A. Dmitriev, and K. Kern, “Supramolecular Architectures and Nanostructures at Metal Surfaces”, *Appl. Phys. A* **76**, 645 (2003).

A. Dmitriev, H. Spillmann, N. Lin, J.V. Barth, and K. Kern, “Modular Assembly of Two-Dimensional Metal-Organic Coordination Networks at a Metal Surface”, *Angew. Chem. Int. Ed.* **23**, 2670 (2003).

M. Abel, A. Dmitriev, R. Fasel, N. Lin, J.V. Barth, K. Kern, “Scanning Tunneling Microscopy and X-ray Photoelectron Diffraction Investigation of C₆₀ Films on

Cu(100)", *Phys. Rev. B* **67**, 245407 (2003).

A. Enders, D. Peterka, D. Repetto, N. Lin, A. Dmitriev, and K. Kern, "Temperature Dependence of the Surface Anisotropy of Fe Ultrathin Films on Cu(001)", *Phys. Rev. Lett.* **90**, 217203 (2003).

H. Spillmann, A. Dmitriev, N. Lin, P. Messina, J.V. Barth, K. Kern, "Hierarchical Assembly of Two-Dimensional Homochiral Nanocavity Arrays", *J. Am. Chem. Soc.* **125**, 10725 (2003).

M. Lingenfelder, H. Spillmann, A. Dmitriev, S. Stepanow, N. Lin, J.V. Barth, K. Kern, "Tailored Assembly of Low-Dimensional Metal-Organic Coordination Systems at a Metal Surface", *Chemistry Eur. J.*, in press (2003).

S. Stepanow, M. Lingenfelder, A. Dmitriev, H. Spillmann, E. Delvigne, N. Lin, C. Cai, J.V. Barth, K. Kern, "Steering host-guest interactions using tailor-made two-dimensional nanoporous coordination systems", submitted (2003).

A. Dmitriev, S. Stepanow, A. Seitsonen, H. Spillmann, M. Lingenfelder, M. Abel, N. Lin, J. V. Barth, T. Strunskus, A. Nicklewski, Ch. Wöll, K. Kern and M. Parrinello "Chiral Functionalization of Metal Surface by an Organic Adlayer", in preparation (2003).